SISSA ISAS
SCUOLA INTERNAZIONALE SUPERIORE DI STUDI AVANZATI
INTERNATIONAL SCHOOL FOR ADVANCED STUDIES

The Mott Transition: Role of Frustration and Orbital Degeneracy

Thesis submitted for the degree of

Doctor Philosophiæ

Candidate
Massimo Capone

Supervisors
Dr. Michele Fabrizio
Prof. Erio Tosatti

October 2000

Contents

Introduction

The Mott transition, i.e. the metal insulator transition (MIT) driven by the correlation between the electrons, represents the most important physical phenomenon in which the ordinary theory of solids fails[1, 2, 3]. In the band theory of solids the electronic state is described as a set of rigid bands, that are filled with the correct number of electrons. The theory relies on the approximation that the electrons in a many-particle state can be described as independent particles. In other words, the effects of electron-electron correlations are neglected. Early in the first decades of quantum mechanics, this theory has provided the first successful characterization of metals and insulators. At zero temperature, the last occupied band of a metal is only partially filled, while it is completely filled in an insulator. As a matter of fact, various compounds seem to invalidate this classification scheme. In 1937 de Boer and Verwey [4] reported that many transition-metal oxides with partially filled bands, presented in fact poor conductivity or even insulating behaviour. Moreover, transitions between a metal and an insulator driven by pressure (or chemical substitution), hardly understandable within a band picture, have been observed.

Peierls [5] was probably the first to put the blame on correlation for such an unpredicted behaviour. Peierls realized that :"it is quite possible that the electrostatic interaction between the electrons prevents them from moving at all. At low temperature the majority of electrons are in their proper places in the ions. The minority which have happened to cross the potential barrier find therefore all the other atoms occupied, and in order to get through the lattice have to spend a long time in ions already occupied by other electrons. This needs a considerable addition of energy and so is extremely improbable at low temperatures.".

These words may be seen as the opening of a new branch of condensed matter physics: the strongly correlated electrons field. Mott [6, 1] has gone forward along this direction identifying the reason why correlation should transform a metal in an insulator. Without loss of generality he considered the idealized case of a lattice with a single orbital on each site. In absence of electron-electron correlation, a single band is

formed by the overlap of the atomic wave functions. The band can host one electron per site with spin up and one with spin down. If the number of electrons equals the number of lattice sites, half of the band is filled, and the chemical potential falls in the centre of the symmetric band (half-filling). If correlation is considered, then two electrons sitting on the same site experience a strong repulsion. Mott argued that such an effect would split the band in two: a lower band filled by electrons occupying a previously empty site, and an upper band occupied by electrons sitting in a site already hosting another electron. For one electron per site (half-filled system) the lower band would be filled, and the upper empty, leading to an insulator. After the path-breaking work by Mott, the metal-to-insulator transition driven by the electron-electron interaction is usually referred to as the Mott transition. We underline that the possible occurrence of antiferromagnetic (AFM) ordering is not crucial in this argument. On the other hand, Slater [7], starting from the observation that most "Mott insulators" have AFM long-range order at low temperature, attributed the MIT to the opening of a gap associated to the formation of magnetic superlattices.

In recent years, a renewed interest has been growing around strongly correlated systems and related models. The driving force for this revival has been the discovery of the High T_c superconductors. These compounds are in fact doped Mott insulators, the stoichiometric compounds being AFM insulators [8]. Many other interesting systems present strong correlation effects and are Mott insulators, or at least close to the Mott transition. Among these we mention the alkali-doped fullerides [9], the colossal magnetoresistance manganites [10], the longstanding V_2O_3 [11], the adlayer structures on semiconductor surfaces, such as SiC(0001) [12] or K/Si(111) : B [13], and layered organic conductors like $\kappa - (\mathrm{BEDT} - \mathrm{TTF})_2\mathrm{X}$ [14].

The renewed interest in strongly correlated systems has evidenced the weaknesses of the "early" approaches to the strongly correlated systems, and in particular to the Mott transition, and has generated the development of powerful new techniques.

The unavoidable problem in dealing with strongly correlated systems is that a highly non-trivial competition rules their physical properties. The effect of kinetic energy, that tends to form delocalized metallic states, contrasts with the correlation effects that result in constraints on the electronic motion. In the metallic, weakly-correlated, side of the transition, the electron is properly described as a propagating wave. Even if the Coulomb interaction is clearly present, the low-energy physics of metals can be described as a renormalized non-interacting system according to Landau's Fermi-liquid theory. The system of interacting particles can be mapped onto a gas of non-interacting quasiparticles, characterized by a long lifetime, and the transport properties are ruled

by the Boltzmann theory. As a result, the Density Functional Theory, even in the Local Density Approximation turns out to be a quantitatively reliable tool for the investigation of metallic systems. On the other hand, in the insulating state, the electron is better described in real space. The electrons are tightly bound to the ions (each ion binds an integer number of electrons), and the transport occurs by carrying an electron from a site to a neighbouring one, giving rise to a charge unbalance. In this limit one can start from the atomic physics, and reintroduce the electronic motion as a perturbation. This approach gives rise to spin Hamiltonians which correctly reproduce the low-energy physics. As a result the spectrum is basically given by the atomic excitation that get broadened by the electron hopping to neighbouring sites, giving rise to incoherent bands, usually referred to as "Hubbard bands". It should be clear from the discussion above that the basic problem of strongly correlated systems, that is definitely relevant to the Mott transition, is the search for a unique framework to describe both limits or to properly handle the intermediate region of parameters, in which both of the limiting schemes outlined do not work well.

As mentioned above, a rich variety of compounds presents strong correlations, and Mott insulating states. In the various compounds the electron-electron correlation is usually accompanied by other physical effects, like lattice effects leading to polaron formation or to the Jahn-Teller effect, orbital and charge ordering, and many others. Nevertheless, the physical mechanism leading to the MIT is expected to be generic and idealized models are expected to give a qualitatively good description of this phenomenon. The Hubbard model, in which tight-binding electrons interact via a local repulsion, is the archetyp model for the Mott transition. When the Mott phenomenon is studied in this model it is usually referred to as the Mott-Hubbard transition. Much effort has been devoted to the understanding of the Mott transition, but only recently many points have been clarified, at least for the single-band Hubbard model. In recent years, the Dynamical Mean Field Theory (DMFT) has been widely used to enlarge our comprehension of the Mott phenomenon. This theory, exact in the limit of infinite dimensions, has provided a unique framework, in which both the metallic and the insulating properties can be handled on the same footing. The development of DMFT has allowed to gain a deep insight on the Mott-Hubbard transition. The transition between a paramagnetic metal and a paramagnetic insulator by increasing the correlation strength has been fully characterized by means of a mapping onto an Anderson impurity model subject to a self-consistency equation [2].

In this thesis, we select some open points regarding the Mott-Hubbard transition. One of the main open questions in our understanding of the Mott transition is the pos-

sibility of a "real" Mott transition, not associated to any symmetry-breakings. Despite the argument by Mott does not rely on the possibility of magnetic ordering, in most theoretical and experimental realization of correlation-induced insulators, one has to deal with AFM ordering or other symmetry-breaking. The AFM long-range order may be viewed as a doubling of the unit-cell in real space, that implies a folding of the Brillouin zone, leading to an effective band insulator. In the single-band Hubbard model on bipartite lattices with nearest-neighbours hopping only, AFM long-range order takes place as soon as a non-zero U is considered, due to the perfect nesting of the Fermi surface, making the scenario of the paramagnetic metal- paramagnetic insulator not appropriate to the groundstate of the model. A possible route to a Mott transition without associated broken magnetic symmetry is frustration of magnetic ordering. In one of the chapters of this thesis we will study the Mott-Hubbard transition in the single-band Hubbard model on the triangular lattice, looking for a possible Mott transition within the paramagnetic sector.

Another, alternative, route to a Mott transition without broken symmetries, is the introduction of orbital degeneracy. This effect leads to a richer physics in the atomic limit with respect to the single-band model. In orbitally degenerate systems, besides the local repulsion U, we must also consider exchange terms between the electrons in different orbitals on the same lattice site, that result in a splitting of the degenerate atomic multiplets according to the Hund's rules. Furthermore, the orbital degeneracy may be partially lifted by the Jahn-Teller effect, i.e. by a coupling of electrons with lattice distortions. As a general result, we expect that, even when the correlation is so strong to completely forbid the motion of electrons from site to site, a non-trivial physics is present, due to the on-site interaction terms. This non-trivial physics must be somehow recovered in the infinite-correlation limit, and may influence both the nature of the Mott insulator, and the mechanism leading to the MIT. We will discuss at length the unusual properties of the tetravalent alkali-metal doped fullerides A_4C_{60}, where A is an alkali-metal atom (K,Rb, Na,Cs). Even if less popular than their superconducting brothers of the family A_3C_{60}, these compounds present interesting properties. The K and Rb doped compounds are in fact narrow-gap insulators at room pressure, and turn metallic by increasing pressure. Moreover, the insulating state is *nonmagnetic*, with a sizeable spin-gap. The transition occurs between a nonmagnetic insulator and a nonmagnetic metal. These systems are insulators, even if the four extra-electrons donated by the alkali-metal atoms partially fill a threefold degenerate p-like t_{1u} band. Band-structure calculations completely fail, providing a metallic groundstate. It is natural to blame correlation for this unpredicted behaviour, but at least two points are non-standard. As

a first point, we have a nonmagnetic groundstate, whereas usually Mott-insulators have magnetic properties. As a second point, the half-filled A_3C_{60} compounds are instead metallic, even if the bandwidth and the correlation strength are almost the same in the two families. A single-band Hubbard model can not account for these properties. The model we propose and carefully study is a threefold degenerate Hubbard model enriched by the multiplet-exchange and the Jahn-Teller interactions. The Jahn-Teller effect has the crucial role to render the atomic limit a singlet both in spin and in orbital space ($S = 0, L = 0$). If we vary the correlation strength we expect the MIT to occur without magnetic ordering. The nonmagnetic insulating state of A_4C_{60} can be understood as a Mott-Jahn-Teller state[15, 16], in which the correlation frustrates the electronic motion, and the Jahn-Teller effect leads to a singlet state. The DMFT of the Mott transition in the threefold degenerate model described above allows to completely characterize the properties of these Mott-Jahn-Teller insulators. The understanding of the mechanism in which the non-trivial molecular physics is recovered in the Mott insulating limit is important both from the theoretical and the experimental side. On one hand, it sheds light on some features of the Mott transition that can be hidden in the single-band model. On the other hand, it allows to fully understand many spectroscopic features of the fullerides.

The model introduced for A_4C_{60} acquires a more general theoretical significance since it represents a simple model in which the Mott transition really occurs within the paramagnetic sector. Even more interestingly, we have a transition from a metal to an insulator with zero entropy (non-degenerate), without any explicit change of symmetry (like e.g. in the first-order MIT between a paramagnetic metal and an AFM insulator). This transition represents a really interesting theoretical problem, in which peculiar features are expected to enlarge our understanding of the Mott transition beyond the single-band model.

In the first chapter we review the most popular methods to deal with the Mott transition and emphasize the successes of the Dynamical Mean Field Theory (DMFT) in characterizing the properties of the Mott insulating state and the evolution of physical quantities across the transition.

In the second chapter we present the DMFT of the Mott transition in the alkali-metal doped fullerides A_4C_{60}, studying the threefold degenerate Hubbard model with multiplet-exchange and Jahn-Teller effect for realistic values of the parameters. We completely characterize the properties of these insulators, showing that only the DMFT can give such a complete description. Spectral quantities for this compound are computed, showing that the molecular spectroscopic features are recovered in the Mott state.

In Chapter 3 we consider the threefold degenerate model introduced in Chapter 2 in more general terms. As a first point we study the dependence of the transition upon filling, a point that can partially help in understanding the different behaviour between the trivalent-superconducting and the tetravalent-insulating fullerides. We also consider the effect of a negative multiplet-exchange interaction, arising from the Jahn-Teller effect, and leading to a non-degenerate atomic limit, like in A_4C_{60}. The MIT for this model is compared with the single-band model, and the qualitative differences are evidenced. In particular, it will be shown that a second order transition between a paramagnetic metal and a non-degenerate insulator is not compatible with a Fermi-liquid regime for the metal.

In Chapter 4 we turn to the Mott-Hubbard transition in the two-dimensional single-band Hubbard model on the triangular lattice. In this case, we cannot resort to DMFT, since we are interested in the effect of the actual topological structure of the lattice which is lost in DMFT. We use therefore the slave boson approach [17] and the exact-diagonalization of small clusters. The study is focused on the presence of incommensurate magnetic ordering and/or nonmagnetic insulating phases.

Chapter 1

The Hubbard model and the Mott transition

The electron-electron (e-e) correlation has been identified as the cause of the insulating behaviour of otherwise metallic systems already in the 50's, but only recently, a comprehensive understanding of the correlation-induced metal-insulator transition (MIT) has been achieved. After Mott's ideas, it turned out that the mechanism leading to this kind of MIT was the competition between the delocalizing effect of the kinetic energy, and the correlation that constraints the electronic motion. This is a really basic mechanism, that can be understood in terms of idealized models. Simplified models of solids are in fact usually introduced to gain insight on general physical effects neglecting many of the complications of real materials. The "Hubbard model", introduced independently by Hubbard[18], Gutzwiller[19] and Kanamori[20] is the simplest lattice model in which the competition between the electronic kinetic energy and the correlation effects can give rise to the MIT. In this model tight-binding electrons, moving on a lattice, interact via a short-range repulsion acting when two electrons of opposite spin sit on the same lattice site. The local repulsion, despite the extreme short-range character, results in a significant frustration of the electronic motion.

The Hamiltonian is

$$\mathcal{H} = -t \sum_{\substack{<ij> \\ \sigma}} \left(c^{\dagger}_{i\sigma} c_{j\sigma} + h.c. \right) - \mu \sum_{i\sigma} c^{\dagger}_{i\sigma} c_{i\sigma} + U \sum_{i} n_{i\uparrow} n_{i\downarrow}, \tag{1.1}$$

where $c^{\dagger}_{i\sigma}$ ($c_{i\sigma}$) are creation (destruction) operators for an electron with spin σ on the site i and $n_{i\sigma} = c^{\dagger}_{i\sigma} c_{i\sigma}$ is the number operator; t is the hopping amplitude, U is the Hubbard on-site repulsion, μ is the chemical potential. The indices i, j label the sites of a given lattice, and the sum in the first term extends over pairs of sites. In the following we will

only consider the sum restricted to nearest-neighbour sites only.

The first term is the kinetic energy for tight-binding electrons, describing the motion (hopping) of the electrons from site to site. The hopping term can be diagonalized in momentum space, where is becomes $\mathcal{H}_t = \sum_{k\sigma} \varepsilon_k c^\dagger_{k\sigma} c_{k\sigma}$, with a dispersion $\varepsilon_k = -2t \sum_d cos(k_d)$, and eigenfunctions given by delocalized plane waves with momenta k. The interaction term is instead diagonal in real space. The two terms do not commute, and this leads unavoidably to a non-trivial competition between them. This competition is the ultimate reason for the non-trivial properties of the model. Varying the parameters, the Hubbard model presents both the insulating and the metallic phases. It is easy to show that, for a number of electrons equal to the number of lattice sites (half-filling), this model undergoes a MIT by increasing the interaction strength U. At $U = 0$, the model describes in fact a free metal with a half-filled band, while for $U \gg t$ the charges get localized due to the large energy cost in creating double occupancies. In the $U = \infty$ limit (atomic limit), double occupancies are strictly forbidden, and all the configurations with one electron per site are degenerate. In this limit the mobility of the electrons is completely suppressed, leading to an insulating system. If the hopping is introduced as a small perturbation ($t \ll U$), we can resort to perturbation theory in t/U. A simple argument helps to understand how magnetic correlations arise in this limit. The leading-order corrections to the atomic limit derive from virtual transitions to states with a single double-occupied site, whose energy is U above the groundstate. Let's consider two neighbouring sites, occupied each by one electron: if their spins are parallel, no virtual transition involving hopping between the two sites is possible, due to Pauli principle. On the other hand, if the spins are opposite, a negative contribution of order t^2/U is obtained. Therefore antiparallel alignment of spins on neighbouring sites is favoured. This simple argument shows that in the strong-coupling limit, the Hubbard model displays antiferromagnetic (AFM) correlations. The AFM correlations in the strong coupling limit arise also in more rigorous treatments. The half-filled Hubbard model maps in fact onto an AFM Heisenberg model with $J = 4t^2/U$ in the $U \gg t$ limit. This can be seen using strong-coupling perturbation theory, projecting out doubly occupied sites [21], or a Schrieffer-Wolff transformation[22]. Both the naive argument and the mapping onto the Heisenberg model do not depend on the lattice and the dimensionality. If the lattice and dimensionality allow for long-range AFM ordering in the Heisenberg model, then the Hubbard model has an AFM strong-coupling groundstate. One can ask himself what is the relationship between the MIT and the onset of antiferromagnetic long-range order. In principle, the transition between a metal and an insulator (Mott transition) and the Néel transition may occur for different coupling val-

ues, and one can define a critical $U = U_c$ for the MIT and a magnetic-ordering coupling $U = U_M$. The values of U_c and U_M are dependent on the dimensionality and the lattice under consideration.

In the Hubbard model on a d-dimensional (hyper)cubic lattice with nearest neighbours hopping only, the groundstate is insulating for arbitrarily small U, and it is always AFM ordered. In the following we will limit to the two-dimensional case. The absence of a finite U_c can be easily understood within Hartree-Fock theory, which gives reliable results for small U values. The stability of the paramagnetic metallic phase with respect to magnetic ordering with wave-vector $\mathbf{q}$ is signaled by a divergent spin susceptibility

$$\chi(\mathbf{q}) = \frac{2\mu_B^2 \Gamma(\mathbf{q})}{1 - U\Gamma(\mathbf{q})}, \tag{1.2}$$

where μ_B is the Bohr magneton, and $\Gamma(\mathbf{q})$ is the Lindhardt bubble

$$\Gamma(\mathbf{q}) = -\frac{1}{N}\sum_k \left[\frac{f(\varepsilon_{\mathbf{k}-\mathbf{q}}) - f(\varepsilon_{\mathbf{k}})}{\varepsilon_{\mathbf{k}-\mathbf{q}} - \varepsilon_{\mathbf{k}}}\right]. \tag{1.3}$$

The instability occurs when the denominator in (1.2) vanishes, that is for $U\Gamma(\mathbf{q}) = 1$ (Stoner criterion). If $\mathbf{q}$ is the classical AFM ordering vector $\mathbf{Q_{AFM}} \equiv (\pi, \pi)$, the sum in Eq.(1.3) is divergent, and the Stoner criterion is satisfied for any non-vanishing U. As it will be discussed in Chapter 4, the divergence is associated with the perfect nesting of the Fermi surface, which is peculiar to the square lattice with nearest-neighbours hopping. A vanishing U makes the system unstable towards antiferromagnetism. Moreover, the model has a long-range ordered state [23] in the $U \gg t$ (Heisenberg) limit. The two-dimensional Hubbard model has therefore AFM long-range order both in weak- and strong-coupling. There is no physical reason why intermediate couplings should present a metallic behaviour. The MIT then occurs at arbitrarily small U, as a transition between the uncorrelated metal for $U = 0$, and an AFM insulator for every non-zero coupling. The absence of a metallic phase for small U is a pathology of the square lattice with nearest-neighbours hopping, and every effect breaking the perfect nesting property is expected to push the transition to finite U. The possibility to have instead a Mott transition with no concurrent symmetry breaking is a much more intriguing and debated issue, that we will address in the following chapters. As we shall see extensively, a possible route towards a transition at finite U/t, and eventually to a Mott transition in which the insulator has no broken symmetry, is frustration. In Chapter 4 we will study the Mott-Hubbard transition on the two-dimensional triangular lattice, in which the AFM order is frustrated and the perfect nesting is no longer present.

These hand-waving arguments are the milestones of the description of the MIT in the Hubbard model, but more detailed calculations are needed to properly characterize this

transition. Despite the apparent simplicity, this model has proved really hard to solve. Exact solutions are available only in one dimension, thanks to the Bethe *ansatz* [24], whereas for higher dimensions approximate techniques or numerical tools are required. In this chapter we briefly review the most common approaches to the Mott transition in the Hubbard model, and finally describe the Dynamical Mean Field Theory[2], which is probably the most reliable instrument for the inspection of the Mott transition.

1.1 Early approaches

As soon as the idea of the correlation-driven MIT was established, and experimental realizations have been discovered, many alternative approaches have been proposed to attack the problem. All the early approaches concentrate on one of the opposite limits we have described in the previous section, and move towards the transition point introducing perturbatively the missing physics. Due to the non-trivial competition between the kinetic and the interaction terms, which gives rise to the transition, all these tools are bound to fail when used too far away from their starting point. The insight provided by these methods is anyway valuable, and it has contributed to characterize the limiting phases, opening the way to more sophisticated methods able to treat the different physical regimes on the same footing.

The early work by Hubbard [18] is pretty close to Mott's original point of view. The main idea is to provide an effective band picture for the Mott transition. Hubbard characterizes the insulator with a density of states (DOS) made by two bands centred at $\pm U/2$ of width $W = 2dt$, associated respectively to holes (lower band) and doubly occupied sites (upper band). The gap between the bands is of the order $U - W$. Decreasing U the gap shrinks, up to a critical value $U \simeq W$ for which the gap closes. The MIT is associated with the closure of the Hubbard gap, when the two bands merge giving rise to a metal. This description starts from the insulating side of the transition, with a the atomic DOS, made by two δ-functions at $\pm U/2$, broadened by the hopping. The opening of the Hubbard gap is not associated with antiferromagnetic ordering and the corresponding folding of the bands.

On the opposite side, Brinkman and Rice [25], following the Gutzwiller technique[19], start from the metallic phase, which is characterized as a renormalized Fermi liquid. In their approach the MIT is associated with a diverging effective mass for the carriers $m^*/m \propto (U - U_{BR})^{-1}$. The MIT occurs as a disappearance of the metallic phase, but no description of the insulating state is given.

Finally, in the Slater picture [7], the driving force to the MIT is long-range antiferro-

magnetic ordering, that gives rise to an effective doubling of the unit cell. The Brillouin zone becomes half of the original one, and the folding of the band gives rise to a band insulator.

In the following sections we briefly give more detailed account for the Hubbard and the Brinkman-Rice approaches and to the more refined techniques that originate from these pioneering works.

1.1.1 The Hubbard approach

The Hubbard approach relies on an approximation scheme on the equations of motion for the Green's functions. For generic interacting systems, the equations of motion form an infinite hierarchy of coupled equations. The system is unsolvable unless one resorts to some approximation scheme. Hubbard's starting point is the (insulating) atomic limit $t = 0$. Close to this limit, it is likely that vertices involving a high number of sites can be neglected. This leads to a closed set of equation. In his first work on the subject[18], Hubbard obtains an insulating paramagnetic solution for every value of U, while in a successive refinement[26], a closed form for the single-particle Green's function is obtained, for a half-filled semicircular band under the hypothesis of a paramagnetic solution. Within this approximate scheme, Hubbard analytically describes the evolution of the density of states by decreasing U. The two separated bands of width W centred at distances $\pm U/2$ form the Fermi level (Hubbard bands) get closer and closer and finally merge in a unique metallic band. Despite being the first successful attempt to describe the correlation-driven MIT, the Hubbard's solution still presents a relevant drawback, since it is not able to describe the metallic phase as a Fermi liquid. The low-energy excitation in the Hubbard's solution have indeed finite lifetime. This approach does not forget the starting point in the atomic limit and it is not able to properly reconstruct the metallic behaviour. In summary, the Hubbard approach describes the MIT as the opening of a gap in the single-particle spectrum. The opening of the gap signals the MIT between a "non-Fermi-liquid" metal and an insulator.

1.1.2 The Brinkman-Rice approach

The Gutzwiller approximation[19], applied to the problem of the MIT by Brinkman and Rice[25], is a variational approach, based on a *metallic* wavefunction in which correlation is taken into account by means of a projector. The variational wave function is

chosen as

$$|\psi_{BR}\rangle = \prod_i (1 - g n_{i\uparrow} n_{i\downarrow})|FS\rangle, \tag{1.4}$$

where $|FS\rangle$ is the Fermi sea, and g is a variational parameter that controls the number of doubly occupied sites; $g = 0$ describes the uncorrelated metal ($U = 0$), and $g = 1$ describes a state in which doubly occupied sites are completely forbidden, as it happens for $U \to \infty$. The groundstate energy can be obtained by minimizing the quantity

$$E_{BR} = \frac{\langle \psi_{BR}|H|\psi_{BR}\rangle}{\langle \psi_{BR}|\psi_{BR}\rangle} \tag{1.5}$$

as a function of g. If we use the number of doubly occupied sites $D = 1/N\langle \sum_i n_{i\uparrow} n_{i\downarrow}\rangle$ as a parameter, then the expectation value of the interaction term is obviously given by DU. To obtain analytical estimates of the kinetic energy, Gutzwiller has introduced a non-perturbative approximation scheme, in which spatial correlation between spin on different sites are neglected[19]. Using this approximation and restricting to the paramagnetic phase ($\langle n_\uparrow \rangle = \langle n_\downarrow \rangle$), Brinkman and Rice[25] obtain that the number of doubly occupied sites vanishes for a critical value $U = U_{BR}$, giving rise to an insulating phase with exactly one electron per site. In the Brinkman-Rice approach, the metal is a Fermi-liquid up to the transition, and the effective mass diverges at the transition $m^*/m \propto (U - U_{BR})^{-1}$. The transition is therefore associated with the disappearance of the metallic phase associated with a diverging effective mass and a vanishing spectral weight for the quasiparticles at the Fermi-level. This result suffers from the intrinsic limitations of a variational approach; the choice of the wavefunction is a strong constraint to the solutions. A metallic wavefunction can not access the insulating state, and improvement can only be achieved changing the variational wavefunction to allow for different physics. The Brinkman-Rice approach is clearly complementary to the Hubbard's picture. While the Hubbard approach properly describes the high-energy Hubbard bands and the insulating phase, the Brinkman-Rice results correctly describe the coherent low-energy physics in the metallic phase. A coherent framework able to capture both the features is therefore needed to properly analyze the Mott transition in the Hubbard model.

1.1.3 The Slave Boson approach

The slave bosons technique [17] may be used to implement an accurate mean-field approach for quantum systems. In this section we only briefly sketch the basic ideas of the slave boson technique, that we will describe in detail in section 4.2. In the Kotliar-Ruckenstein slave boson approach four auxiliary bosonic operators are introduced on

each site labeling empty, doubly occupied and singly occupied sites[27]. Renormalized fermionic operators substitute the original ones. The Hamiltonian is quadratic in the new fermions, that can be integrated out. We are left with a bosonic Hamiltonian. The saddle-point mean-field approximation on this Hamiltonian gives the same results of the Gutzwiller approximation. The SB technique represents therefore a systematic way to improve the Gutzwiller approximation results leading to the Brinkman-Rice scenario, allowing fluctuations of the bosonic fields around their mean-field values. Unfortunately, to take into account fluctuations in the SB approach proves really hard from a technical point of view, and no further insight on the Mott transition has been achieved along this path. It has been shown, anyway, that fluctuations around the saddle-point reconstruct the lower and the upper Hubbard bands, and that the disappearance of the resonance coincides with the closure of the gap [28, 29].

1.2 The Dynamical Mean Field Theory

In recent years, the Dynamical Mean Field Theory (DMFT) of strongly correlated electron systems has acquired a key role as a tool able to attack the problem of strong correlation without the need to move perturbatively from a well-defined physical regime. This property is of particular value for the study of the Mott transition, because it allows to treat on the same footing both the Fermi-liquid properties and the incoherent Hubbard bands. The DMFT becomes exact in the limit of infinite correlation on various lattices. Historically, it has been mainly developed as a $d \to \infty$ limit of a finite-dimensional theory [30], even though nowadays it is better viewed as a quantum dynamical counterpart of the mean-field approaches[2].

The basic idea is to map the *lattice* Hamiltonian onto a *single-site effective theory* in order to significantly reduce the number of relevant degrees of freedom. In the classical mean-field theory a lattice Hamiltonian is mapped onto a single-site Hamiltonian. For sake of concreteness, we consider the Ising model

$$\mathcal{H} = -\sum_{\langle i,j \rangle} J S_i S_j - h \sum_i S_i. \tag{1.6}$$

The mean-field approach assumes that the physics is the same on each site; we arbitrarily take "site 0" as of all the others. The site Hamiltonian is

$$\mathcal{H}_{eff} = -h_{eff} S_0, \tag{1.7}$$

where h_{eff} is an effective magnetic field, that keeps into account the effect of neighbouring sites on the "chosen" one. It is given by $h_{eff} = h + zJm$, where z is the

lattice coordination number, and $m = \langle S_i \rangle$ is the magnetization (site-independent). h_{eff} is therefore expressed in terms of a quantity (m) that can be in turn calculated from the effective Hamiltonian (1.7). Since $m = \tanh(\beta h_{eff})$, we arrive to the well-known Curie-Weiss *self-consistency* equation.

$$m = \tanh \beta(h + zJm). \tag{1.8}$$

The Dynamical Mean-Field Theory can be seen as the extension to a quantum interacting system of this approach. In this case we will consider the single-band Hubbard model (1.1). We associate to the lattice model an effective single-site dynamics, described by an imaginary-time action for the fermionic degrees of freedom on the "site 0":

$$S_{eff} = -\int_0^\beta d\tau \int_0^\beta d\tau' \sum_\sigma c^\dagger_{0\sigma}(\tau) G_0(\tau - \tau')^{-1} c_{0\sigma}(\tau') + U \int_0^\beta d\tau n_{0\uparrow}(\tau) n_{0\downarrow}(\tau). \tag{1.9}$$

$G_0(\tau - \tau')^{-1}$ plays exactly the same role of the effective magnetic field in Eq.(1.7), and may be called a "Dynamical Weiss field". It is the probability amplitude for a fermion to be created on site 0 at time τ and destroyed at time τ'. The time dependence of the "Weiss field" is the main difference with respect to the classical case, and it the origin of the adjective "dynamical". The full local quantum dynamics is retained, while the spatial fluctuations are frozen. The analogy with the classical case should help to avoid misinterpretation of G_0. This quantity must not be viewed as a bare Green's function for the original lattice model, but as an effective field that rules the local quantum fluctuations in our local theory. In close analogy with the classical case, the mean-field theory must be supplemented with a self-consistency equation, that relates G_0 to quantities computable from the effective action S_{eff}. A few alternative derivations of the self-consistency equation can be find in Ref. [2]. Here we only report the result

$$G_0(i\omega_n)^{-1} = i\omega_n + \mu + G(i\omega_n)^{-1} - R[G(i\omega_n)]. \tag{1.10}$$

The local Green's function $G(i\omega_n)$ plays the role of the magnetization in the Ising model. It can be computed from the effective action as

$$G(\tau) \equiv -\langle T c(\tau) c^\dagger(0) \rangle_{S_{eff}}. \tag{1.11}$$

$R(G)$ is defined as the inverse function of the Hilbert transform of the density of states for non-interacting electrons on the lattice under consideration. For specific lattices, Eq. (1.10) takes more friendly forms. For the infinite-coordination Bethe lattice with nearest-neighbours hopping the DOS is semicircular [31]

$$D(\varepsilon) = \frac{2}{\pi t^2}\sqrt{t^2 - \varepsilon^2} \tag{1.12}$$

and the self-consistency equation reads

$$G_0(i\omega_n)^{-1} = i\omega_n + \mu - \frac{t^2}{4}G(i\omega_n). \tag{1.13}$$

Note that the original lattice enters the DMFT equations only through the bare DOS in Eq. (1.10). Since the single-site theory can not be critical, criticality can be introduced in the context of DMFT only through the self-consistency. The Eq. (1.9) and (1.10) form a closed set of mean-field equations. Once they are solved, we can also access to non-local quantities. The lattice Green's function in momentum space is given by

$$G(k, i\omega_n) = \frac{1}{i\omega_n + \mu - \varepsilon_k - \Sigma(i\omega_n)}. \tag{1.14}$$

The self-energy can be computed from the solution of the effective single-site problem and it is given by

$$\Sigma(i\omega_n) = G_0(i\omega_n)^{-1} - G(i\omega_n)^{-1}, \tag{1.15}$$

It is easy to see that the locality of the self-energy $\Sigma(i\omega_n)$, i.e. the independence on k, is a direct consequence of the DMFT approximation. It is also easy to check that the local component of the Green's function $G(i\omega_n) = \sum_k G(k, i\omega_n)$ coincides with the local Green's function computed from the effective action.

1.2.1 The Local Impurity Self-Consistent Approximation (LISA)

Despite the strong simplification of the original lattice problem introduced by the DMFT approximation, the solution of the effective action S_{eff} is still a non-trivial many-body problem. As a matter of fact, due to the dynamical nature of our mean-field approach, no *local* Hamiltonian formulation can be cast. The quantum fluctuations of the effective Weiss field $G_0(i\omega_n)^{-1}$ substantially describe the transitions between "site 0" and the rest of the system which is interpreted as an external bath. If we want to describe within the Hamiltonian formalism the transitions among the various quantum states on "site 0", we have to re-introduce the bath degrees of freedom as a conduction band hybridized with the site.

A possible Hamiltonian corresponding to the action (1.9) is

$$\mathcal{H}_{AM} = \sum_{k\sigma} \tilde{\varepsilon}_k a^\dagger_{k\sigma} a_{k\sigma} + \sum_{k\sigma} V_k (a^\dagger_{k\sigma} c_{0\sigma} + c^\dagger_{0\sigma} a_{k\sigma}) - \mu \sum_{\sigma} c^\dagger_{0\sigma} c_{0\sigma} + U n_{0\uparrow} n_{0\downarrow}. \tag{1.16}$$

The subscript AM stays for Anderson Model. We have in fact constructed an effective Anderson impurity model, in which the $c_{0\sigma}$ is the destruction operator for the

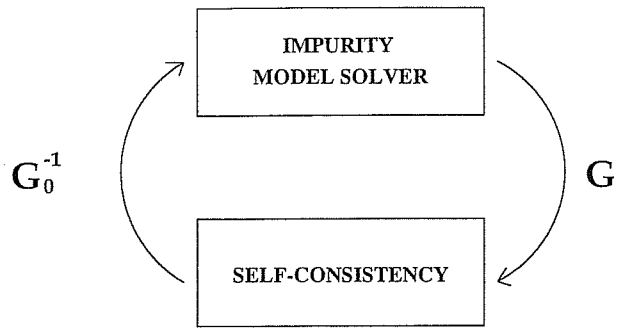

Figure 1.1: Schematic flow-chart of every method of solution of the DMFT equations. The impurity problem solver may be an exact numerical method, like ED or QMC, or some approximate analytical tool, like IPT. The self-consistency generates a new impurity model via a new value of G_0^{-1}.

impurity site, and $a_{k\sigma}$ are destruction operators for the conduction bath. Since the Hamiltonian is quadratic in the bath operators, the latter can be integrated out, giving rise to the action (1.9) if $G_0(i\omega_n)^{-1}$ is related to the Anderson model parameters by the relation

$$G_0(i\omega_n)^{-1} = i\omega_n + \mu - \sum_k \frac{V_k^2}{i\omega_n - \tilde{\varepsilon}_k}. \tag{1.17}$$

The choice of (1.16) as the Hamiltonian translation of (1.9) is not unique, but it is the most popular one. In really general terms, the DMFT approach can be viewed as the solution of an impurity model subject to a self-consistency equation, hence the name Local Impurity Self-consistent Approximation (LISA). The basic step of the DMFT algorithm is therefore an "impurity solver", i.e. a technique that allows to compute the local Green's function for the Anderson impurity model (1.16). Many tools have been used to this aim, ranging from approximate analytical methods like the Iterated Perturbation Theory (IPT)[32], to numerical techniques, like the Quantum Monte Carlo (QMC)[33] and the Exact Diagonalization (ED)[34] methods. We will describe advantages and disadvantages of the various approaches in the next section.

In really general terms, we can draw a flow chart for a DMFT calculation made by two simple steps:

1. Start from a given $G_0(i\omega_n)^{-1}$. Solve the associated Hamiltonian (1.16) with the chosen solver, computing $G(i\omega_n)$.

2. Compute new $G_0^{new}(i\omega_n)^{-1}$ from Eq. (1.10). Repeat step 1 until convergence.

A sketch of the procedure is shown in Fig. 1.1.

1.3 Solutions of DMFT equations

Despite the enormous simplification introduced by the LISA approach, the solution of the impurity model (1.16) is still a difficult task. No analytical solution is known, and approximate or numerical solutions are needed. Among the analytical techniques, the iterated perturbation theory (IPT) deserves a special place[32]. This method is exact both at weak- and strong-coupling, and represents a useful interpolation scheme. Comparison with numerical techniques has confirmed the reliability of this technique over a wide range of couplings, with the exception of the proximity of the critical coupling U_{c2} (see section 1.4). The two most powerful numerical strategies applied to the DMFT method are the Quantum Monte Carlo (QMC) and the Exact Diagonalization (ED). Both the techniques have no bias or systematic error, and may be considered exact within numerical accuracy. The only approximation is the discretization of the equations. Extrapolation to vanishing discretization limit gives the exact result in both cases.

More specifically, the QMC approach, based on the Hirsch-Fye algorithm [33], solves the impurity model in discretized imaginary time. The conduction bath described by $G_0(i\omega_n)^{-1}$ is instead not discretized. The ED method, introduced by Caffarel and Krauth [34], involves instead a discretization of the conduction bath, which is approximated by only a small number of orbitals. The number of orbitals is severely limited by the exponential growth of the Hilbert space size with the number of orbitals. The impact of the limitation is strongly reduced by the freedom of choice of the parameters of the impurity Hamiltonian at every iteration, and we believe that the advantages of ED are more relevant than the disadvantages.

1.3.1 The Hirsch-Fye QMC algorithm

The Hirsch-Fye algorithm [33] is the most successful QMC method for a general impurity model. It is suited for the calculation of the local Green's function at finite temperature, exactly the quantity needed by the DMFT equations. The effective action (1.9) is discretized in imaginary time:

$$S_{eff} \simeq \sum_{\tau\tau'\sigma} c^{\dagger}_{0\sigma}(\tau) G_0(\tau,\tau')^{-1} c_{0\sigma}(\tau') + U \sum_{\tau} n_{0\uparrow}(\tau) n_{0\downarrow}(\tau). \tag{1.18}$$

With $\tau = 1, 2, ...L$, and the imaginary time interval β is cut in L slices of width $\Delta\tau$, with $\beta = L\Delta\tau$. The interaction term is decoupled by means of a discrete Hubbard-Stratonovich transformation that allows to replace a quartic interaction term with a quadratic term for auxiliary Ising variables.

It can be shown that the algorithm does not suffer from the well-known nemesis of QMC calculation for fermionic systems, the so-called "sign problem". Therefore, the method is numerically stable at arbitrarily low temperatures, regardless of the interaction strength. Nevertheless, there are still at least two remaining limitations:

1. The algorithm involves multiplication of large matrices ($Ln_s \times Ln_s$), whose dimension increases linearly with the number of time slices. As a result, one can handle only a limited number of slices. On the other hand, if the system is strongly correlated, a small value of $\Delta\tau$ is needed to obtained reliable results (see Ref. [35]). Being $\beta = L\Delta\tau$, large β values are hard to study, since it is not possible to arbitrarily increase L to compensate the small value of $\Delta\tau$. As a matter of fact, the highest accessible values of β can not exceed 100 (in units of the half-bandwidth).

2. Only imaginary-time (and Matsubara frequency) quantities are computable, and real-time and frequency calculation involve analytic continuations, that are not usually completely reliable.

1.3.2 The Exact Diagonalization

In the ED approach to the DMFT equations, the Anderson impurity Hamiltonian is first of all discretized, and then exactly diagonalized and the local Green's function is computed by means of the Lanczos algorithm (at zero temperature) or by full diagonalization (at finite temperature). Since ED algorithms strongly suffer from the exponential growth of the Hilbert space, the sum over k in Eq. (1.16) is truncated to a finite small number of orbitals ($n_s \sim$ 5–12). Let us stress that the truncation does not mean that we are considering a finite small number of sites, since the DMFT equations are defined in the thermodynamic limit. The real approximation is to take

$$G_0^{n_s}(i\omega_n)^{-1} = i\omega_n + \mu - \sum_{k=2}^{n_s} \frac{V_k^2}{i\omega_n - \tilde{\varepsilon}_k}. \tag{1.19}$$

We can think about this truncation as a *projection* over a reduced subspace of functions. The algorithm can be divided in three steps:

1. The Weiss field is discretized according to Eq. (1.19). This step can be seen as the projection of G_0 onto $G_0^{n_s}$.

2. $\mathcal{H}_{AM}$ is exactly solved for parameters corresponding to $G_0^{n_s}$, and the local Green's function G is computed.

3. Using the self-consistency equation (1.10), G is used to compute a new G_0'. Step 1 is repeated until convergence is achieved.

The ED algorithm can be used at finite temperature, when the full spectrum must be used to compute the Green's function, and at zero temperature, when, by means of the standard Lanczos algorithm, the Green's function is computable as a continued fraction if the groundstate vector is known[36]. Since the finite temperature calculation requires the full diagonalization of the Hamiltonian, it is severely limited ($n_s \leq 6$ for the single-band Hubbard model). The $T = 0$ algorithm instead, being based on the much more powerful Lanczos technique, allows to go to larger n_s values, up to $12 - 13$ or even more. The great advantage of this technique is the possibility to use an adaptive grid. At each iteration the parameters describing the Anderson model are modified in order to better approximate with a finite number of orbitals the hybridization function coming from the self-consistency equation. Another advantage is that real-time and real-frequency quantities can be directly evaluated without the need of tricky analytical continuations like in QMC. Furthermore, these method turns to be rather insensitive to the different regimes. The accuracy is almost the same in the insulating and the metallic phase at fixed number of orbitals. Therefore even a really small number of orbitals gives a good estimate of U_c. On the other hand, it has been shown that the QMC technique needs a really small $\Delta\tau$ to obtain converged solutions close to the transition and in the insulating phase[35]. This difficulty in convergence has sometimes lead different authors to opposite conclusions even about the nature of the transition [35].

1.4 The Mott-Hubbard transition

In the recent years, a coherent picture of the Mott-Hubbard transition for the half-filled single-band Hubbard model has emerged from the DMFT. Within this framework we can describe both the insulating and the metallic phases with no bias in favour of one or the other. In some sense, this approach retains many feature of the scenarios introduced by Hubbard and by Brinkman and Rice, merging them in a unified picture. In the following sections we briefly present the characterization of the metallic and the insulating phases in the standard analysis of the DMFT results, and then the scenario for the MIT.

1.4.1 The metallic phase

If we assume that the metallic phase is a Fermi liquid, the zero-frequency limit of the self-energy $\Sigma(i0^+)$ must be real. Then, particle-hole symmetry implies that $\Sigma(i0^+) =$

$U/2$. Plugging this constraint into Eq. (1.10), we obtain $G(i0^+) = 2i/D$ regardless of U. The local Green's function determines then the zero frequency value of the Weiss field $G_0(i0^+)^{-1} = -D^2/4G(i0^+)$. This quantity is the hybridization function for the effective Anderson model. The LISA brings us to a mapping onto an Anderson model with a non-vanishing hybridazation at zero frequency. This model is known to display different metallic regimes[37]. It is usually believed that the metallic state in the Hubbard model at half-filling is associated with a Kondo resonance at the Fermi level leading to the formation of the quasiparticles. The low-frequency behaviour of the self-energy computed with IPT is that of a Fermi liquid:

$$\begin{aligned} \mathcal{R}e\Sigma(\omega + i0^+) &= \frac{U}{2} + \left(1 - \frac{1}{Z}\right)\omega + O(\omega^2) \\ \mathcal{I}m\Sigma(\omega + i0^+) &= -B\omega^2 + O(\omega^3) \end{aligned} \tag{1.20}$$

The quasiparticle residue Z is the only control parameter for the Fermi liquid phase, setting the effective width of the coherent peak at the Fermi level ($D^* = DZ$), and the effective mass ($m/m^* = Z$). Z decreases if U increases, leading to a shrinking of the width of quasiparticle peak and to a divergence of the effective mass. The disappearance of the metallic phase is associated, as in the Brinkman-Rice picture, to the vanishing of the quasiparticle weight at the Fermi level. Note that the Luttinger theorem for a k-independent self-energy leads to a pinning of the density of states to its non-interacting value[38]. Hence, increasing U does not change the peak height, but only decreases the width. A solution of the DMFT equations moving from the metallic phase is expected to present a critical value for $U = U_{c2}$ [1] in which the metallic solutions is destroyed as a consequence of an infinite effective mass.

1.4.2 The insulating phase

For large U the correct starting point is the atomic limit, in which the Green's function is given by

$$G(i\omega_n) = \frac{1}{2}\left(\frac{1}{i\omega_n + U/2} + \frac{1}{i\omega_n - U/2}\right). \tag{1.21}$$

Since $G(i0^+) = -4/D^2 G_0(i0^+)^{-1}$, in this limit the effective Anderson model as a zero hybridization at zero energy, so we have an impurity embedded in an insulator. If we

[1] The following discussions will clarify the reason for the subscript 2

move form the atomic limit we can use the *ansatz* [39]

$$G(i\omega_n) = \frac{1}{2}\left(\frac{1}{G_0(i\omega_n)^{-1} + U/2} + \frac{1}{G_0(i\omega_n)^{-1} - U/2}\right), \tag{1.22}$$

that can be understood as a superposition of magnetic Hartree-Fock or as a resummation of a t/U expansion. This kind of solution is very close to the spirit of the Hubbard approach [26]. With this choice we have $G(i\omega_n) \sim i\omega_n$, which leads to $G_0(i\omega_n)^{-1} \sim i\omega_n$. The effective bath is therefore gapped at the Fermi level. It is known that no special effect (Kondo effect or mixed-valence phase) occurs for an impurity in an insulator. The intrinsic weakness of this limiting solution is the inability to catch the appearance of the resonance at the Fermi level that generates the metallic phase. It is evident that the atomic solution (1.21) has a gap $\Delta = U$. For finite t and decreasing U the gap tends to close. The solution disappears as Δ vanishes. We label U_{c1} the critical value for the existence of the insulating (gapped) solution.

We have shown that DMFT can describe a metallic (Fermi-liquid) and an insulating solution. The zero-frequency density of states plays the role of an order parameter for the transition between one phase and the other.

1.4.3 The Metal-Insulator transition

The metal-insulator transition is well defined only at $T = 0$, where a qualitative distinction between a metal and an insulator is possible. At finite temperature there is no clear-cut transition, but the existence of two families of solutions that can be continuously connected to the $T = 0$ solutions allows us to draw an unambiguous phase diagram.

The characterization of the Mott-Hubbard transition both at zero and at finite temperature has been carried out in the recent years by means of the joint use of the analytical IPT approach, and the numerical techniques. The IPT approach has proven quantitatively accurate for almost any value of the coupling except really close to U_{c2}.

We previously stated that there are two critical values of the interaction U_{c1} and U_{c2}, associated respectively with the vanishing of the insulating and the metallic phases. It turns out both from IPT and from numerical results that $U_{c1} < U_{c2}$. Moreover, we can show that the actual MIT occurs at $U_c = U_{c2}$[40]. The derivative of the energy with respect to U is given by the expectation value of the double occupation

$$\frac{dE}{dU} = \langle n_\uparrow n_\downarrow \rangle. \tag{1.23}$$

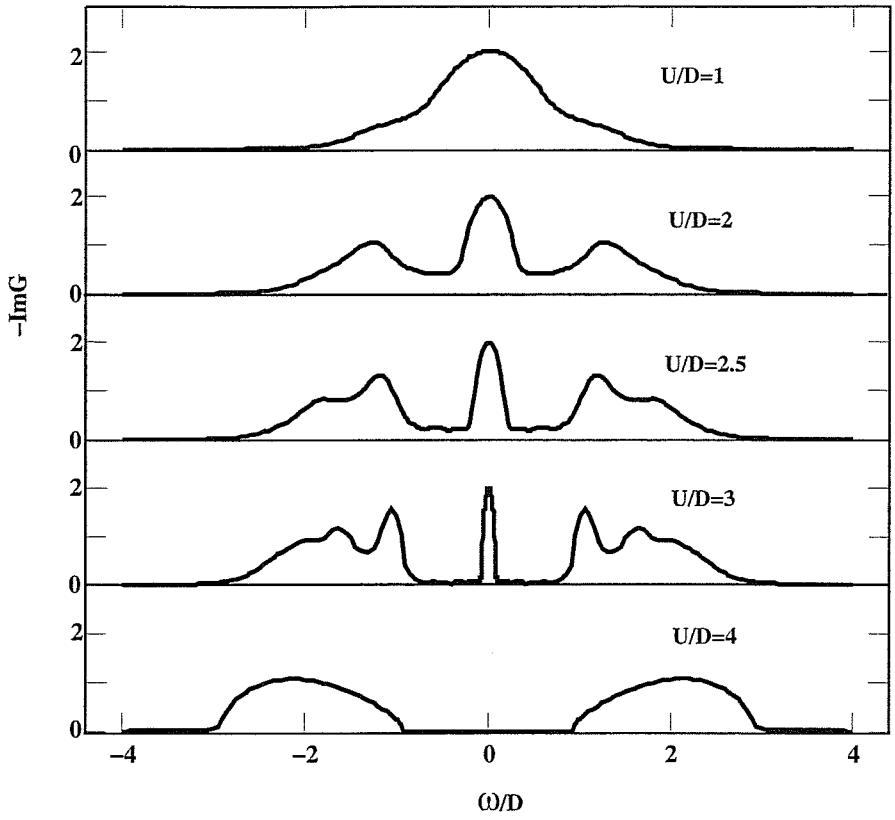

Figure 1.2: The evolution of the spectral density $\pi D\rho(\omega)$ for the half-filled single-band Hubbard model as obtained with IPT (from Ref. [2]). From top to bottom are shown $U/D = 1, 2, 2.5, 3$ (metallic) and i$U/D = 4$ (insulator).

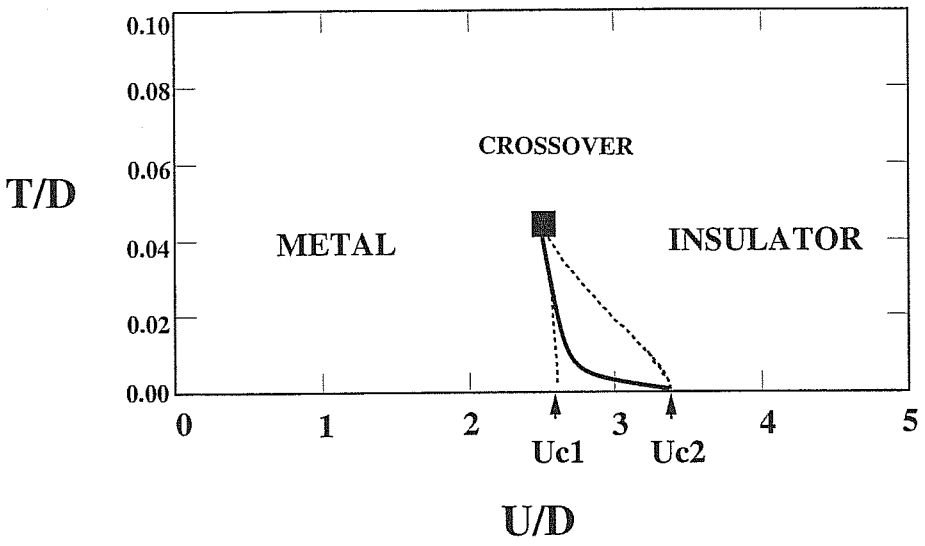

Figure 1.3: Phase diagram of the half-filled single-band Hubbard model within IPT in the paramagnetic sector. The dashed lines are the critical temperatures $U_{c1}(T)$ and $U_{c2}(T)$ (see text), and delimit the coexistence region, the solid line is the actual first-order MIT line $U_c(T)$. Both the ends of the line are second-order points.

Numerical studies confirm the expectation that $\langle n_\uparrow n_\downarrow \rangle$ is larger in the metallic phase than in the insulating one. Hence, integrating (1.23) from an arbitrary U up to U_{c2} where the two solutions merge, one obtains that the energy of the insulating solution is always higher than the energy of the metal for every value of U in which they coexist. Möller at al.[40] have also shown that the transition is of second order. In Fig. 1.2 we report the evolution of the spectral density $\rho(\omega) = -1/\pi \mathcal{I}mG(\omega)$ obtained by IPT. The disappearance of the metallic solution at U_{c2} coincides with the MIT. The resonance at the Fermi level appears in the middle of a preformed insulating gap, since $U_{c2} > U_{c1}$. Note also that the peak gets thinner and thinner increasing U but its height is pinned to the non-interacting value[38]. For intermediate metallic couplings the spectral density contains both the quasiparticle features (coherent peak at the Fermi level), and the atomic features (Hubbard bands). The transition is associated to a dramatic transfer of spectral weight from the low-energy sector to the high-energy bands, leading to the divergence of the effective mass.

Continuously increasing the temperature, we can follow the $T = 0$ solutions, defining $U_{c1}(T)$ and $U_{c2}(T)$. $U_{c1}(T) < U_{c2}(T)$ for every T value. The phase diagram in the $T - U$ space can be drawn comparing the free energies for the two solutions. The

result of IPT is shown in Fig. 1.3. The dotted lines are $U_{c1}(T)$ and $U_{c2}(T)$ and delimit the coexistence region. The solid line is a line of first-order metal-insulator transitions. It departs from the $T = 0$ second order transition on one side, and on the other side it ends in a second-order critical point. For higher temperature no transition occurs and a smooth crossover connects the phases. In this regime the tunnelling between the incoherent bands is allowed by thermal excitations. Even if $U_c(T = 0) = U_{c2}(T = 0)$, for finite temperatures U_c is close to $U_{c1}(T)$, and the curvature is such that increasing temperature the metal turns into the insulator. This apparently surprising result is easily understood recognizing that the paramagnetic insulator has a larger entropy than the metal ($N \log 2$). This is a general feature of strongly correlated materials that can be found, for example, in the phase diagram of V_2O_3.

Chapter 2

The Alkali-metal doped Fullerides A_4C_{60}

2.1 The fullerides

After the discovery of the fullerenes (C_{60}, C_{70}, ...) [41] much interest has been devoted to these large and highly symmetrical molecules. It is hard to believe that at least a part of the interest attracted by the C_{60} molecule is not due to its appealing shape. Besides being the most symmetric existing molecule (The icosahedral point group of the C_{60} molecule is in fact the largest symmetry group of the known molecules), the C_{60} molecule has a special place among the fullerenes, since it can be produced in large quantities [42], giving rise to solid structures that can be object of many experiments. The 60 carbon atoms are all equivalent and lie on the corners of a soccer ball, forming 12 pentagons and 20 hexagons. Obviously, the interest in this system is not only due to aesthtetical reasons, but mainly to its interesting physical properties. Some of the alkali metal-doped fullerides are indeed superconducting with relatively high critical temperatures (T_c) that are lower only to the ones of the cuprates. As well as the cuprates or the manganites, these compounds represent a new class of conductors, and present interesting and peculiar properties that forced the scientific community to reconsider many milestones of solid state physics, like the Migdal-Eliashberg theory of electron-phonon (e-ph) interaction or the Hubbard picture of the metal-insulator transition (MIT) driven by correlation.

The fullerene molecules form solids of relatively weakly bound molecules. The shortest separation between two carbon atoms on different molecules is about 3.1Å, while the shortest separation between atoms within the same molecule is 1.4Å. The dif-

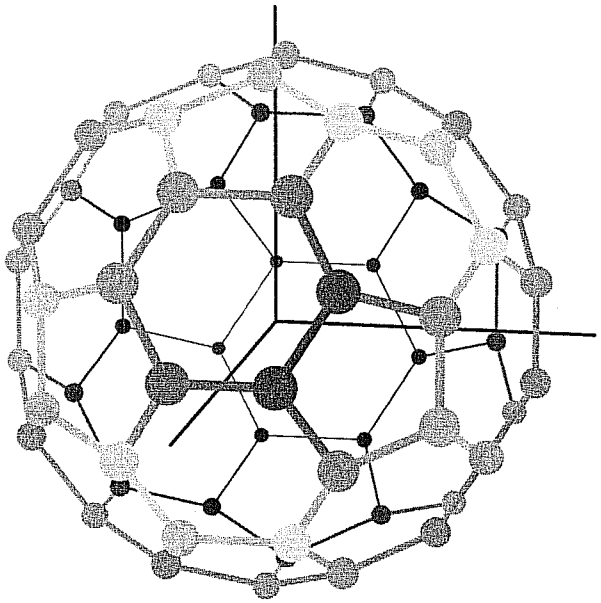

Figure 2.1: The C_{60} molecule

ferent molecules preserve therefore their identity in forming the solid, and the fullerites represent therefore molecular solids. Some fingerprints of the molecular properties are expected to be recognizable in the solids as well.

The discrete levels of the C_{60} molecule are only weakly broadened by the hopping between adjacent balls, leading to a set of non-overlapping bands strongly reminiscent of the molecular levels. The relevant levels (close to the Fermi level for the undoped molecule) have bandwidth of the order $\sim$ 0.5 eV. For the undoped C_{60} solid, the h_u level (highest occupied molecular orbital, HOMO) is completely filled, and the threefold degenerate t_{1u} band (lowest unoccupied molecular orbital, LUMO) is empty. The system is therefore a band insulator. When the system is doped by alkali-metal atoms, basically no hybridization occurs between the alkali bands and the ones of the C_{60}, so that each alkali atom basically donates one electron to the t_{1u} band.

In Fig.2.2 the band-structure for solid C_{60} is shown (from Ref. [43]). The chemical potential (zero energy) is chosen for the undoped system, so the h_u band lies just below it and the t_{1u} band is the first one above it, separated by a gap of more than 1 eV.

The t_{1u} levels are the counterparts of the p levels within the icosahedral point group, so the manifold is triply degenerate, and it can host up to six electrons. In principle all A_nC_{60} compounds with $0 < n < 6$ should then be metals with a partially filled band. The half-filled compounds ($n = 3$) are indeed metallic[44], and turn superconducting with a relatively high T_c that can reach 40 K (in Cs_3C_{60} under pressure[45]), but A_4C_{60}

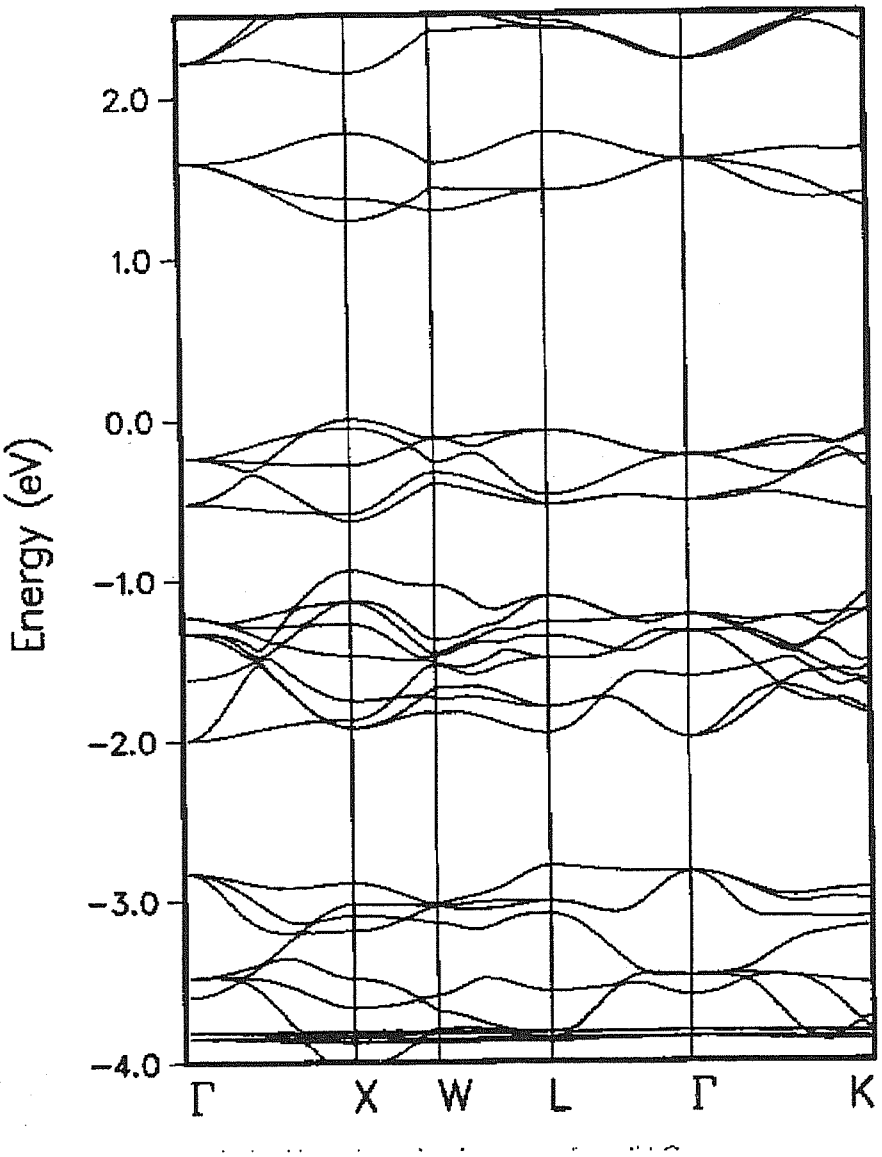

Figure 2.2: The band-structure for solid C_{60}. (from Ref.[43])

are insulators, with the exception of Na_4C_{60} [46, 47, 48]. This chapter is entirely devoted to the understanding of the anomalous properties of these insulators.

Not only the rough argument given above, but also accurate band-structure calculations predict that all these systems should be metallic[43]. As we will discuss in the following, the failure of band-structure calculations is a clear signature of the role of electron-electron (e-e) correlations. The effective Coulomb interaction between two electrons on a C_{60} molecule is about 1–1.5 eV [49, 50], significantly larger than the bandwidths, which are of the order of 0.5 eV. These systems are therefore highly correlated compounds. We emphasize that the effects of strong correlation effects in orbitally degenerate systems give rise to interesting physics that can not be described using single band models. The presence of orbital degeneracy has a quantitative effect on the critical coupling for an insulating state in the Hubbard model [51, 52, 53], and prompts for the inclusion of multiplet exchange correlations giving rise to the Hund's rules.

The C_{60} molecule has also molecular vibrations (phonons) with characteristic vibration energies up to 0.2 eV, therefore comparable to the electronic energy scales.. In particular, the eight fivefold degenerate H_g modes are Jahn-Teller (JT) active, i.e., they are coupled to the electronic degrees of freedom, partially lifting the degeneracy of the t_{1u} levels. The interaction strength is quite large, the typical electron-phonon (e-ph) interaction energy E_{JT} being several tenths of an eV, and the coupling λ of order 1. This e-ph interaction has quite non-standard features, since the ratio between the typical phononic scales $\omega_{ph} \simeq 0.2$ eV, and the bandwidth $W \simeq 0.5$ eV is not negligible, making the ordinary Migdal-Eliashberg theory not justified[54], and the electron-phonon couplings are of intermediate strength, not allowing weak- and strong-coupling treatments. Therefore, even the e-ph problem in the absence of e-e correlations for the C_{60} molecule is non-trivial.

In all these compounds many energy scales are rather similar, being $\omega_{ph} \sim E_{JT} \lesssim W \lesssim U$ and also the electron-phonon couplings are of intermediate strength. The alkali-doped fullerides are therefore quite complicated systems in which the interplay between strong electron-electron correlations, the Jahn-Teller effect, and the orbital degeneracy gives rise to interesting physical properties [55]. The competition between all these different terms gives rise to many stable phases (magnetic and nonmagnetic insulator, metal, superconductor) as a function of external parameters. The problem of the alkali-doped fullerides is therefore inherently a many-body problem, and powerful tools must be used to properly treat the competition between different physics. The reader may notice that basically the same ingredients we have outlined are relevant to the understanding of the Colossal MagnetoResistance (CMR) manganites, in which the phase diagram

is complicated by the crucial role of magnetism and its relationship with the other properties. The alkali-doped fullerides, besides their intrinsic interest, can be thought as an almost ideal playground to study the interplay between e-ph and e-e interactions beyond the weak- and strong-coupling limits.

2.2 The alkali doped fullerides A_4C_{60}

In this section we consider more specifically the properties of the tetravalent fullerides A_4C_{60}, where A is an atom of an alkali-metal (Na,K,Rb,Cs).

The threefold degenerate t_{1u} level of the isolated molecule leads to three bands hosting the valence electrons provided by the alkali metals. Hence all compounds A_nC_{60} with $0 < n < 6$ should in principle be metallic if, as one expects, the bandwidth (of order 0.5 eV both in the $n = 3$ and the $n = 4$ compounds), is larger than the relatively small crystal field splittings.

The $n = 3$ fullerides are in fact generally metals, and become superconducting with T_c as high as 40 K [56] for Cs_3C_{60} under pressure. All the $n = 3$ compounds present a face-centred cubic (FCC) non-bipartite crystal structure. Among the $n = 4$ compounds, however, only Na_4C_{60} is a nonmagnetic metal and it shows an FCC structure at low temperatures[57], and a body-centred tetragonal structure (BCT) structure at high temperature[58]. K_4C_{60} and Rb_4C_{60} are instead stable BCT structures down to low temperatures, and nonmagnetic narrow-gap insulators. The first difference between the $n = 3$ and $n = 4$ insulating compounds is the lattice structure. The BCT crystal of the quadrivalent fullerides is a body-centered cubic lattice in which the c-axis lattice constant is smaller than the distances on the plane. The distortion leaves the lattice bipartite, while the FCC lattice of the trivalent fullerides is frustrated.

The experimental evidences for a narrow-gap insulating state in K_4C_{60} and Rb_4C_{60} are well settled and come from various independent techniques. Resonant Raman studies [59] on K_4C_{60} indicate an activation energy of 0.055 eV, associated with an indirect energy gap, in close agreement with the estimates coming from NMR [60]. Kiefl et al.[47] report a significantly larger gap of $\sim$ 0.3 eV by inspection of the μSR spectrum, but it has been shown [59] that the data reported are inconclusive and a fit to them may give results ranging from 0.04 to 0.3 eV. NMR provides an estimate for the spin-gap of $E_t \sim 0.13$ eV [60], in close agreement to bulk magnetic measurements for Rb_4C_{60} that indicate a value of 0.10 eV[61]. ^{13}C-NMR measurements on Rb_4C_{60} confirm the nonmagnetic insulating behaviour for this compound at ambient pressure, but increasing pressure up to 12 kbar, T_1^{-1} displays a Korringa-like behaviour, characteristic of a

metal[62]. An optical conductivity study based on Electron Energy Loss Spectroscopy shows a sizeable optical gap for different A_4C_{60} compounds. A study of the optical gap Δ as a function of the different alkali ions shows that Δ increases with increasing size of the ions[57]. The values range from 0.5 eV (K_4C_{60}) to 0.6 eV (Rb_4C_{60} and Cs_4C_{60}). Reminding that Na_4C_{60} is metallic, the behaviour as a function of the dimension of the alkali atoms can be understood as a sort of chemically induced variation of pressure. The Na ion is the smallest alkali-metal atom, so going from K to Na may be viewed as an increasing chemical pressure due to the shortening of the bondlenght. Further increasing the alkali-atom size results in a decreased chemical pressure leading to a larger gap. Notice that both the metallic Na_4C_{60}, and the insulating K_4C_{60} are nonmagnetic, so this transition occurs without any magnetic effect even at low temperatures. The picture of the Mott transition between a paramagnetic metal and a paramagnetic insulator seems to fit the experimental scenario, but we still have to walk a rather long path to confirm or disprove this explanation. We also mention that no static JT distortion has been observed in K_4C_{60} [63]. Unfortunately, the energy resolution of the X-ray scattering that provide this negative result is 0.04 Å, almost exactly the estimated value of the JT distortion for an isolated ion, that represents an upper bound for the solid, where the electron motion can only quench the distortions. As a matter of fact, these results are inconclusive. In any case, the absence of a static JT effect would not rule out a possible dynamical JT effect with the molecules resonating between different distorted configurations.

Various physical ingredients may be advocated to explain the properties of these compounds in the light of the experimental evidences we have reported. It is anyway rather safe to divide the possible explanations of the insulating behaviour of these compounds in two alternative scenarios:

1. A large splitting of the t_{1u} bands may give rise to a band insulator, in which the two lower bands are filled and the upper one is empty. The splitting can be either due to the BCT crystal field or, more likely, to a collective JT distortion of the C_{60} molecules. The JT may in turn be dynamical or static.

2. The strong Coulomb repulsion strongly suppresses the electron hopping between adjacent molecules. The systems can be regarded as Mott insulators. In this case the Jahn-Teller effect takes place as a molecular JT effect, without collective distortions.

In the case of the band insulator, the nonmagnetic groundstate can be easily understood, since the four electrons per site can fill completely the two lower bands. In the case of a Mott insulator, the explanation of the nonmagnetic behaviour is not so simple. The eventual Mott state of these compounds can not be described by means of a single-

band Hubbard model for two main reasons. The groundstate of the single-band model in the insulating state is always antiferromagnetic, while we need to describe a non-magnetic insulator. Moreover, a single-band model can not account for the difference between the metallic $n = 3$ compounds and the insulating $n = 4$, since the bandwidths are quite similar. In this chapter we report results of many different calculations that allow to discuss the actual realization of one or the other scenario[16]. In section 2.3 we study first of all the isolated molecular ion, including both electron-electron interactions, and the molecular JT coupling. In section 2.4 we investigate the possible band origin of the insulating state of K_4C_{60} by Tight-Binding Hartree-Fock (TBHF) and, more accurately, by density functional theory [1]. The failure of these band structure approaches to provide a reasonable description of the insulating state leads us to consider the alternative viewpoint, in which the Mott phenomenon takes place, and strong correlation must be taken into account. This is done in section 2.5 by means of the Dynamical Mean Field Theory (DMFT) of the Mott transition in these compounds. Our final conclusion will be that the A_4C_{60} insulators should indeed be regarded as Mott-Jahn-Teller insulators[15, 16]. Moreover, many observable quantities will be shown to recover the molecular values in the Mott insulating state . In particular, the molecular Jahn-Teller effect brings the system towards a nonmagnetic (singlet) groundstate.

2.3 The single C_{60}^{4-} ion

There are at least two reasons to begin our analysis of the properties of A_4C_{60} from the isolated C_{60}^{4-} ion. On one hand, since the fullerides are molecular solids, and the molecular structures clearly survive in the solid phase, some reminder of the molecular physics is anyway expected to be present in the solid state; moreover, if the system were a Mott insulator, the frustration of the electronic motion would lead to a state in which four electrons would reside on each molecule, without hopping frequently from site to site. Then the molecular physics would be recovered in order to minimize the energy on each ion. Within the triply degenerate t_{1u} orbital, assuming rotational (icosahedral) symmetry, a general interaction among electrons can be written as

$$\mathcal{H}_{int} = \mathcal{H}_U + \mathcal{H}_{m-e} = \frac{U}{2} n(n+1) + \frac{J_H}{6} \sum_{m=1}^{5} W_{(m)}^2, \tag{2.1}$$

where $n_\alpha = \sum_\sigma c_{\alpha\sigma}^\dagger c_{\alpha\sigma}$ is the electron number on each orbital ($\alpha = 1, 2, 3$), $n = n_1 + n_2 + n_3$ is the total density on the molecule. U and J_H are Coulomb interaction

[1] The DFT calculations have been performed by P. Giannozzi [16]

energies; while U has the familiar meaning of an on-site repulsion controlling the total charge, the second term is responsible for the multiplet splitting according to the Hund's rule. $W_{(m)}$ are the multiplet-exchange operators

$$\begin{aligned} W_{(1)} &= \sqrt{3}(n_1 - n_2) \\ W_{(2)} &= n_1 + n_2 - 2n_3 \\ W_{(3)} &= \sqrt{3}\sum_\sigma (c_{1\sigma}c_{2\sigma} + h.c.) = \sqrt{3}\Delta_{12} \\ W_{(4)} &= \sqrt{3}\sum_\sigma (c_{2\sigma}c_{3\sigma} + h.c.) = \sqrt{3}\Delta_{23} \\ W_{(5)} &= \sqrt{3}\sum_\sigma (c_{3\sigma}c_{1\sigma} + h.c.) = \sqrt{3}\Delta_{31}. \end{aligned} \tag{2.2}$$

Using Eqs. (2.2) we can rewrite (2.1) as

$$\mathcal{H}_{int} = \frac{U}{2}n(n+1) + \frac{2J_H}{3}\sum_\alpha n_\alpha^2 - \frac{2J_H}{3}\sum_{\alpha<\beta} n_\alpha n_\beta + \frac{J_H}{2}\sum_{\alpha<\beta}\Delta_{\alpha\beta}^2, \tag{2.3}$$

which is manifestly symmetric in the orbital indices.

The first term, proportional to U is the usual Hubbard term, which gives rise to the Mott transition. This term alone does not split the degeneracy of the $n = 4$ manifold. For a fixed number of electrons, the molecular spectrum is determined by the second term. The exchange coupling J_H is not expected to be significantly screened by the t_{1u} electrons, so that a reasonable estimate can be obtained by optical measurements on solid C_{60}, which give $J_H \simeq 0.05$ eV[49].

In Appendix A we compute the spectrum for the interaction Hamiltonian (2.3) for $n = 1, 2, 3$ (the other fillings can be obtained by symmetry around half-filling). For $n = 4$ and positive J_H the spectrum follows the Hund's rules: the lowest energy state is the ${}^3T_{1g}$ triplet ($S = 1, L = 1$), followed at energy $2J_H$ by a ${}^1H_g$ singlet ($S = 0, L = 2$), and at $5J_H$ by a ${}^1A_g$ singlet ($S = 0, L = 0$). The multiplet exchange terms alone would give a molecular spin as well as orbital triplet groundstate. If this terms were dominant, it would be indeed hard to understand the nonmagnetic groundstate of the solid A_4C_{60}.

Next, we consider the JT coupling to the eight H_g vibrational modes. The electron-vibron Hamiltonian is

$$\begin{aligned} \mathcal{H}_{JT} &= \sum_{\nu=1}^{8}\omega_\nu \sum_{m=1}^{5}(b_{\nu m}^\dagger b_{\nu m} + \frac{1}{2}) \\ &+ \sum_{\nu=1}^{8}\frac{g_\nu}{2}\sum_{m=1}^{5} W_{(m)}(b_{\nu m} + b_{\nu m}^\dagger), \end{aligned} \tag{2.4}$$

where $b_{\nu m}(b_{\nu m}^{\dagger})$ are annihilation (creation) operators for the vibronic modes, and g_ν and ω_ν are, respectively, electron-vibron coupling and vibron frequencies for each of the H_g modes. Their values can be extracted from gas phase $C_{60}^{(-)}$ photoemission[64]. $W_{(m)}$ are the fermionic quadratic operators (2.2) that couple to the vibronic modes[64]. For symmetry reasons, the same operators appear in the e-e interaction term and in the e-ph coupling.

Instead of an exact solution of $\mathcal{H}_{int} + \mathcal{H}_{JT}$, we consider two opposite limits, antiadiabatic and adiabatic for the e-ph interaction term. The adiabatic limit assumes the phonon dynamics to be much slower than the electronic one. On the opposite, the antiadiabatic limit amounts to average out the phonon degrees of freedom, assumed to be rapidly varying. The role of the degree of adiabaticity in the e-ph coupling, measured by the ratio between a typical phonon scale ω_0 and the hopping amplitude, has been studied in the recent years[65, 54] in the context of the Holstein model. One of the main outcomes is that the extreme adiabatic limit is not representative of the physics at finite frequencies.

Although neither of the opposite limits strictly applies, since the vibronic frequencies involved are comparable to all splittings[64] and the coupling is of intermediate strength, the simplicity of the opposite extreme limits will help us to better understand the relevant physics. We will discuss in more details the relevance of both limits in section 2.5. We anticipate here that the antiadiabatic limit is a more faithful image of the symmetries of the actual solution if a dynamical JT effect takes place, whereas the adiabatic limit proves quantitatively more accurate if compared to exact numerical solutions.

In the antiadiabatic limit, the phononic degrees of freedom can be integrated out, since their dynamics is assumed to be fast with respect to the other time scales. The antiadiabatic treatment of the JT term (2.4) gives rise to a non-retarded electron-electron interaction, which has exactly the same form of the Hund's rule splitting term (2.1), but the opposite sign [2]. The antiadiabatic effective Hamiltonian has then the form (2.3) once J_H is suitably changed, $J_H \longmapsto J_H - (3/4)E_{JT}$, being $E_{JT} = \sum_\nu g_\nu^2/\omega_\nu = 0.169$ eV. J_H changes therefore sign from 0.05 eV to -0.076 eV. The result of the Jahn-Teller interaction is therefore an inversion of the molecular multiplets. The lowest energy state is now the ${}^1A_g$ singlet, followed at 0.23 eV by the ${}^1H_g$ singlet, and at 0.38 eV by the ${}^3T_{1g}$ triplet. The overall JT energy gain in this limit is very large, 0.84 eV, about a factor three larger than the bare adiabatic JT energy (see below). This signals a true enhancement, due to the gain in zero point energy corresponding to the frequency collapse of

[2]This is exactly the equivalent of the Holstein molecular crystal model, in which a phonic mode is coupled to the electron density, that is mapped onto an attractive Hubbard model in the antiadiabatic limit.

the tangential vibron modes, first pointed out in Ref.[66], as a possible mechanism for explaining the high critical temperature of A_3C_{60} compounds. The inclusion of the JT coupling has an important effect. The groundstate of the ion at least in this limit becomes *non-degenerate* with $L = 0$ and $S = 0$.

In the adiabatic limit, the electronic model is solved at fixed phonon coordinates. In the fully-adiabatic limit, where the phonon frequencies are assumed to be negligible, but the ratios g_ν^2/ω_ν are kept constant, the phonon dynamic is neglected and the molecular vibrations can be treated as classical variables. As a consequence, the eight fivefold degenerate vibrations can be treated within a *single mode* approximation[67] for (2.4), which, once we consider one of the equivalent JT distortions, leads to

$$\begin{aligned} \mathcal{H}_{JT} &= \frac{g_*^2}{2\omega_\nu}\left\{\left(z^2+r^2\right)+\right. \\ &\left. z\left(n_1+n_2-2n_3\right)+r\sqrt{3}\left(n_1-n_2\right)\right\}. \end{aligned} \tag{2.5}$$

In this limit the Jahn-Teller term explicitly breaks the orbital symmetry, and the electrons are coupled to classical variables r and z. Using the values from [64] we have $\omega_* = 0.117$ eV, and an effective e-ph coupling $g_* = 1.409$ eV, so that the characteristic Jahn-Teller energy is $E_{JT} = g_*^2/\omega_* = 0.169$ eV. We diagonalize (2.3) plus (2.5) for $n = 4$, minimizing with respect to z and r treated as classical variables. The groundstate is found to be a singlet with classical distortions $z = -1.987$ and $r = 0$, and a JT energy gain of 0.293 eV, as shown in panel (a) of Fig. 2.3. The large Jahn-Teller splitting makes orbitals 1 and 2 significantly favourable with respect to orbital 3, while there is no energy gain in lifting the degeneracy between levels 1 and 2, since they are completely filled by four electrons. Adding the zero point energy gain ω_*[66], we obtain a total gain of 0.41 eV. A similar total gain of 0.42 eV was obtained by uncorrelated eight-mode calculations[64, 67]. The adiabatic limit accurately describes the energetics of the Jahn-Teller effect, even if it implies a symmetry breaking.

The lowest triplet state has instead $z = 1.0$ and $r = 0$ and lies above the groundstate by $E_t = 0.108$ eV (spin gap). In this state the Jahn-Teller favours orbital 3, which is filled with two electrons, and each of the other two electrons occupies one of the remaining orbitals, as shown in Fig.2.3 (b). The next lowest singlet, denoted by (c) in Fig. 2.3 (with $z = 1.0$ and $r = 0$), is at $E_s = 0.208$ eV above the groundstate. Finally, the *optical* gap, identified with the JT orbital splitting, is $\Delta = (3/2)zE_{JT} \simeq 0.504$ eV and it is associated to transitions from the groundstate (a) to the state (d), in which the orbital splitting is frozen.

Also in the adiabatic limit the C_{60}^{4-} ion is in a singlet groundstate with a sizeable energy gap to the closest triplet state. The JT energy gain is therefore large enough to

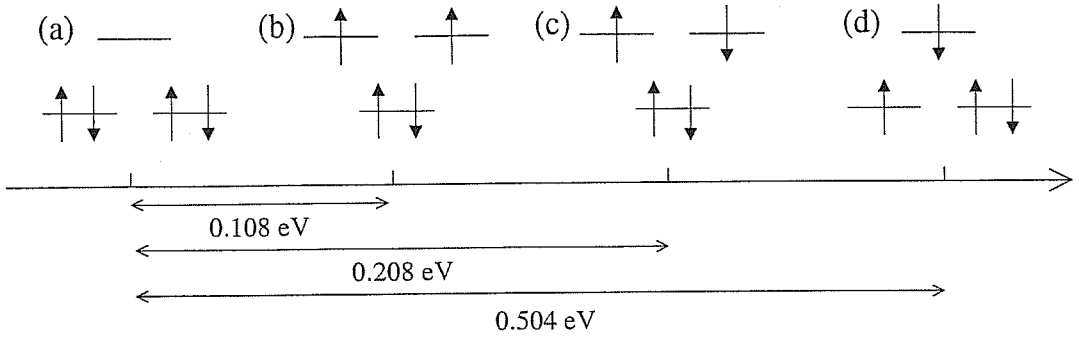

Figure 2.3: The lowest energy states for an isolated C_{60}^{4-} ion when the JT effect is treated in the extreme adiabatic limit. (a) is the singlet groundstate; (b) is the lowest triplet; (c) is the next-singlet; (d) is the lowest state accessible by optical transitions. The difference between (a) and (b) gives the spin-gap, while the difference between (a) and (d) is the optical gap. Both quantities are extremely close to the experimental values for K_4C_{60}.

overcome the Hund's rule and to give rise to a singlet groundstate. This property is then expected to hold also for an exact treatment of the molecular Hamiltonian. In both scenarios for A_4C_{60}, this is a crucial step to explain the nonmagnetic behaviour.

Moreover, the observable spin gap and optical gap computed for the isolated ion in the adiabatic limit (that are quantitatively almost identical to the values coming from the exact numerical solution) are really close to the experimental values for K_4C_{60} and Rb_4C_{60}[62, 57, 60]. This finding strongly suggests that the low-lying excitations in the solid are essentially intermolecular, as it would be in the case of a Mott insulator. It is hard to believe that this could be a coincidence, but the results of the following sections are meant to rule out this chance, discussing the possibility of the formation of a band insulator starting from the lattice of C_{60}^{4-} ions.

2.4 Band structure calculations: Hartree-Fock and Density Functional Theory

The first, and simplest, explanation of the insulating properties of A_4C_{60} fullerides would be a small value of the hybridization between the different C_{60} molecules. If the electron hopping matrix elements between adjacent molecules were much smaller than all the intra-molecular energy gaps involved, then a lattice of C_{60}^{4-} molecules would indeed be a nonmagnetic insulator, with a spin gap E_t and an optical gap Δ close to their molecular values of about 0.1 and 0.5 eV.

In that case of nearly uncoupled ions, we would expect a band insulator in which

the molecular levels were split by the Jahn-Teller effect and the Hund's rule, and weakly broadened by the (assumed small) hopping between balls. An electronic structure calculation for the A_4C_{60} lattice should yield a t_{1u} triplet of bands, split by the atomic insulating gap. The gap would in turn be supported by a collective JT distortion that could be either dynamical and static. In the latter case, the collective distortion pattern could be uniform or staggered[43].

2.4.1 Tight-Binding Hartree-Fock

The simplest calculation of the band-structure is a Tight-Binding Hartree-Fock (TBHF) approach, in which the electronic hopping matrix element are obtained with realistic models of atomic hopping amplitudes [68], and the Hubbard interaction is linearized by means of a Hartree-Fock decoupling. We performed this kind of calculations using parameters appropriate for K_4C_{60}. The Hamiltonian may be written

$$\mathcal{H} = \sum_{i,j,\alpha,\beta,\sigma} t_{ij}^{\alpha\beta} c_{i\alpha\sigma}^{\dagger} c_{j\beta\sigma} + \mathcal{H}_{int} + \mathcal{H}_{JT}, \tag{2.6}$$

where $c_{i\alpha\sigma}^{\dagger}$ ($c_{i\alpha\sigma}$) is the creation (destruction) operator for an electron with spin σ on orbital α ($\alpha = 1, 2, 3$). $\mathcal{H}_{int}$ and $\mathcal{H}_{JT}$ are the lattice version of (2.3) and (2.4) respectively, i.e. the same local Hamiltonian repeated on every lattice site. The hopping amplitudes $t_{ij}^{\alpha\beta}$ are evaluated along the lines outlined in Ref.[69] taking explicitly into account the hybridization between all the C_{60} atoms within a single molecule and between adjacent molecules, and projecting onto the t_{1u} levels. The alkali-atoms levels only negligibly hybridize with the t_{1u} levels, and can be safely neglected.[3] The BCT structure is used with lattice parameters appropriate for K_4C_{60} of $a = b = 11.886$Åand $c = 10.774$Å[43]. Given the actual lattice distances, and the spatial dependence of the hopping matrix elements between carbon atoms[68], the band-structure is essentially given by an effective hopping between nearest-neighbours and next-nearest-neighbours C_{60} molecules, with the longer range hoppings negligible. The bands obtained neglecting the interaction term and the JT coupling are rather similar to the LDA bands[43].

The Jahn-Teller interaction is treated in the adiabatic approximation, as in Eq.(2.5) with the realistic values for the effective coupling and frequency, giving $E_{JT} = 0.169$ eV. We look for a HF state with broken orbital symmetry, in which the average density in a given orbital, $n_\alpha = \langle c_\alpha^{\dagger} c_\alpha \rangle$, is assumed non-zero and uniform, and with $n_1 = n_2 \neq n_3$, in order to represent the electronic state associated with a collective static JT distortion.

[3] Calculations explicitly taking into account potassium atoms have been carried out, but the effect on the band-structure does not effect our conclusions.

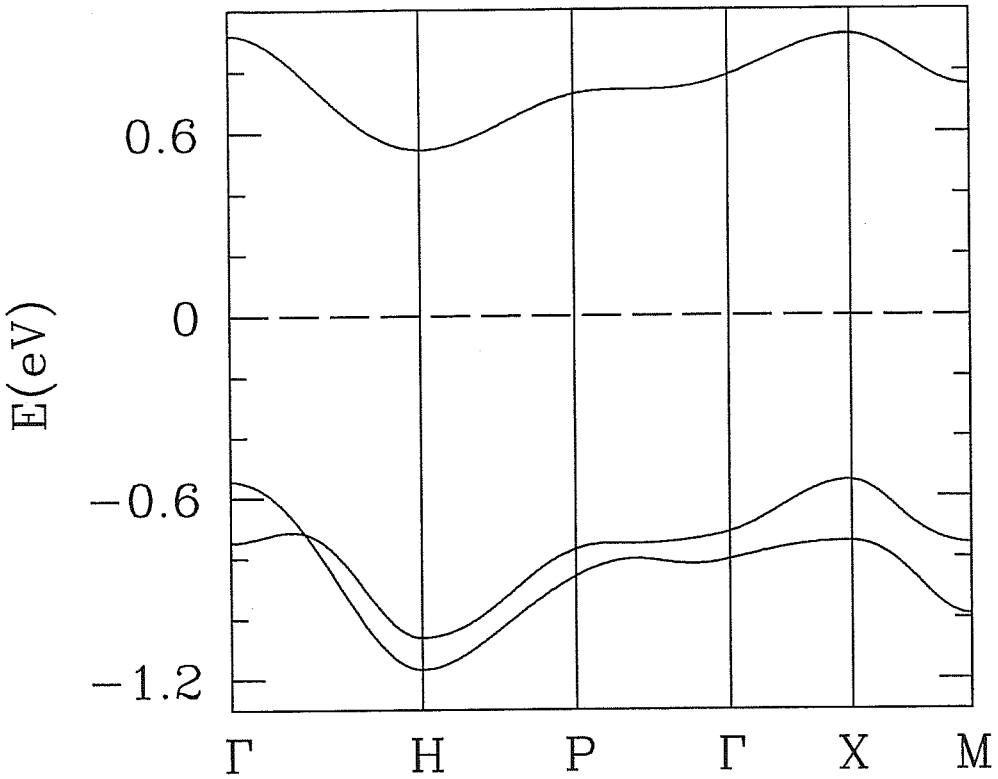

Figure 2.4: The t_{1u} bands for K_4C_{60} according to HF. The HF state sustains a collective JT distortion and is wide gapped, while experiments indicate a narrow gap semiconductor.

We choose

$$\Delta = \frac{1}{2}\langle n_1 + n_2 - 2n_3 \rangle, \tag{2.7}$$

as the order parameter, the potential energy with this choice of Hartree-Fock decoupling can be written

$$\mathcal{H}_{int}^{HF} = -\left[gx + \frac{\Delta}{18}(3U - 11J_H)\right](n_1 + n_2 - 2n_3) \equiv V^*(n_1 + n_2 - 2n_3) \tag{2.8}$$

The outcome for realistic values of all the interaction terms ($U = 1.1$ eV, $J_H = 0.05$ eV[49]) gives a stable band insulator with direct gap and spin gap of $\sim$ 1.48 eV and an indirect gap of $\sim$ 1.03 eV, much larger than the experimental values. Our calculated TBHF band-structure is shown in Fig. 2.4. The gross discrepancy with the much smaller experimental gaps indicates that the HF approximation, well known to overestimate insulating tendencies, may not be reliable for this problem. No improvement is achieved

by considering staggered distortion patterns. We note however that by a different choice of effective hamiltonian parameters, gaps slightly closer to experiment may actually be obtained[70], and that further improvements may be obtained by including corrections such as GW [71]. The feeling we get from our calculations is that rather unrealistic and fine-tuned parameters must be used to decently reproduce the actual physical measurable quantities within this framework. The question whether a band picture would predict an insulator or a metal, requires a more realistic first principles approach than TBHF. To this end we compare TBHF to *ab initio* density functional calculations, whose applicability to fullerene and fullerides is well documented[72], and whose predictive power, including total energy minimization as a function of ionic coordinates, is greater.

2.4.2 Density Functional Theory: Local Density Approximation

In this section we report results of electronic structure calculations within the density functional theory in the Local Density Approximation (LDA) for K_4C_{60}, performed by P. Giannozzi[16]. A BCT configurations compatible with X-ray data[63] has been taken as a starting point, allowing ions to relax towards the total energy minimum. As a first approximation, only the molecules and alkali ions were left able to move in order to minimize the total energy, without allowing for a Jahn-Teller deformation within each C_{60} unit. In agreement with previous results[43], a stable metallic groundstate with t_{1u} bands of width $W \simeq 0.6$ eV has been found. Such a result is evidently contrary to the experimental findings, but this is not a surprise since the calculations neglected the Jahn-Teller coupling, as a consequence of the assumption of undistorted molecules. This finding simply proves that the BCT crystal field is not strong enough to give rise to an insulator starting from the degenerate t_{1u} levels.

Since the LDA has proven successful in the description of electron-ion coupling and therefore static Jahn-Teller too[72], the next step has been to search for a spontaneous collective JT distortion allowing the relaxation of the atomic positions according to Hellmann-Feynman forces. As a check of the capability of the calculation to properly reproduce a delicate feature like the JT distortion, test calculation have been performed for a single ion, by artificially increasing the intermolecular spacing to 13.3Å. At this (unphysical for the solid) distance, the electrons are essentially unable to hop between molecules, so that we are actually simulating an isolated molecule. As expected for that case, the calculation successfully reproduced the Jahn-Teller deformation of the ion. The computed distances of the atoms from the centre range between 3.511 and 3.553Å. This distortion amplitude $\Delta R = 0.042$Å, although apparently small, is very close to that

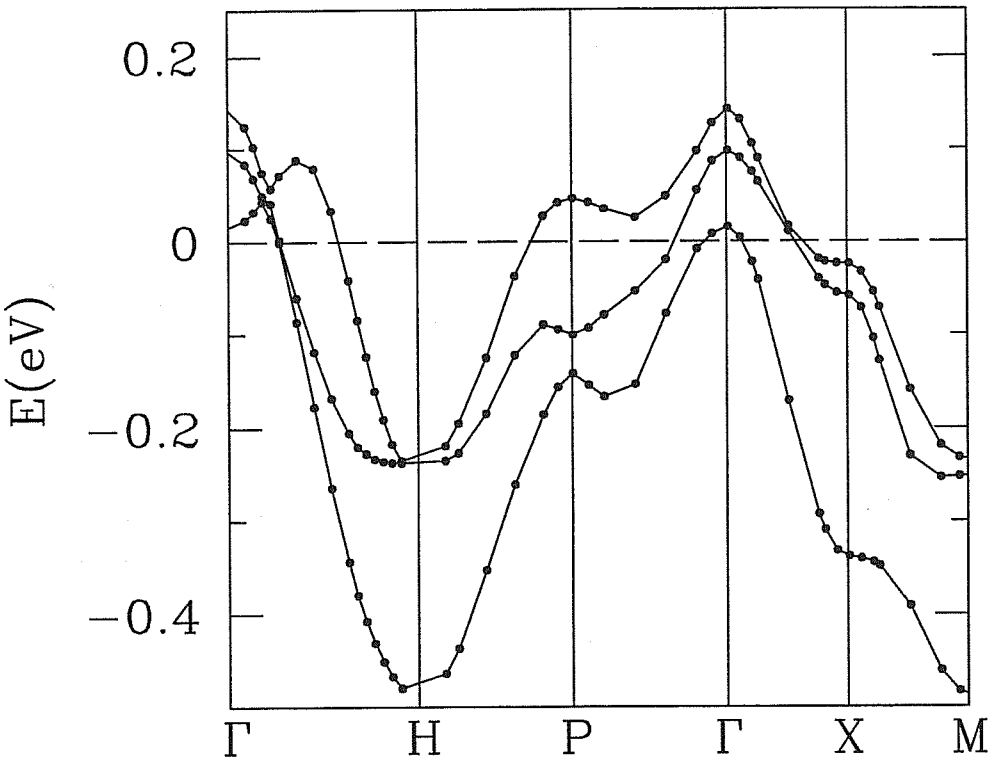

Figure 2.5: The t_{1u} bands for K_4C_{60} according to LDA. The LDA state is undistorted and metallic, in strong disagreement with experiments.

reported for $[PPN(+)]_2C_{60}(2-)$ salts[73], namely 0.043Å. This finding is very gratifying, since JT distortions of C_{60}^{2-} and C_{60}^{4-} should be the same due to electron-hole symmetry of the Hamiltonian (2.3) + (2.4). The LDA calculations are therefore able to provide an almost perfect description of the actual deformations due to the Jahn-Teller coupling. As an intrinsic drawback of LDA calculation, the single-particle JT gap is only about 0.1 eV, instead of the expected 0.5 eV. Since we are interested in the actual existence of sizeable distortions, this shortcoming does not affect our conclusions.

The true BCT structure was then considered, and an extensive search for a possible JT distortion was carried out, looking for uniform distortion patterns. The search yielded however negative results, and the final conclusion was that the groundstate of K_4C_{60} within LDA and one molecule per cell is undistorted, and metallic , with bands as shown in Fig. 2.5.

The undistorted metallic state is actually very robust, and rather independent of small details. In other words, it is really hard to imagine that some small physical effect could open a gap at the chemical potential starting from the bands of Fig. 2.5 thus giving rise to an insulator. The last reasonable possibility for the opening of a gap in the spectrum within a band approach is to consider staggered distortions. Selected calculations with two molecules per unit cell also failed in finding a stable distorted groundstate. This failure rules out (within a band-structure calculation) charge-density-waves [43] or a staggered collective JT state. The molecular JT energy gain is quenched in the solid in favour of intermolecular band electron kinetic energy. The LDA being a much more reliable calculation that TBHF, where quenching of molecular JT may not be very well described, we conclude that the undistorted metallic state genuinely represents the most faithful representation of the system within a single-particle picture.

As already mentioned, neither the presence or the absence of a JT distortion are well established in K_4C_{60}. X-rays fail to find a static JT distortion[63], but the experimental resolution is indeed not sufficent to rule out the possibility of a distortion. The metallicity is nonetheless clearly at odds with experiment. We temporarily surmise that, since accurate density functional calculations cannot account for its insulating behaviour, K_4C_{60} might not be a band insulator, with electron-electron correlations a possible culprit.

2.5 Dynamical Mean Field Approach

Electron-electron correlations are rather strong in many fulleride compounds. A realistic estimate[9, 49] of the intra-molecular Hubbard U of Eq.(2.3) is $\simeq$ 1.0–1.6 eV, which is about twice the full electron bandwidth. The failure of density functional calculations

does not appear surprising in this light. The relatively strong value of the correlation strength implies that we are dealing with a fully many-body problem, beyond the field of validity of band-structure calculations. It is thus desirable to implement a reliable, even if by necessity more schematic, description of the insulating state, and of the possible MIT induced by electronic correlation. In this spirit we resort to dynamical mean-field theory (DMFT)[2], which has proved to be the most reliable tool for the description of the Mott transition in the Hubbard model, as discussed in Chapter 1. Within DMFT, the spatial fluctuations are frozen, but local quantum fluctuations are fully taken into account. As a result, the original lattice model is mapped onto a single-site effective action subject to a self-consistency condition. At least in its standard version, DMFT does not keep track of the details of the band-structure, and we will use the semicircular density of states (DOS) of an infinite coordination Bethe lattice, that only qualitatively resembles the one of a three-dimensional system. Although we do not explicitly consider possible merohedral disorder effects, discussed by other authors[71, 74], the assumption of a smooth, singularity-free, semicircular electron DOS may to some extent make that inclusion superfluous within the DMFT.

On the positive side, we expect a DMFT treatment of this problem to be extremely instructive, because of its ability to handle simultaneously the orbital degeneracy, the molecular JT coupling, and the strong inter-orbital and intra-orbital correlations without further approximations. Gunnarsson's group has recently implemented quantum Monte Carlo calculations within the DMFT which indicate that one source of the insulating state of tetravalent fullerides may be the lack of frustration implied by the BCT lattice. By contrast, the presence of frustration typical of non-bipartite FCC lattices, favours metallicity in the trivalent fullerides. [74].

The effective action corresponding to the Hamiltonian (2.6) can be written as

$$S_{eff} = -\sum_{\alpha} \int_0^{\beta} d\tau \int_0^{\beta} d\tau' c^{\dagger}_{0\alpha}(\tau) G_{0\alpha}(\tau - \tau')^{-1} c_{0\alpha}(\tau') + S_0, \tag{2.9}$$

where S_0 is the local action associated with the interaction terms (2.3)in

$$\begin{aligned} S_0 \;=\; & -\frac{U}{2}\int_0^{\beta} n_0(\tau)^2 d\tau + \frac{2J_H}{3}\sum_{\alpha}\int_0^{\beta} n_{0\alpha}(\tau)^2 d\tau \\ & -\frac{2J_H}{3}\sum_{\alpha<\gamma}\int_0^{\beta} n_{0\alpha}(\tau) n_{0\gamma}(\tau) d\tau \\ & +\frac{J_H}{2}\sum_{\alpha<\gamma}\int_0^{\beta} [\sum_{\sigma} c^{\dagger}_{0\alpha\sigma}(\tau) c_{0\gamma\sigma}(\tau) + h.c.]^2 d\tau. \end{aligned} \tag{2.10}$$

In the presence of the Jahn-Teller interaction of the form (2.4), a local electron-phonon interaction term appears of the form

$$\begin{aligned} S_0^{JT} &= \sum_{\nu=1}^{8} \omega_\nu \sum_{m=1}^{5} \int_0^\beta \left(b^\dagger_{0\nu m}(\tau) b_{0\nu m}(\tau) + \frac{1}{2} \right) d\tau \\ &+ \sum_{\nu=1}^{8} \frac{g_\nu}{2} \sum_{m=1}^{5} \int_0^\beta W_{(m)0}(\tau) (b^\dagger_{0\nu m}(\tau) + b_{0\nu m}(\tau)) d\tau \end{aligned} \tag{2.11}$$

The Weiss field $G_{0\alpha}(i\omega_n)$ and the local Green's function are now dependent on the orbital index $\alpha = 1, 2, 3$. The self-consistency equations for a Bethe lattice read

$$G_{0\alpha}(i\omega_n)^{-1} = i\omega_n + \mu + \varepsilon_\alpha - \frac{t_\alpha^2}{4} G_\alpha(i\omega_n), \tag{2.12}$$

where $W_\alpha = 2t_\alpha$ is the bandwidth for the α-th band, ε_α is a shift for the energy of the band, μ is the chemical potential chosen to provide the desired density, and $G_\alpha(i\omega_n)$ is the local Green's function for the orbital α. Since both the interaction (2.3) and the Jahn-Teller coupling (2.4) are invariant under rotation in the orbital indices, we work in the basis in which the bands are diagonal. Therefore, without loss of generality, the self-consistency equations can be taken diagonal in the orbital indices, even if different shifts ε_α and/or hopping amplitudes can be chosen for the different bands. In this section, we take three bands with the same bandwidth ($t_\alpha \equiv t$), taken equal to the full bandwidth coming from LDA calculation ($W \simeq 0.61$ eV), and do not consider shifts for the various bands ($\varepsilon_\alpha \equiv 0$). The values of the Coulomb integrals and the JT couplings come from realistic estimates.

Then we turn to the LISA approach described in section 1.2.1. Obviously, in our case, we have to deal with a triply degenerate Anderson model. The hamiltonian can be written as

$$\begin{aligned} \mathcal{H}_{AM} &= \sum_{k\alpha\sigma} \tilde{\varepsilon}_{k\alpha\sigma} a^\dagger_{k\alpha\sigma} a_{k\alpha\sigma} + \sum_{k\alpha\sigma} V_{k\alpha\sigma} (a^\dagger_{k\alpha\sigma} c_{0\alpha\sigma} + + c^\dagger_{0\alpha\sigma} a_{k\alpha\sigma}) + \\ &- \mu \sum_{\alpha\sigma} c^\dagger_{0\alpha\sigma} c_{0\alpha\sigma} + \mathcal{H}_0^{int}. \end{aligned} \tag{2.13}$$

To avoid too lengthy notations, we denote by $\mathcal{H}_0^{int}$ the local interaction Hamiltonian taking into account both the e-e correlation (2.3) and the e-ph interaction (2.4). The Hamiltonian (2.13) is solved by means of exact diagonalization (ED) with a finite number (n_s) of conduction electron degrees of freedom[34], checking convergence as a function of n_s, as described in section 1.3.2. Following Krauth [35], one can easily convince that the ED method is by far more reliable and useful than QMC for the single-band model,

since really small values of n_s assure converged results in both the metallic and the insulating phase, while the QMC method requires really small values of $\Delta\tau$ to give reliable results in the insulating phase and mostly in the transition region. One could argue that the ED may loose its appeal for orbitally degenerate systems, since the presence of degenerate levels amounts to an effective increase of the number of sites (the number of degrees of freedom needed to describe n_s sites with N_{deg} degenerate levels is exactly the same as for $n_s N_{deg}$ sites). We still believe that ED is the best technique even in the $N_{deg} = 3$ case, for some different reasons. First of all, it safely allows to study directly the $T = 0$ limit in which the MIT is well-defined, whereas the QMC approach is limited to finite temperature by computer memory requirements even in the absence of fermionic sign problem. As a second point, we have verified for the single-band model that even a surprisingly small number of conduction bath levels ($n_s = 4 - 5$) gives an almost converged solution, and that QMC must be pushed to really small $\Delta\tau$ to obtain equally accurate results. Last, but not least, for the specific problem we discuss, the ED method allows to straightforwardly implement the multiplet exchange terms, while they can not be included in the Hirsch-Fye QMC algorithm, since no reasonable Hubbard-Stratonovich decoupling is known for them. In previous QMC calculation for analogous problems, the non-diagonal part of the multiplet-exchange interaction (last term in Eq. (2.3)) has in fact been neglected[53, 74]. The results we show are for $n_s = 5$. They have been checked against $n_s = 6$ for special cases, in which the latter case was feasible, and the quantitative variation of the physical quantities was found to be negligible. In particular, the location of the MIT is basically unchanged. Since the A_4C_{60} compounds are always nonmagnetic, we confine ourselves to the paramagnetic sector, as it usually done in DMFT. In the problem at hand, we have a further choice, concerning the orbital degrees of freedom. DMFT allows us to look for either broken or unbroken orbital symmetry phases. In this respect, it must be stressed that the capability to describe a true Mott insulator without any symmetry breaking is a unique feature of DMFT, which is not shared by HF or density functional-based calculations, always implying symmetry breaking at metal-insulator transitions.

For simplicity, we restricted our search to insulating solutions either without orbital symmetry breaking, i.e. with $V_{k\alpha\sigma} \equiv V_k$ and $\tilde{\varepsilon}_{k\alpha\sigma} \equiv \tilde{\varepsilon}_k$, or with uniform JT ordering, i.e. without considering super-cells made by two or more sites. The expectation value of the density is fixed to $n = 4$ by tuning the chemical potential μ.

As we have seen in the general introduction to the DMFT, the MIT can be located

by computing a single quantity, the quasiparticle residue Z given by

$$\frac{1}{Z} = 1 - \frac{\partial}{\partial\omega}\mathcal{R}e\Sigma(\omega + i0^+)|_{\omega=0}. \tag{2.14}$$

Since the self-energy is momentum independent within the DMFT approach, $Z = m/m^*$, and a vanishing Z is equivalent to a diverging effective mass. Also in the orbitally degenerate case, it can be easily shown that, if there is a coexistence region between metallic and insulating solutions, in the whole region the metallic solution has lower energy, o it is stable at $T = 0$. The vanishing of the metallic solution (indicated with U_{c2}) coincides with the actual transition [40].

Again, we restrict our analysis to instructive limiting cases:

1. No JT effect
2. Antiadiabatic JT effect
3. Adiabatic JT effect

2.5.1 No Jahn-Teller effect

We start from the interaction hamiltonian (2.3), in absence of JT coupling. As we will discuss in detail in Chapter 3, mostly in Section 3.1, the orbitally degenerate Hubbard model with $N_{deg} = 3$ has been already studied within DMFT, only at half-filling and mostly for $J_H = 0$[53]. We will come back later to these results in the following chapter, considering the dependence of the critical U upon filling, and discussing the qualitative features of the transition. Here we focus our attention to the $n = 4$ case using suitable parameters for A_4C_{60}. In the presence of a finite positive $J_H/W = 0.08$, which corresponds to the realistic situation for C_{60}, we find a critical value of $U_c/W \simeq 1.414$ for orbitally-symmetric solutions, sizeably reduced with respect to the critical value in the absence of multiplet exchange terms ($J_H = 0$) which is found to be $U_c/W \simeq 1.92$. This qualitative behaviour is in agreement with Ref. [53, 74], where a reduction of U_c in presence of a positive J_H was reported. It must be noted however that these works did not consider, for technical reasons, non-diagonal contributions to the multiplet exchange terms (last term in the interaction Hamiltonian (2.3)). This neglect leads to an underestimate of the effect of these terms on U_c. In presence of the full interaction Hamiltonian (2.3), but in absence of the Jahn-Teller coupling, the Hund's rules are restored, and in the Mott limit, when the molecular groundstate is recovered, the system is expected to be a spin and orbital triplet ($S = 1$, and $L = 1$). Nevertheless, even within the paramagnetic subspace, the presence of finite Hund's rule coupling results in an effective partial quenching of orbital degeneracy.

2.5.2 Antiadiabatic limit for the Jahn-Teller interaction

In the antiadiabatic limit, the vibronic degrees of freedom are assumed to be fast and can be integrated away leading to a negative contribution to the dipolar integral J_H, exactly as in the case of a single molecule. As a result, a purely electronic model of the form (2.3) is obtained, with an effective negative $J_H/W = -0.127$. The molecular multiplets are therefore inverted with respect to the positive-J_H case, and the $S = 0$, $L = 0$ state becomes the groundstate. The insulating state is expected to be a non-degenerate singlet both in spin and orbital space. The critical value for the MIT is shifted in this limit to $U_c/W \simeq 0.707$, much lower than for positive J_H.

The antiadiabatic limit may seem unphysical, since it assumes that the vibrational dynamics is faster than the electronic one. In the fullerides the vibrational frequencies are indeed roughly of the same order of the electronic energy scales. It is then likely that a dynamical JT effect takes place. By dynamical JT effect, we mean a state in which the symmetry is not broken even in presence of large deformations, due to quantum fluctuations. Every molecule is in a coherent superposition of distorted states with different directions for the distortions [4]. The physical picture of the dynamical JT effect is well described by an antiadiabatic limit, in which no symmetry is broken, even if a quantitative agreement with the exact solution for realistic parameters is not expected. Therefore $U_c/W \simeq 0.707$ is probably an underestimate of the true critical value, but the features of the transitions are expected to be well described in this approximation. According to the arguments above, we expect that the qualitative picture of the Mott-Hubbard transition emerging from this limit is the more appropriate description of the actual transition, despite the quantitative disagreement with more involved and less instructive intermediate-coupling solutions.

2.5.3 Adiabatic limit for the Jahn-Teller interaction

The adiabatic limit assumes the vibrational dynamics to be much slower than the electronic one. In the extreme adiabatic limit $\omega_* \to 0$, with g_*^2/ω_* constant, the vibronic degrees of freedom are treated as classical variables. As in the single molecule, the adiabatic calculation implies a broken orbital symmetry solution, but the numerical values of energies and distortions it generates are accurate enough[64].

[4] This is basically the same thing it happens in the simplest model of e-ph interaction, the Holstein molecular crystal model, in which for non-zero phonon frequency, the translational symmetry is never broken, even in strong-coupling, and no localization transition occurs The formation of a small polaron state is only a crossover, without symmetry-breaking[65].

Solution of DMFT equations is now more involved, since self-consistency must be implemented only after averaging the local Green's function over the classical vibrational variable Q [75, 76]. In the broken-symmetry case the average simplifies, at $T = 0$, as the probability distribution of Q becomes a single δ-function. We obtain a critical $U/W \simeq 0.9 - 1.0$ (the uncertainty due to convergence difficulty). The orbitally-symmetric insulating solution, instead, becomes stable at $U/W \simeq 1.237$, and is higher in energy. Nonetheless, it is of particular interest since it describes a molecular insulator where each molecule is distorted with equal probability in all possible directions and independently from any other molecule. This state has therefore a very large entropy which could be reduced by including quantum fluctuations, for instance in the form of tunnelling between the equivalent local distortions. This would in fact represent an alternative way to describe the dynamical JT effect, not included at the adiabatic level. It should particularly be noted in that respect that our adiabatic treatment does not include the vibron zero-point energy gain upon JT distortion, whose magnitude may be non-negligible[66, 64]. Being it present in the symmetric case only, zero-point energy gain could lower the true critical U/W value of this phase, possibly even below that of the broken symmetry case. Moreover, finite temperature would also favour the symmetric state, which has an higher entropy.

2.5.4 Comparison between the various limits

A summary of all the results presented in the previous paragraphs is reported in Fig. 2.6. The quasiparticle weight Z given by Eq. (2.14) is shown as a function of U/W for the different cases discussed above. In the adiabatic case, we show both the solution with broken orbital symmetry (dot-dashed line + heavy dots), which is the most stable at $T = 0$, and the orbitally-symmetric one (dotted line), expected to be a more faithful picture of the real physics beyond the fully adiabatic limit. The solid line refers to the solution in the absence of the JT effect, and the dashed line to the antiadiabatic limit. We can now compare the critical U_c/W's with the realistic estimates of the Coulomb interaction for K_4C_{60}. The calculated critical values are in all cases substantially smaller than the actual U/W values, i.e. 1.5–2.5.

Notice that for the pure Hubbard model, in the absence of both the Hund's term and the Jahn-Teller interaction, the critical value lies in the middle of the physical range. The overall conclusion of this study is that the strong e-e correlation in A_4C_{60} compound is able to drive the system to a Mott insulating state as soon as the multiplet-exchange coupling is considered. The Jahn-Teller effect further increases the region of stability of

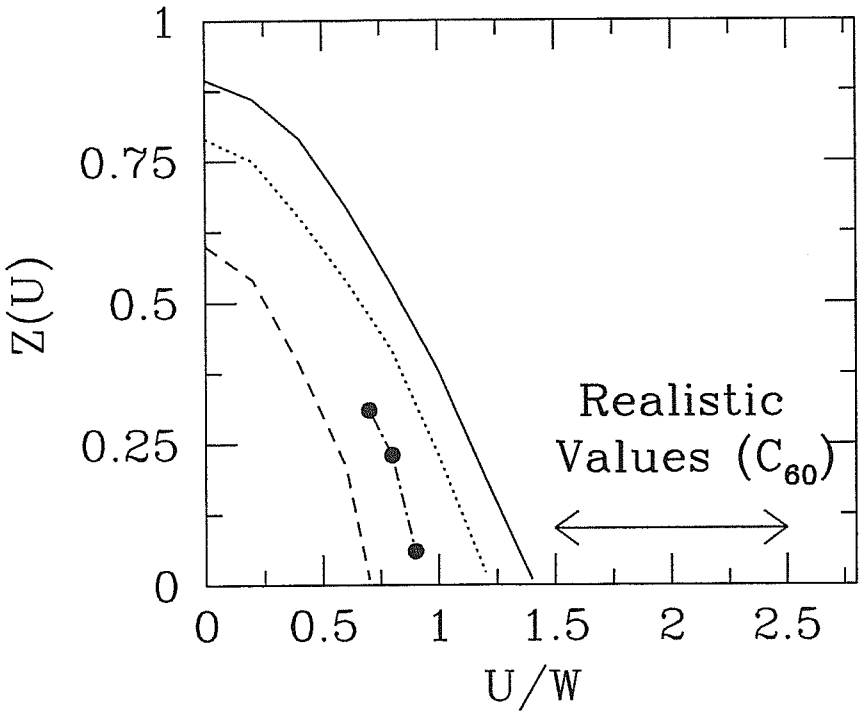

Figure 2.6: Quasiparticle weight Z as a function of U/W: the solid line is the solution in the absence of JT effect; the dotted line is the symmetric solution in the adiabatic limit; the dot-dashed line with heavy dots is the symmetry-broken solution in the adiabatic limit, and the dashed line is in the antiadiabatic limit. All results are for $n_s = 5$. Realistic values of U/W lie in the insulating side.

the insulating phase, both in the adiabatic and in the antiadiabatic limit. All the solutions have critical U's smaller that the range of realistic parameters. It is likely that the critical value for the real parameters is close to the orbitally-symmetric adiabatic solution. The Jahn-Teller interaction is not expected to only have a quantitative effect on the transition, shifting the critical U to smaller values, but also to qualitatively affect the nature of both the insulating and the metallic states. We expect in fact that the Mott insulating state, due to a strong suppression of the hopping, should be strongly reminiscent of the molecular physics. In the next section, inspection of the dynamical properties (spectral density, spin susceptibility, and optical conductivity) will help us to better understand the way the molecular limit is approached, and also to compute observable quantities.

2.6 Dynamical properties

We have shown that the e-e correlation in A_4C_{60} is strong enough to drive the system towards a Mott insulating state. One of the most striking successes of DMFT is the characterization of the mechanism of the transition, and of the intermediate coupling region. This technique is therefore the most appropriate to understand the details of the Mott transition in these compounds. It is reasonable to expect that, in the strong-coupling limit, the molecular physics should be recovered, but the actual physical parameters for K_4C_60 and Rb_4C_60 are not so large to put us deep in the molecular limit. The aim of this section is to provide insights on the way the atomic limit is recovered by increasing the coupling strength. As we have discussed previously, the inclusion of the Jahn-Teller effect is crucial for the proper description of the transition in the fullerides. Besides a quantitative effect on the critical U, described in the previous section, the Jahn-Teller effect has the much more relevant qualitative effect to render the groundstate of the isolated ion a non-degenerate singlet. This property can explain why the actual compounds are nonmagnetic Mott insulators, and it has relevant consequences on the Mott transition, as we will discuss in the next chapter. Throughout this section we will only consider the antiadiabatic limit for the Jahn-Teller effect, that represents the simplest regime from a computational point of view, and yields solution with the correct symmetry. The only drawback is that the optical and spin gap one obtains in the antiadiabatic limit are not close to the exact values for the single ion, in turn almost coincident with the experimental values. We believe that the mechanism leading to the recovery of the molecular physics in the Mott limit is basically independent on the details of the molecular spectrum, and that our antiadiabatic study can be generalized in a straightforward, though computationally heavy, way to a realistic case in which quantitative agreement

is expected.

To characterize the transition, we consider various dynamical properties that describe various experimental spectra: namely we computed the spectral function (photoemission), and the optical and spin response for different values of the interaction strength. It should be noted that there are some small problems with the evaluation of real-frequency dynamical properties within the DMFT. The whole formalism is in fact defined in imaginary (Matsubara) frequencies, and must be extended to the real axis. In QMC one needs to resort to analytical continuation schemes, like maximum entropy, that are usually not reliable when we are interested in delicate features of the spectra. In ED, no analytical continuation is necessary, and real-frequency properties can be computed without further approximation besides the truncation to a given number of orbitals n_s. The result of the truncation is that every spectral function is constituted by a series of δ-functions. This limits the amount of information we can extract, but still allows to draw relevant conclusions.

In the following calculations, We will consider different bandwidths for the three different levels to introduce the effect of the BCT lattice and mimic the realistic bandstructure: LDA calculations present in fact one band with large width $W \simeq 0.61$ eV and two narrower bands of width $W \simeq 0.35$ eV, as one expects in a BCT symmetry.

2.6.1 Spectral density

The first quantity we compute is the spectral density, proportional to the imaginary part of the Green's function, $\rho(\omega) = -1/\pi G(\omega)$. This function can be thought as a photoemission spectrum, taking into account transitions involving the creation or the destruction of a single electron. As a consequence, the allowed transition connect the $n = 4$ manifold with the $n = 3$ and $n = 5$ sectors, according to the selection rules $\Delta S = 1/2$ and $\Delta L = 1$. in Fig. 2.8 we show $\rho(\omega)$ as a function of U for fixed value of $J_H/W = -0.128$. We stress that this is not the correct way to describe the MIT under pressure in A_4C_{60}, since pressure has the effect to increase the overlap between the electronic wavefunctions, and consequently the hopping integral t. Therefore the transition occurs because U/t increases, but J_H/U stays constant, since all the interaction terms are local, and hence not affected by pressure. On the other hand, the choice of keeping J_H/t fixed assures that the position of the molecular multiplets is unchanged, and allows us to better follow their evolution as a function of U. Anyway, in the small range of parameters in which the system changes from metal to insulator, J_H should be only weakly rescaled. Therefore, the qualitative features of the transition are not expected to

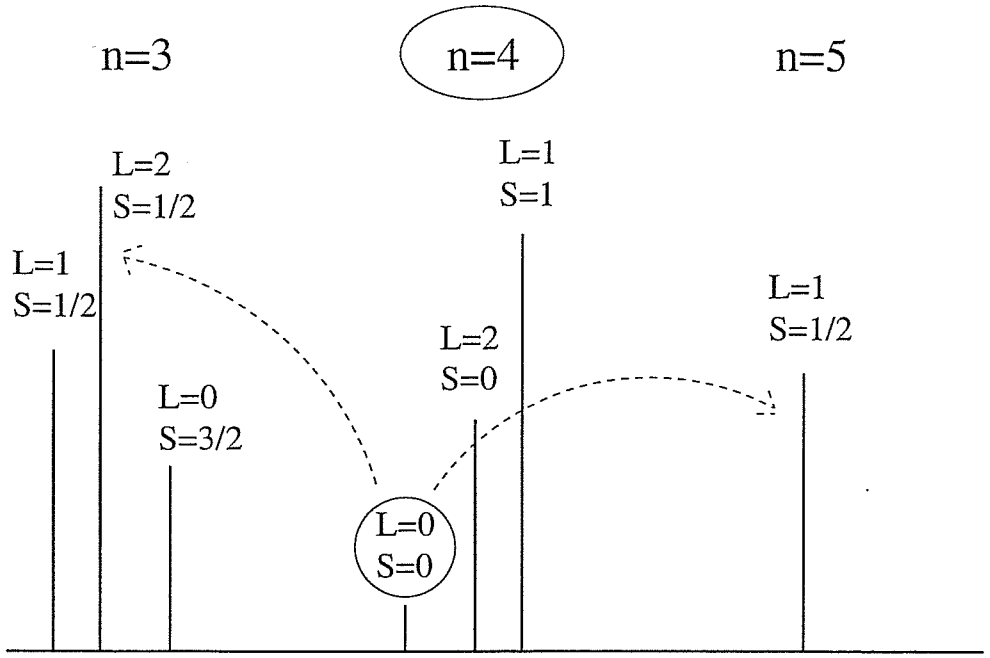

Figure 2.7: The Spectrum of an isolated C_{60}^{n-} ion for $n = 3, 4, 5$. The groundstate for $n = 4$ is non-degenerate ($S = 0$, $L = 0$), and only the transition to $S = 1/2$,$L = 1$ are allowed by the selection rules.

depend on the scaling of J_H.

To better understand the results, we report the spectrum of the single ion, for $n = 3, 4, 5$ in Fig. 2.7.

In the molecular limit, only two transitions are permitted, going from the $S = 0$, $L = 0$ groundstate for $n = 4$ to the $S = 1/2$,$L = 1$ states in the $n = 3$ and the $n = 5$ sectors. The transitions are denoted by dashed lines in the picture. As a result, the molecular Green's function is formed by two isolated peaks at energies $-U/2 - 5|J_H|$ and $U/2 + 5/3|J_H|$. These peaks are the equivalent of the peaks at $\pm U/2$ observed for the single band Hubbard model, but they are shifted by the other interaction terms.

As it can be seen in Fig. 2.8, for really large values of U (last two panels) the spectral density almost exactly coincides with the molecular one, with just a small broadening due to hopping processes. For these coupling values, the electrons are basically localized, four on each molecule, and the allowed transitions are the molecular ones. Since the spectral function is made by δ-functions, it is hard to measure the width of these peaks, but we can learn how to interpret these data comparing them with the single-band case. In that case, the spectral function in the extreme strong-coupling limit is composed by two bands of width W centered at $\pm U/2$. In ED this limit presented two

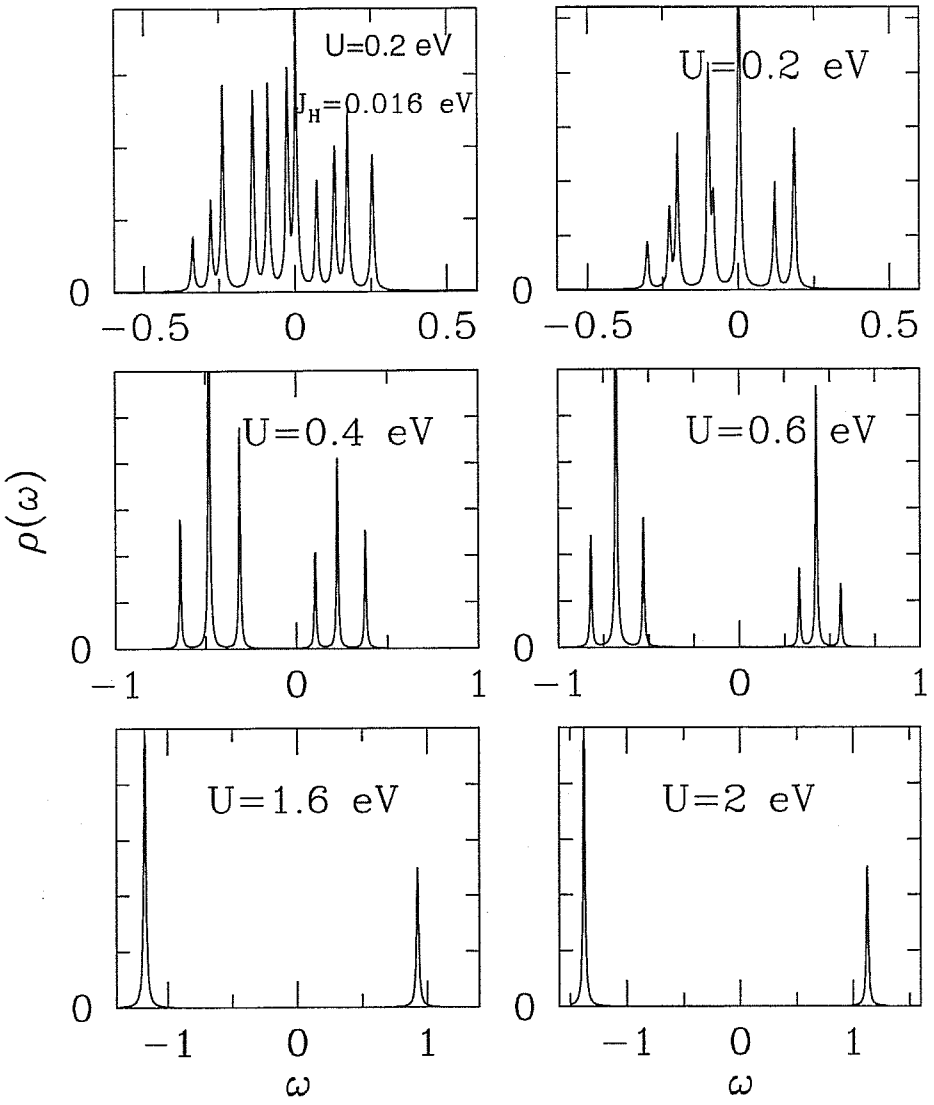

Figure 2.8: The spectral function $\rho(\omega)$ for various values of the interaction strength U (arbitrary units). Frequencies are expressed in eV. $J_H = -0.076$ eV except for the topmost left panel, where $J_H = -0.016$ eV. The two upmost panels display metallic solutions, all the others insulating solutions. The bandwidth is $W = 0.61$ eV.

large peaks at $\pm U/2$ surrounded both by two lateral peaks of smaller but visible weight, at distance $W/2$ from the large ones. In our case, the atomic peaks are undoubtedly much sharper, and the width is substantially smaller than the bandwidth. A strong motional line-narrowing occurs, due to the drastically reduced mobility of the molecular excitations[77]. By decreasing U, a broadening of the molecular excitations associated with a larger effective bandwidth occurs.

This situation, with the atomic peaks clearly present and only weakly broadened, persists down to relatively small values of U, just above the transition. As the correlation is strong enough to give an insulating groundstate, the spectral function displays evident molecular features. In the two upmost panels two metallic solutions for small U are shown. In the right one we show a metallic solution for $U = 0.2$ eV, but with unscaled $J_H = -0.076$ eV, in which the ratio J_H/U is unphysically large. Though unphysical, this case allows to observe a persistence of the molecular peaks in the metallic phase. This property is not so evident here in the spectral function, but it is much more evident in the spin and optical response functions we present in the subsequent sections. In the left upmost panel, the metallic solution is instead computed for suitably rescaled $J_H = -0.016$ eV, such that $J_H/U = -0.08$. The molecular features are now much less evident, but they can still be identified (see, also in this case, the other response functions). Note that, while the positions of the molecular excitations with respect to $\pm U/2$ is the same for all the calculation with fixed J_H, here they are shifted to much lower energies.

2.6.2 Spin susceptibility

The analysis of the spectrum in our DMFT solution has suggested that the molecular physics is almost immediately recovered in the insulating state and that traces of the ionic features can be seen already in the metallic state. In this section and the following, we compute observable quantities, to understand whether the recovery of the molecular limit is limited to the features of the spectrum, or it extends to experimentally accessible quantities like the spin- and optical-gaps. We start from the magnetic response. We notice that, if we want to compare our results with a spin-gap measured by NMR, we cannot simply consider an orbital-diagonal spin susceptibility, that takes into account the spin transitions within the orbitals, and is not able to measure the inter-orbital magnetic transitions, but a more complicated quantity, taking into explicit account the spin response on each C atom.

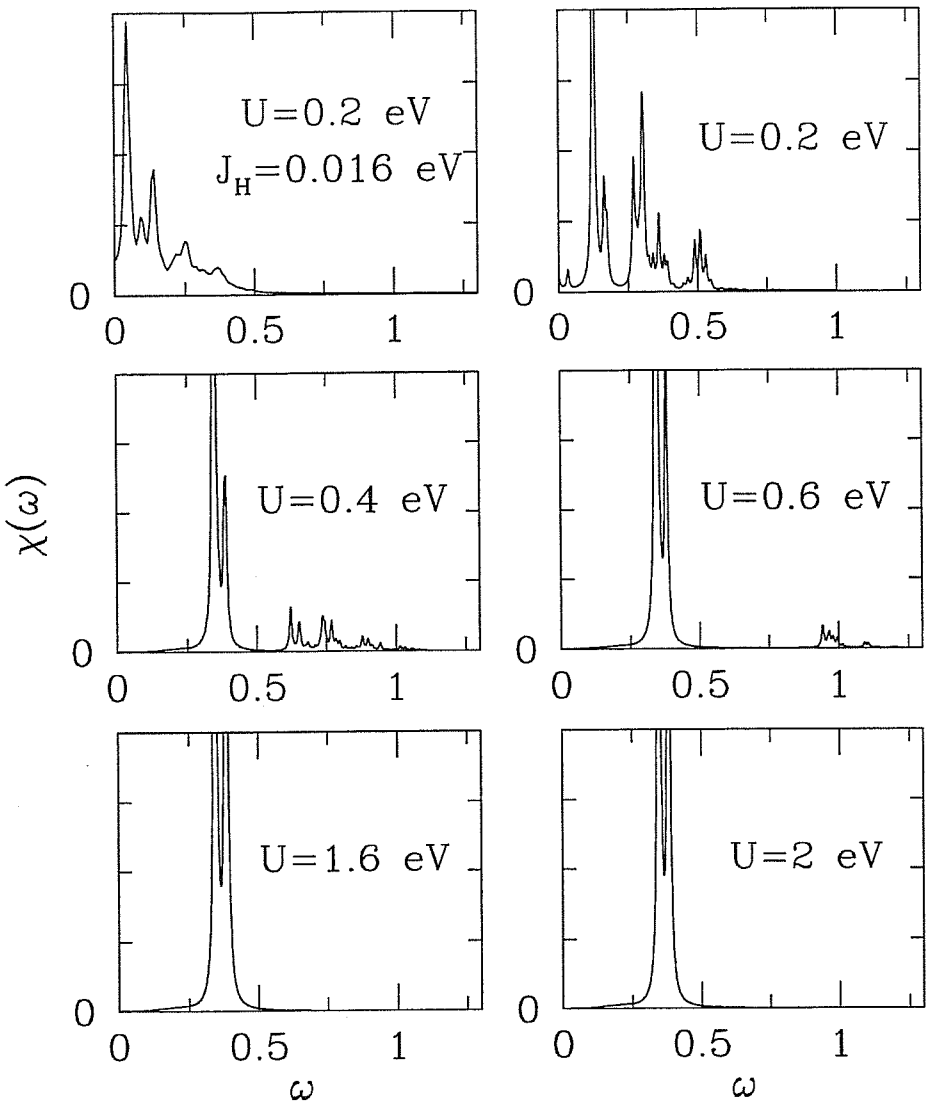

Figure 2.9: The spin susceptibility $\chi(\omega)$ given by Eq. (2.15) (arbitrary units). The parameters are the same as in Fig. 2.8. The two upmost panels are metallic solutions, and the others are insulating.

We computed

$$\chi(\omega) = \sum_{R=1}^{60} \mathcal{I}m \sum_{n=0}^{\infty} \frac{|\langle \phi_n | S_z^R | \phi_0 \rangle|^2}{\omega - (E_n - E_0) + i\delta}. \tag{2.15}$$

Where $|\phi_n\rangle$ and E_n are the eigenfunctions and eigenvalues, and S_z^R is the z component of the spin operator on site $R = 1, \ldots, 60$ on a given C_{60} molecule. The operator is related to the creation and annihilation operators for the orbitals by the relations

$$\begin{aligned} S_z^R &= c_{R\uparrow}^\dagger c_{R\uparrow} - c_{R\downarrow}^\dagger c_{R\downarrow} \\ c_{R\sigma} &= \sum_\alpha u_{R\alpha} c_{\alpha\sigma}, \end{aligned} \tag{2.16}$$

where $u_{R\alpha}$ are the coefficients of the α-th orbital wavefunction in the coordinate representation. $\chi(\omega)$ is shown in Fig. 2.9 for the same values of U and J_H as in Fig. 2.8. Also for this quantity, the recovery of the molecular physics in the insulating state is sudden, all the four insulating solution (lower panels) basically present a single structure at the same energy, associated to the transition from the molecular singlet groundstate ($S = 0$, $L = 0$) to the first triplet state ($S = 1$, $L = 1$) within the $n = 4$ sector. The presence of two close, almost coincident, peaks within this structure is probably due to the use of different bandwidths. The spin-gap calculated within DMFT in the insulating state is basically given by the molecular value. Analogously to the spectral density, the metallic solutions also display some reminder of the molecular spectrum. This is more clearly seen in the metallic solution with unscaled J_H (topmost right panel), but it is also present in the solution with rescaled J_H (topmost left panel).

2.6.3 Optical conductivity

As a last point, we also computed the real part of the optical conductivity $\sigma(\omega)$, which is given, within the DMFT, by[78, 79]

$$\sigma(\omega) = \frac{1}{\omega} \frac{2e^2 t^2 a^2}{\hbar V} \int_{-\infty}^{\infty} d\varepsilon D(\varepsilon) \int_{-\infty}^{\infty} d\omega' \rho(\varepsilon, \omega') \rho(\varepsilon, +\omega' + \omega) [f(\omega') - f(\omega' + \omega)]. \tag{2.17}$$

Where e is the electron charge, V the volume of the unit cell, a the lattice constant, $\rho(\varepsilon, \nu) = -1/\pi \mathcal{I}mG(\varepsilon, \nu + i0^+)$, $D(\varepsilon)$ is the non-interacting DOS and $f(\omega)$ is the Fermi function. The results are organized on the usual way in Fig.2.10. Also in this case, the insulating state has always the molecular character, i.e. a large gap to the first charge transition, and high-energy features at energies of order U, while the metallic solutions, besides a clear weight at zero-frequency (Drude weight), present some trace of the molecular spectrum. As usual, we show a metallic solution with non-scaled J_H

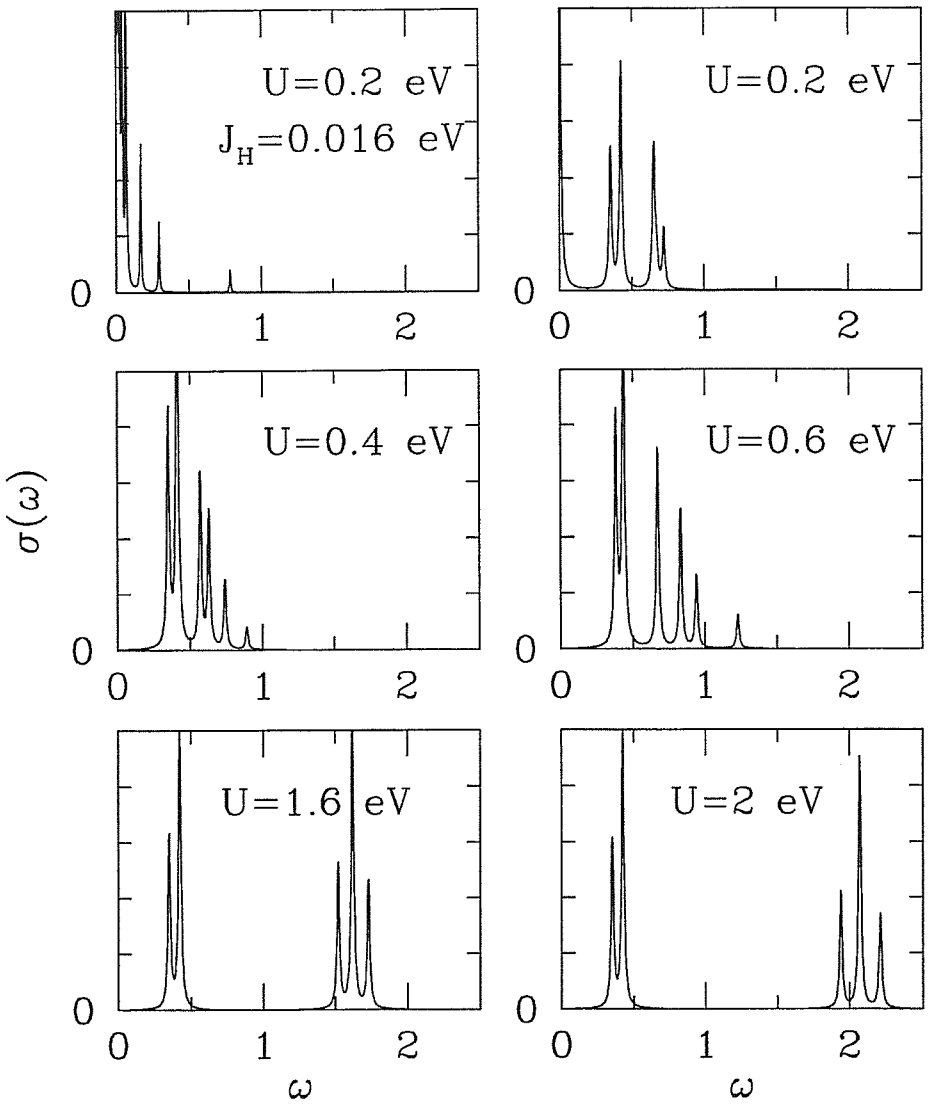

Figure 2.10: The optical conductivity $\sigma(\omega)$ given by Eq. (2.17) (arbitrary units). The parameters are the same as in Fig. 2.8. The two upmost panels are metallic solutions, and the zero-frequency Drude weight is visible, and the others are insulating.

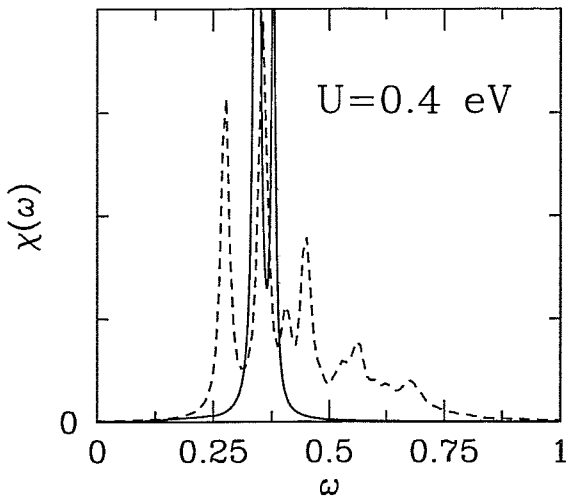

Figure 2.11: Comparison between the spin susceptibilities $\chi(\omega)$ (arbitrary units) for the Mott insulator (solid line), and the band insulator (dashed line) for $U = 0.4$ eV and bandwidth $W = 0.61$ eV. The width of the insulating susceptibility is roughly given by the bandwidth.

in which the molecular features are clearly visible, and a solution with rescaled J_H. The charge-gap is then also almost coincident with its molecular value.

2.7 Comparison with a band insulator

The orbitally symmetric solution, representative of a genuine Mott insulator with no broken-symmetry, does always show a sudden recovery of the molecular physics for all couplings large enough to give an insulating state. We can ask ourselves if the recovery of the molecular features is peculiar to the Mott state, or if this property is shared by some band insulator. The best way to mimic a sort of band insulator within the DMFT is to let the different orbitals free to have different Green's functions and Weiss fields. In other words, $\tilde{\varepsilon}_{k\alpha\sigma}$ and $V_{k\alpha\sigma}$ are no longer α independent. We considered solutions in which two of the three orbitals are equivalent and favoured. This solutions represent a band insulator within DMFT. In Fig. 2.11 we compare the spin susceptibility $\chi(\omega)$

for this solution and for $U = 0.4$ eV with the corresponding symmetric solution. The spectrum for the band insulator is much broader than for the Mott insulator, and the molecular peak is basically washed out in a wide feature. Notice also that the width of the feature is of the order of the bandwidth for the band insulator, in which the motional line-narrowing can not take place.

2.8 Discussion and conclusions

The insulating state of K_4C_{60}, not reproduced by LDA calculations even when allowing a collective JT distortion, may instead be explained as a Mott-Jahn-Teller state, where both inter-orbital and intra-orbital electron-electron correlations on one side, and electron-phonon coupling on the other side, play an essential role. The electron-electron correlation drives the originally metallic system close to a Mott insulating phase. The critical value for this paramagnetic MIT is first of all lowered by Hund's rule coupling, a mechanism absent in the band calculations, where Hund's rule can only stabilize a magnetic insulator. Introduction of JT coupling further stabilizes the paramagnetic insulating state, through a distortion, which splits the orbital degeneracy as in molecular C_{60}^{4-}[66]. The stabilization of the insulating phase due to the JT coupling is completely general, and occurs either if the JT effect is dynamical, or if it static and cooperative. The inclusion of the proper molecular physics (multiplet-exchange and JT effect) allows us to conclude that K_4C_{60} and Rb_4C_{60} are safely on the insulating side of the transition. Furthermore, the JT effect makes the molecular groundstate a singlet.

The close, apparently accidental, agreement between the spin and optical gaps of C_{60}^{4-}, 0.1 and 0.5 eV, with experimental optical and spin gaps in K_4C_{60} and Rb_4C_{60} acquires a strong physical significance in this light. It represents possibly the strongest spectroscopic evidence in qualitative favour of a Mott-Jahn-Teller state for these compounds. Suppose in fact we considered them band insulators, for example by trusting the TBHF results, or devising some other method of band structure calculation, such as GW[80], which yields an insulating state associated with a stable static collective JT state. In any such band state, the equilibrium collective JT distortion magnitude would have to be substantially smaller than that of the isolated molecular ion, due to band structure quenching: electrons leaving the molecule too frequently in order to hop on other molecules, must weaken the average on-site JT effect. In that case, the predicted optical and spin gaps would be much smaller, corresponding to the delocalization, or spill-out, of the band Wannier function. In a band state, it should not be possible for optical and spin gaps to be of molecular magnitude, as one instead observes. In the Mott state, on

the other hand, the electron spill-out to neighbouring molecules is reduced to order t/U, which is very small. The state on each lattice site is much closer to an isolated ion, since the probability to find a molecular site with three or with five electrons is only of order t/U, instead of order 1/4 as in a delocalized band state. This suggests that molecular multiplets will be much more preserved in the Mott-Jahn-Teller state than in the band state.

This expectation is strongly substantiated by a DMFT analysis of the dynamical response functions of the system. As a general trend, all the response functions basically acquire a molecular behaviour as soon as we enter the Mott insulating state.

The results of a complete DMFT study of the problem allow to safely conclude that the BCT A_4C_{60} are not conventional band insulators, and that both strong correlations and JT effects are crucial for their understanding. The realistic parameters are such that the system is deeply in the insulating region of the phase diagram. The observed spin and optical gaps find a simple explanation in a Mott insulator, and are strikingly recovered in a DMFT calculation. A traditional Mott insulator (i.e. without the help of the JT effect), would be magnetic, since the total spin would be $S = 1$ for each molecular ion, in virtue of Hund's rule. That is in contrast with the clear nonmagnetic, spin-gapped state of these insulators. In our proposed Mott-Jahn-Teller state, inter- and intra-orbital electron correlations drive the Mott insulating state, while a conspiring JT distortion makes the groundstate a singlet. That, incidentally, suggests that also the n=3 superconducting fullerides, whose bandwidth is quite similar, are most likely close to a strongly correlated state [51, 49]. In the next chapter we show that the critical U for a Mott-insulating state is larger for $n = 3$ than for $n = 4$, so that an insulating A_4C_{60} is compatible with a metallic A_3C_{60}. Moreover, the eventual Mott-insulating state of A_3C_{60} would be an antiferromagnet arising from an $S = 1/2$ molecular state. Such a state would be frustrated by the FCC crystal structure of the trivalent fullerides, thus favouring the metallic state. Despite they are not able to drive the system towards an insulating state, the electron-electron correlations are expected to be relevant in the physics of the A_3C_{60}.

Chapter 3

The Mott-Hubbard transition in orbitally degenerate systems

The Single-Band Hubbard Model (SBHM), in its archetyp simplicity, represents an idealized framework for the study of the competition between the electron motion and the electron-electron correlations. This model has provided many insights about the mechanism ruling the Mott transition, but it may appear hazardous to use the results of the SBHM to make quantitative comparisons or predictions regarding real Mott insulators. In fact the orbitals involved in the transition are usually narrow bands arising from degenerate electronic levels.

Nevertheless, once the DMFT has provided a reliable tool to compute static and dynamical properties for the SBHM, it was hard to resist the temptation to quantitatively compare these quantities with the experimental findings for various transition-metal oxides. The success of this comparison was remarkable and, to some extent, surprising. Among the experimental features that are well described by the SBHM, we mention the doping dependence of the electron effective mass and of the specific heat in $La_xSr_{1-x}TiO_3$, that is quantitatively reproduced by using the values of U and W extracted from photoemission data [81], the temperature dependence of optical conductivity of V_2O_3[82] and the spectral properties of $Sr_{1-x}Ca_xVO_3$ [83]. The quantitative agreement between model calculations and experimental data is surprising, if one considers that the electrons of $La_xSr_{1-x}TiO_3$ reside in a quasi-threefold degenerate level, and that the most simplified description of the two electrons in the threefold degenerate t_{2g} levels of V_2O_3 involves a twofold degenerate model[84].

The ability of the SBHM to capture the non-trivial features of real material is even more astonishing if one reminds that the inclusion of orbital degeneracy does not simply introduce additional degrees of freedom, but it also prompts for the inclusion of other

physical effects (multiplet exchange and Jahn-Teller interaction) that are not accounted by the single-band model.

On the opposite side, we have described at length a class of systems for which the SBHM is not able to reproduce even the qualitative features, namely the alkali-doped fullerides. A complete description of the insulating state and of the MIT in A_4C_{60} requires a substantially more involved model. On one hand, the threefold orbital degeneracy has a relevant quantitative effect on the location of the MIT; more significantly, the inclusion of the multiplet-exchange splitting and of the Jahn-Teller interaction is crucial to describe a nonmagnetic insulating state in agreement with experiments. Also the different behaviour between the superconducting half-filled fullerides and the insulating tetravalent parent compounds is not predictable on the basis of the SBHM.

In summary, while some compounds require the inclusion of orbital degeneracy and of the related physical interactions, other systems can be well described by a SBHM, despite all the materials share similar electronic structures. This chapter considers the orbitally degenerate model in more general terms, and represents an attempt to understand the reasons for the different behaviour of different classes of compounds. The scenario for the Mott-Hubbard transition put forward within the DMFT is critically discussed in the light of the results for the degenerate model.

As a first relevant topic, we consider the simple threefold degenerate Hubbard model in the absence of further inter-orbital local interactions. This study represents a necessary starting point for a systematic analysis, and allows us to extract the effect of the orbital degeneracy alone on the Mott-Hubbard transition. This effect is expected to be mainly quantitative. In this simpler limit we also study the dependence upon filling of the critical U for the Mott transition [1]. This effect is shown to be at least a partial reason for the different behaviour between the superconducting trivalent and the insulating tetravalent fullerides.

Then we reconsider the inter-orbital interaction terms we introduced in the previous chapter, namely a threefold degenerate Hubbard model, with a negative multiplet-splitting term (2.3). The latter may be thought as arising from an antiadiabatic Jahn-Teller effect, leading to the inversion of the Hund's rule multiplets. From a theoretical point of view, such an inversion has a relevant qualitative effect. As we have seen in Par. 2.3, in the atomic limit the groundstate for $n = 4$ (or $n = 2$) is a non-degenerate orbital and spin singlet. This means that computing only paramagnetic solutions we are able to follow the groundstate across the transition. The MIT occurs within the paramagnetic

[1] In presence of a number of degenerate levels, the Mott transition does not occur only for an half-filled band, but for every integer filling, i.e. when the number of electrons per site is integer.

sector, and we do not need to describe the competition between paramagnetic and antiferromagnetic phases. Moreover, the non-degeneracy of the atomic limit implies that the Mott insulator is a zero-entropy state. Therefore, the insulator-to-metal transition can not be described as a Kondo screening of spin (or orbital) degeneracy. The consequences of this property on the scenario of the Mott-Hubbard transition put forward by Kotliar and coworkers will be discussed.

We emphasize that the possibility of a zero-entropy insulator is limited to the $n = 4$ (or $n = 2$) case if some effect inverts the atomic multiplets. For negligible inter-orbital interactions, or if the positive Hund's coupling is not overcompensated by a large Jahn-Teller effect, of finally if the number of electrons does not allow for a non-degenerate singlet (for $n = 3$ or $n = 1$ the odd number of electrons does not allow for a singlet state; see Appendix A), the Mott insulating state is expected to have a finite entropy per site, as in the single-band case.

3.1 Previous Results

In this section we try to present in a compact way various results appeared in literature regarding the orbitally degenerate Hubbard model. In the presence of degenerate orbitals one can define the Hubbard Hamiltonian as

$$\mathcal{H} = -\sum_{\substack{\langle ij \\ \rangle \alpha\beta\sigma}} t_{ij}^{\alpha\beta} (c_{i\alpha\sigma}^{\dagger} c_{j\beta\sigma} + h.c.) + U \sum_{i} \frac{n_i(n_i+1)}{2}, \tag{3.1}$$

where $n_i = \sum_{\alpha\sigma} c_{i\alpha\sigma}^{\dagger} c_{i\alpha\sigma}$ is the total density operator on site i, and $c_{i\alpha\sigma}^{\dagger}$ ($c_{i\alpha\sigma}$) is the creation (destruction) operator for an electron of spin σ on site i and orbital α, with $\alpha = 1, \ldots, N_{deg}$, being N_{deg} the number of degenerate levels. The hopping amplitudes $t_{ij}^{\alpha\beta}$ from site i to j are usually taken diagonal in the orbital indices and independent on the particular nearest-neighbours pair $t_{ij}^{\alpha\beta} = t\delta_{\alpha\beta}$. The filling ranges from 0 to $2N_{deg}$. $n = 0$ and $n = 2N_{deg}$ clearly describe (trivial) band insulators, while for intermediate integer fillings, the Mott phenomenon can occur, exactly as for an half-filled SBHM.

The discovery of superconductivity in the trivalent fullerides has been one of the driving forces for the investigation of the degenerate Hubbard model. Soon after the discovery of these materials, it turned out that the electron-electron correlation ($\sim$ 1–1.5 eV)[49] was significantly larger than the bandwidth ($\sim$ 0.5 eV) (see Sec. 2.2). On the basis of a SBHM, the ratio between correlation and the bandwidth would imply a Mott insulator, in strong contradiction with the metallic properties.

In really general terms, one can expect that the increased number of degrees of freedom leads to an enhanced effective hopping amplitude with respect to the SBHM, leading to a stabilization of the metallic phase with respect to the insulator. The results we report in the following substantiate this naive expectation. One of the first calculations aiming to characterize the dependence of the critical U upon the number of degenerate levels N_{deg} has been performed in Ref. [85], where the Gutzwiller approximation predicted that at half-filling $U_c(N_{deg}) \approx (N_{deg}+1)U_c$. The enhancement of the effective hopping is really strong within this approach, and such an effect was invoked to explain why the half-filled A_3C_{60} solids are metallic. The factor $N_{deg}+1 = 4$ would in fact safely put the half-filled fullerides on the metallic side of the transition.

Later, Gunnarsson, Koch, and Martin[52, 51] suggested that the dependence of U_c upon N_{deg} should be much weaker. Using a strong coupling argument that we describe in details in Sec. 3.2, suggested that U_c should behave like $U_c(N_{deg}) \simeq \sqrt{N_{deg}}W$, where W is the full bandwidth. These authors have also compared their predictions with Fixed-Nodes Quantum Monte Carlo results for three-dimensional systems on a FCC lattice suitable for A_3C_{60}, finding a good agreement[51]. Han, Jarrell and Cox have systematically studied the transition at half-filling for different N_{deg} using the QMC solution of the DMFT equations [53]. They also introduced the exchange term, which in the case of a threefold degenerate model can be written as (see Chapter 2, and more specifically Sec. 2.3, for more details)

$$\mathcal{H}_{m-e} = \frac{2J_H}{3}\sum_{\alpha} n_\alpha^2 - \frac{2J_H}{3}\sum_{\alpha<\beta} n_\alpha n_\beta + \frac{J_H}{2}\sum_{\alpha<\beta}\Delta_{\alpha\beta}^2, \tag{3.2}$$

where $\Delta_{\alpha\beta} = \sum_\sigma (c^\dagger_{\alpha\sigma}c_{\beta\sigma} + h.c.)$. For technical reasons the authors were not able to treat the non-diagonal contributions to Eq. (3.2). They arrive to the following approximate expression for the critical U at half-filling[2]:

$$U_c(N_{deg}, J) \approx \sqrt{N_{deg}}U_c(1,0) - \frac{N_{deg}J_H}{6}. \tag{3.3}$$

The effect of the exchange coupling is simply to decrease the critical interaction strength for the MIT. This effect can be understood as a partial quenching of the orbital degeneracy due to the multiplet exchange. Quite naturally, J_H is assumed positive, as it turns out from molecular physics in order to give rise to the correct Hund's rules. A negative J_H arises from an antiadiabatic treatment of the strong Jahn-Teller interaction of the C_{60} molecule.

[2]There is a factor 6 between their definition The effect of the exchange coupling is simply to f J, and our J_H.

The effect of band-filling at fixed number of degenerate levels has been investigated by means of the DMFT by Rozenberg [86] and Kajueter and Kotliar [87] for the $N_{deg} = 2$ case, and by Koch *et al.* [88] for $N_{deg} = 3$. The DMFT investigation carried out in Ref. [86], together with Ref.[87]

The analysis of Ref. [86] accounts for the successive MITs at integer fillings, and finds that the metallic phase is more stable for the half-filled case, being $U_c(n = 2) > U_c(n = 1) = U_c(n = 3)$. The qualitative features of each transition are analogous to the single-band case, with two critical couplings for the disappearance of the insulating (U_{c1}) and the metallic (U_{c2}) solutions. Exactly as for the SBHM, $U_{c1} < U_{c2}$, and the metallic solution is always energetically favoured at $T = 0$[87]. Moreover, besides a qualititative independence on the number of levels, it has been found that certain low-energy quantities like the effective mass, for one electron per site, depend in a weak way on the band degeneracy. The effect of the degeneracy is strong only for the high-energy features. The absence of qualitative differences between the single-band model and the degenerate model for $J_H = 0$ rationalizes why the properties of systems like $La_xSr_{1-x}TiO_3$, V_2O_3 and $Sr_{1-x}Ca_xVO_3$ can be well described by the single-band model[82, 83]. We report a schematic phase diagram from Ref.[86] in Fig. 3.1. In Ref.[87] the qualitative effect of the multiplet-exchange coupling is described. In agreement with [53] J_H is found to lower the critical coupling.

It is a little more difficult to extract general informations on the doping dependence from Ref. [88]. In this work Fixed-Nodes QMC simulations are performed on a FCC lattice, which frustrates the magnetic ordering, but are not restricted to the paramagnetic sector as the DMFT results described above. Moreover, the hopping parameters are chosen in order to realistically represent the electronic bands of A_3C_{60}. the result is that $n = 3$ has the largest critical U, and that $n = 2$ and $n = 4$ are no longer equivalent since the FCC lattice breaks particle-hole symmetry. As a result U_c for $n = 4$ is higher than $n = 2$ and much closer to the one for $n = 3$. Real A_4C_{60} compounds have indeed a BCT structure, where the critical correlation is lower. We finally mention the exact diagonalization of the threefold degenerate Hubbard model on four-site clusters by Mahadevan and Sarma also aiming to describe A_3C_{60}[89], that find the same qualitative behaviour of [88], with the exception that $n = 2$ has a large critical coupling than $n = 4$. The discrepancy with Ref. [88] is probably due to the absence of frustration. The general trend indicated by all the results we reported is anyway still evident, being U_c largest for the half-filled system, and decreasing moving away from it. These tendency can be rationalized with a simple strong-coupling argument we report in the subsequent section. In the next sections we give a comprehensive picture of the Mott transition for $N_{deg} = 3$

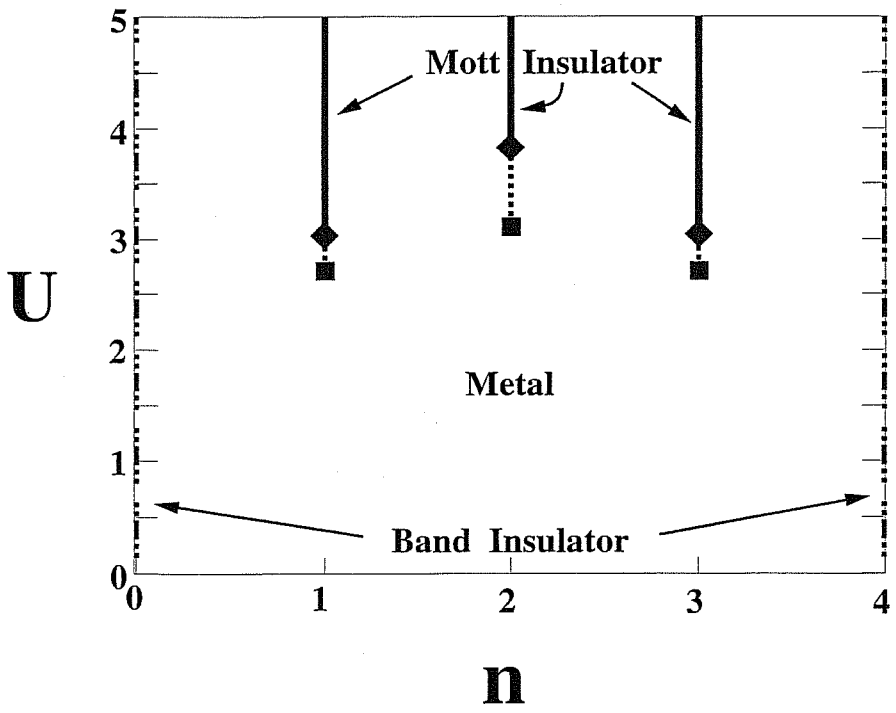

Figure 3.1: Phase diagram in the $U - n$ plane for the paramagnetic solutions of the doubly degenerate Hubbard model. The MITs at $n = 1, 2, 3$ end with critical points. Diamonds indicate the $T = 0$ critical points, and the squares the finite temperature critical point ending the transition line. Solid line are for the Mott insulating state. (From Ref. [86])

within the DMFT, that completes the picture drawn in this paragraph.

3.2 The threefold degenerate Hubbard model: Dependence on filling

In this section we consider the simplest Hubbard model with degenerate levels, i.e. we neglect every further inter-orbital interaction and electron-phonon term. Namely, we study Hamiltonian (3.1) with orbital-diagonal nearest-neighbours only hopping $t_{ij}^{\alpha\beta} = \delta_{\alpha\beta}t$. In particular we concentrate on the dependence of the critical U upon the (integer) filling for the $N_{deg} = 3$ case, which is relevant for the doped fullerides, but also for V_2O_3.

3.2.1 A Strong-coupling argument

Koch, Gunnarsson and Martin [52, 51, 88] have proposed a general intuitive strong-coupling argument to estimate the dependence of the critical U upon the number of degenerate levels and the filling. The MIT can be associated with the opening of a conduction gap given by

$$E_g = E(N+1) - 2E(N) + E(N-1),$$

where $N = nN_s$ is the number of electrons, and N_s the number of sites. An estimate of E_g can be given in strong-coupling. In this limit, n electrons occupy each molecule, and the energy is

$$\frac{E(N)}{N_s} = \frac{n(n-1)}{2}U + \mathcal{O}(\frac{t^2}{U}). \tag{3.4}$$

In the states with $N = nN_s \pm 1$, the extra-electron or hole can hop without creating further double occupancies. In presence of orbital degeneracy, the groundstate for a single electron or hole is not given by the Nagaoka state, but AFM alignment is favoured, since it allows for more hopping channels. Fig. 3.2 clearly shows for $n = 3$ that in the ferromagnetic case a), only one channel is possible, whereas for the antiferromagnetic case b), three channels are available.

An estimate of the effective hopping matrix element in this regime gives $H_{ij} = \sqrt{k}t$, where k is the number of hopping channels connecting sites i and j. Being $\sqrt{k} \geq 1$, the hopping is always enhanced with respect to the single-band model. The gap is given by

$$E_g = U - (\sqrt{k_{N+1}} + \sqrt{k_{N-1}})W/2, \tag{3.5}$$

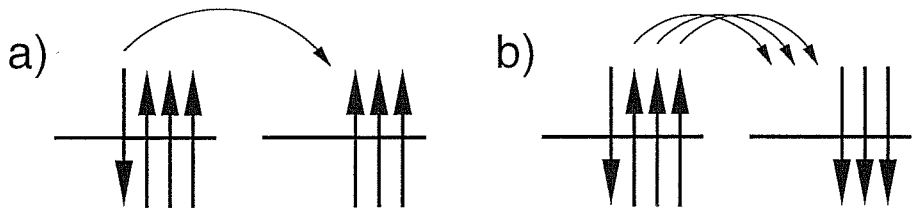

Figure 3.2: Sketch of the possible hoppings of an extra electron against an integer-filled background with $N_{deg} = 3$ and filling $n = 3$. (from Ref.[88]) a) ferromagnetically aligned neighbour: Only one electron can hop. b) antiferromagnetically aligned neighbour: There are three hopping channels ($k = 3$).

where $k_{N\pm1}$ is the number of available hopping channels for the state with $N \pm 1$ electrons. Computing the number of available hopping channels for every filling and number of degenerate levels, we can estimate a critical value for the MIT, obviously given by the value for which E_g vanishes

$$U_c = (\sqrt{k_{N+1}} + \sqrt{k_{N-1}})\frac{W}{2}. \tag{3.6}$$

At half-filling, the increased number of channels pushes the transition to stronger-coupling if N_{deg} is increased. Since at half-filling we have $k_{N+1} = k_{N-1} = N_{deg}$ (see Fig.3.2), we obtain

$$U_c(N_{deg}) \simeq \sqrt{N_{deg}} U_c(1).$$

Keeping N_{deg} fixed and varying n, we obtain that the largest U_c is for the half-filled band and that the value decreases by increasing the distance from half-filling. Koch, Gunnarsson and Martin also performed Fixed-Nodes Quantum Monte Carlo calculations for $N_{deg} = 3$ on a FCC lattice, confirming the qualitative behaviour as a function of filling given by Eq. (3.6)[88]. The values obtained in QMC are actually larger than the strong-coupling estimates. This is not surprising, because the strong-coupling argument is naturally biased in favour of the insulating state, leading to an underestimate of U_c.

3.2.2 DMFT results

In this section we perform a DMFT investigation of the $N_{deg} = 3$ extended Hubbard model of Eq. (3.1). As in Chapter 2, we choose the ED method to perform a quantitative study of the DMFT equations. As usual, we characterize the Mott transition following the evolution of the spectral density by increasing the correlation strength at fixed electron filling. We consider all the independent fillings $n = 3, 4, 5$. Our result perfectly confirm the expectations that arise from the previous data for the half-filled model with

filling	k_+	k_-	U_c/W [Eq.(3.6))]	U_c/W [DMFT]
n=3	3	3	$\sqrt{3} \simeq 1.73$	2.13
n=2	3	2	$\frac{\sqrt{3}+\sqrt{2}}{2} \simeq 1.57$	1.92
n=1	2	1	$\frac{\sqrt{1}+1}{2} \simeq 1.21$	1.44

Table 3.1: Effective hopping enhancement factors for the different filling for $N_{deg} = 3$. In the last column we report our DMFT results for U/W

$N_{deg} = 3$ and for different densities for $N_{deg} = 2$. All the various transitions present the same qualitative features of the SBHM. The transition is associated with the divergence of the effective mass, which is in turn equivalent to the vanishing of the quasiparticle weight Z, given by Eq. (2.14). As usual, we label by U_{c2} the correlation for which Z vanishes. To compute U_{c1}, in which the insulating solution disappears we have followed the insulating solution beyond its region of stability, until the insulating gap closes. The zero-temperature metal-insulator transition coincides with U_{c2}, because the metallic solution is always energetically favoured in the coexistence region [3]. The critical values found are reported in Fig. 3.3.

The qualitative behaviour agrees with Eq. (3.6), being U_c largest for the half-filled case, and decreasing by moving away from half-filling. We also notice that the coexistence region (dotted line) is much larger in the half-filled case. We can make a more quantitative comparison with Eq. (3.6). The k coefficients for $N_{deg} = 3$ are reported in Tab. 3.2.2, together with the overall hopping enhancement factors, and the results from DMFT. If we rescale the critical U obtained for $n = 3$ with the suitable factors, we obtain the values shown in Fig. 3.3 as open dots. The comparison with the actual results from DMFT shows that the trend as a function of n is well described by the strong-coupling result.

The evolution of the spectral density across the transition for our typical reference case $n = 4$ is shown in Fig. 3.4 and displays the usual features. The metallic behaviour appears as a Kondo-like resonance at the Fermi-level in the middle of the preformed charge gap. The behaviour for $n = 3$ and $n = 5$ is completely analogous. In the absence of J_H, there is no substantial difference between the different integer fillings. In all cases the atomic limit has a finite entropy per site. In particular, also $n = 4$ has a degenerate Mott-insulating limit. As a consequence, the birth of a metallic state can be interpreted as a Kondo effect. We note that the strong-coupling argument by Koch *et al.* [52, 88] can be reinterpreted in this light. The number of available hopping channels in

[3] The argument given in Ref. [40] holds also in the presence of orbital degeneracy.

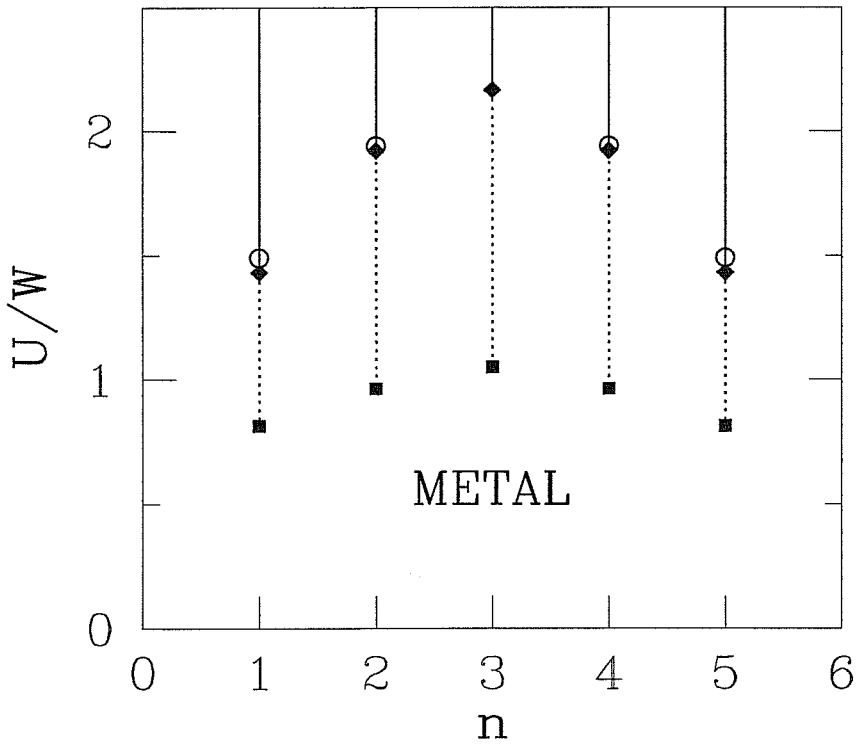

Figure 3.3: Phase diagram in the $U - n$ plane for the paramagnetic solutions of the threefold degenerate Hubbard model. The MITs at $n = 1, 2, 3, 4, 5$ end with critical points. Diamonds indicate the $T = 0$ critical points, in which the metallic solution disappears (U_{c2}), and the squares denote U_{c1}, in which the insulating solution becomes unstable. The solid lines are the regions in which the Mott insulator is stable, whereas the dotted lines indicate the coexistence region between the Mott insulator and a correlated metal. The open dots compare the DMFT results with the prediction of Eq. (3.6). The rest of the diagram has a metallic solution. The $n = 0$ and $n = 6$ lines are band-insulators.

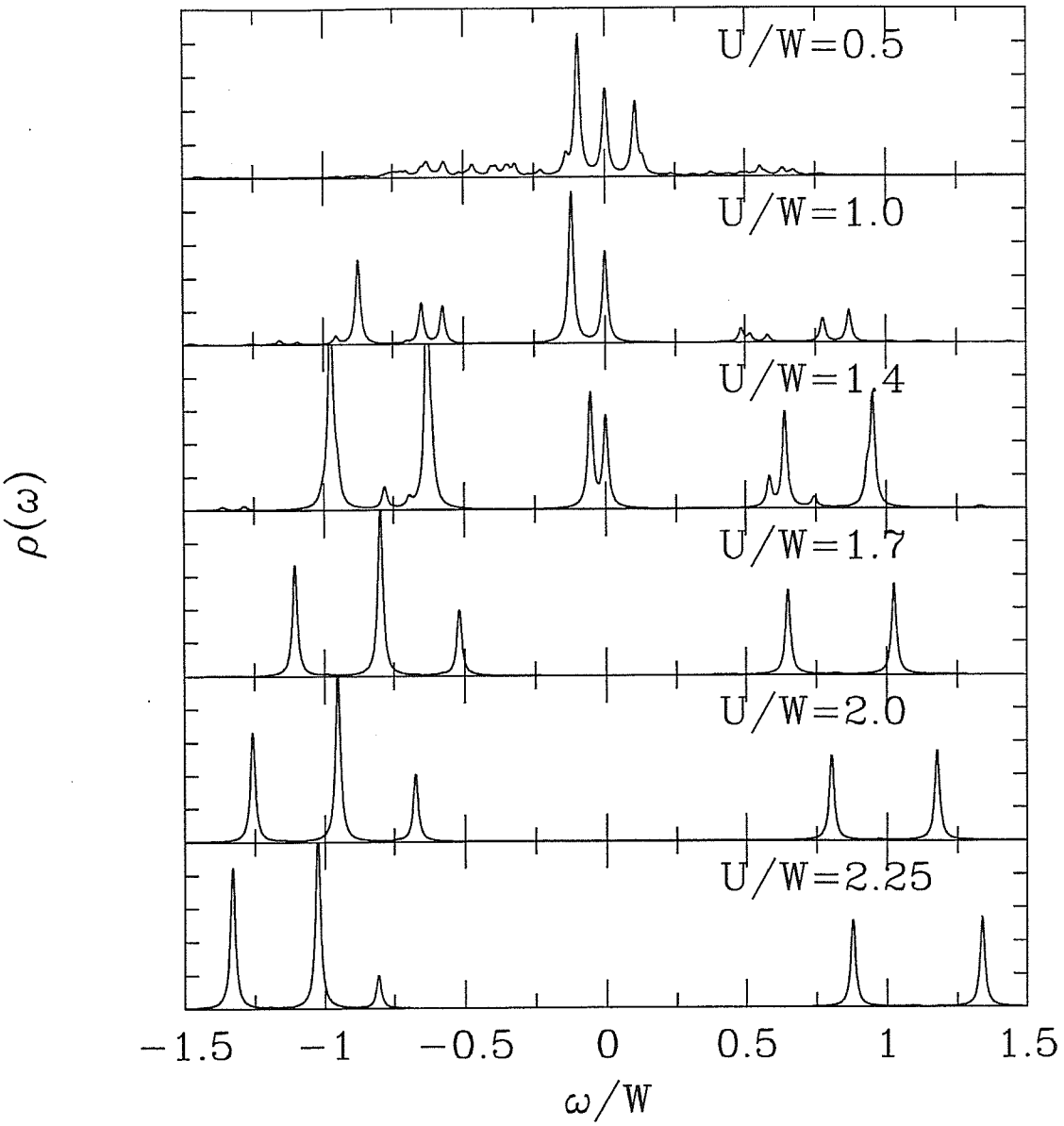

Figure 3.4: The evolution of the spectral density $\rho(\omega) = -1/\pi \mathcal{I}mG(\omega)$ for $n = 4$ and for $J_H = 0$. Clearly, the three top solutions are metallic and the bottom ones are insulating. $\rho(\omega)$ is expressed in arbitrary units.

the presence of orbital degeneracy is clearly related to the entropy per site in the atomic limit $t = 0$. Therefore, if a given filling has a large number of hopping channels, it has also a large entropy in the atomic limit. Both points of view lead to the same conclusion, i.e. that the higher the number of hopping channels (or equivalently the entropy), the higher the critical coupling needed for the MIT. Also in the presence of a positive J_H, as used in Ref.[53], the entropy is only partially quenched because the Hund's rules always favour highly degenerate states, and the transition can in principle occur as a Kondo effect. Only the inversion of the Hund's rule can give rise, in peculiar cases, to a non-degenerate atomic limit.

3.3 The transition for negative J_H

The analysis of the previous section, together with other results, clearly indicates that, in the presence of the Hubbard local repulsion alone, the inclusion of orbitally degenerate levels does not modify qualitatively the scenario for the Mott-Hubbard transition. The main effect is a quantitative reduction of the critical U, that can be understood in terms of an effectively increased hopping for the degenerate case. The metallic behaviour appears as a Kondo-like resonance at the Fermi level in the middle of a preformed gap, regardless the number of levels. As already discussed, the appearance of the resonance is usually interpreted as a Kondo effect, associated with the quenching of the large entropy of the paramagnetic insulating state[2, 37]. Both the absence of qualitative modifications, and the quantitative behaviour as a function of filling and degeneracy are at least compatible with a Kondo effect leading to a Fermi-liquid phase.

When the inter-orbital correlations are turned on, the Mott-Hubbard transition may acquire new features, related to the different atomic limits that positive or negative values of J_H can determine. The multiplet-exchange term partially lifts the degeneracy, splitting the atomic multiplets. For positive J_H, the Hund's rules are satisfied, and the molecular groundstate has a relatively large degeneracy. On the other hand, for a negative J_H, and for $n = 4$ electrons per site, as we stated many times, the atomic limit is non degenerate. Therefore, this is a zero entropy state. It should be clear that the insurgence of the metallic state for this model can not take place as a Kondo effect [4]. In Chapter 2 we only exploited the positive side of this situation, namely the fact that the insulating phase was nonmagnetic, so we could limit ourselves to the paramagnetic sector without considering magnetic solutions. In this chapter we ask ourselves the question of how a

[4]The zero-entropy property holds only for $n = 4$ (or equivalently for $n = 2$). For $n = 3$ and $n = 5$ it is not possible to form a non-degenerate state with both $L = 0$ and $S = 0$.

Mott transition may occur between a Fermi-liquid and a non-degenerate insulator.

3.3.1 The limit $U \to U_{c2}$

In this section we examine the possibility of a direct transition between a Fermi-liquid and a zero-entropy Mott insulator. Let us consider for comparison the SBHM. If we limit to paramagnetic solutions, the atomic limit for the SBHM is dramatically degenerate. On each site, the down and the up spin configurations are in fact degenerate, leading to a finite entropy per site $S/N = \log 2$.

This property has quite important consequences on the transition. In the SBHM, when $U < U_{c2}$, the system is in a metallic Fermi-liquid state. In a Fermi liquid, the leading term in the low-temperature specific heat is given by $C_V = \gamma T$, where $\gamma = \frac{1}{3} m^* k_F k_B^2$. As a consequence,

$$\frac{S(T)}{N} = \int_0^T dT' \frac{C_V(T')}{T'} = \gamma T$$

The entropy is a linear function of T as well. The slope of the entropy curve increases with the effective mass. Within DMFT, as we approach the transition point U_{c2}, the effective mass increases, and finally diverges at the transition. Simultaneously, the energy scale associated with the Fermi-liquid properties (renormalized Fermi-energy) decreases. Since the density of states at the Fermi-level is pinned to the non-interacting value ρ_0, a single quantity Z rules both the divergence of the effective mass ($m/m^* \sim Z$), and the vanishing of the renormalized Fermi-energy ($E_F^* \sim Z$)[38]. The effective Fermi-energy sets the temperature scale below which the system can be described as a Fermi-liquid $k_B T_F^* = E_F^*$. As a result, the entropy at T_F^* is always finite, being

$$\frac{S(T_F^*)}{N} = \gamma T_F^* = \frac{1}{3} m^* k_F k_B^2 \rho_0 T_F^* = \frac{1}{3} \frac{m}{Z} k_F k_B^2 \rho_0 T_F Z = \frac{1}{3} m k_F k_B^2 \rho_0 T_F. \qquad (3.7)$$

This behaviour can be continuously connected with the finite entropy of the paramagnetic insulator for every coupling up to $U \to U_{c2}$, when the slope $\gamma \to \infty$ as it is shown in Fig. 3.5(a). The point in which $\gamma T_F^* \simeq \log 2$ sets the scale for the Kondo temperature under which the entropy of the paramagnetic state is quenched giving rise to the Kondo effect.

In the three-fold degenerate model with negative J_H this picture is no longer valid. The crucial difference is that, since the insulator has zero entropy at $T = 0$, and has a finite spin-gap at the transition, the entropy in the insulating phase has an activated behaviour of the form $S(T)/N = (1 + \beta\Delta)e^{-\beta\Delta}$, where the gap Δ is of order J_H. The

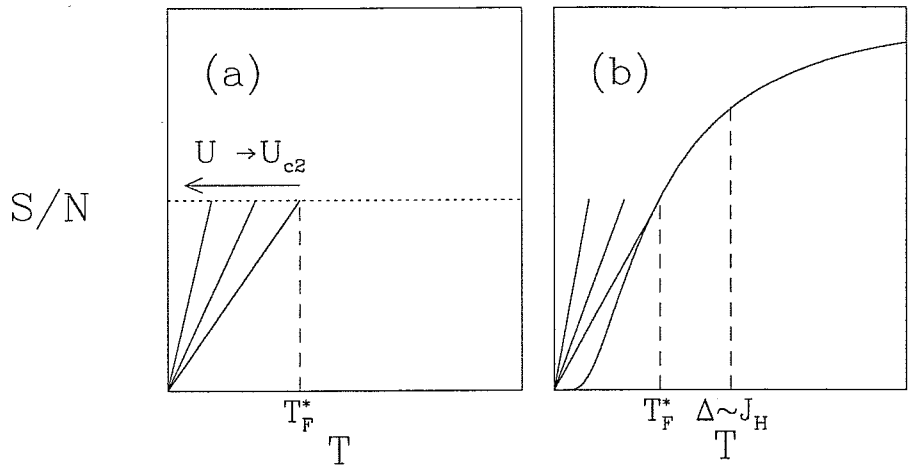

Figure 3.5: The Entropy as a function of temperature in proximity of the Mott transition between a Fermi-liquid and an insulator with finite entropy per site (a), and between a Fermi-liquid and an insulator with zero entropy (b). In case (a) the system can approach the transition as a Fermi-liquid, while in case (b), it is not possible to connect a Fermi-liquid with diverging effective mass with the insulator.

entropy of this phase goes exponentially to zero as $T \to 0$, as shown in Fig. 3.5(b). For $T \gg J_H$ the activated behaviour disappears because thermal fluctuations prevent the formation of local singlets.

The problem is to connect the non-degenerate insulating phase with a Fermi-liquid. The properties of the Fermi-liquid close to the transition must be the same we have outlined above, so if we suppose the existence of a renormalized Fermi energy, the entropy at the transition $S(T_F^*)$ must be finite and related to the free-electron properties by Eq. (3.7). Fig. 3.5(b) shows that we can connect continuously the linear Fermi-liquid behaviour of the entropy with the insulating entropy only for finite slopes, i.e. for finite effective masses, due to the rapid vanishing of the entropy of the spin-gapped insulator for $T \to 0$. The occurrence of a Mott transition is incompatible with a continuous connection between the Fermi-liquid behaviour for $T < T_F^*$, and the activated behaviour for $T_F^* < T < J_H$.

The argument above implies that the system can not be a Fermi liquid up to the transition, if the transition occurs with a diverging effective mass[5]. We are basically left

[5]We have described the impossibility of a direct transition between a Fermi liquid with a diverging effective mass to a zero-entropy insulator by means of a finite-temperature argument. We underline that

with three scenarios for the transition to a non-degenerate insulator:

- The inclusion of a negative J_H implies a *qualitative* modification of the appearance of the metallic solution. For example, the transition may acquire a band-like nature in which one of the two Hubbard bands acquires more weight, and the chemical potential lies in this band.

- The effective mass does not diverge at the transition, but it is finite at $U = U_{c2}$. This is a sort of first-order transition, even if $Z = m/m^*$ is not a derivative of the free-energy with respect to some parameter. This phenomenon could be associated with a quenching of the spin degrees of freedom below J_H.

- The system is not a Fermi-liquid in the proximity of the transition. A possible non Fermi-liquid state is a superconducting state, in which the local pairs present in the Mott insulating state form a coherent superconducting state. This scenario has several theoretical and experimental implications.

3.3.2 Spectral properties close to the transition

In this section we present various DMFT results for the intriguing case described in the previous section, i.e. $n = 4$ with a negative J_H in Hamiltonian (3.2). This investigation is aimed to discriminate between the various options outlined above. As a first step, we follow the usual strategy to describe the MIT within the DMFT, namely we consider the evolution of the spectral density by increasing the correlation strength U. Figs. 3.6 and 3.7 present this quantity for two different values of J_H. The goal of this section is to discuss the effect of a non-degenerate atomic limit on the mechanism of the Mott transition. We have therefore chosen relatively small values of J_H to avoid too drastic modifications to the usual scenario that could occur for large J_H. The chosen values $J_H = -0.01W$ and $J_H = -0.02W$ are instead likely to have the only effect to make the groundstate non-degenerate.

As a matter of fact, as it appears from Figs. 3.6 and 3.7, the qualitative features of the transition are basically unaffected by the inclusion of a negative J_H. The metallic phase still appears as a Fermi-level resonance in the middle of the insulating gap, and the Hubbard bands are well separated when the MIT occurs. Also the presence of a lower critical U_{c1} for the disappearance of the insulating solution is recovered.

---

the argument above shows that it is not possible to define an energy scale above which the system is a Fermi liquid. The argument could be recast in terms of frequencies, and rules out the possibility of a zero-temperature second-order transition.

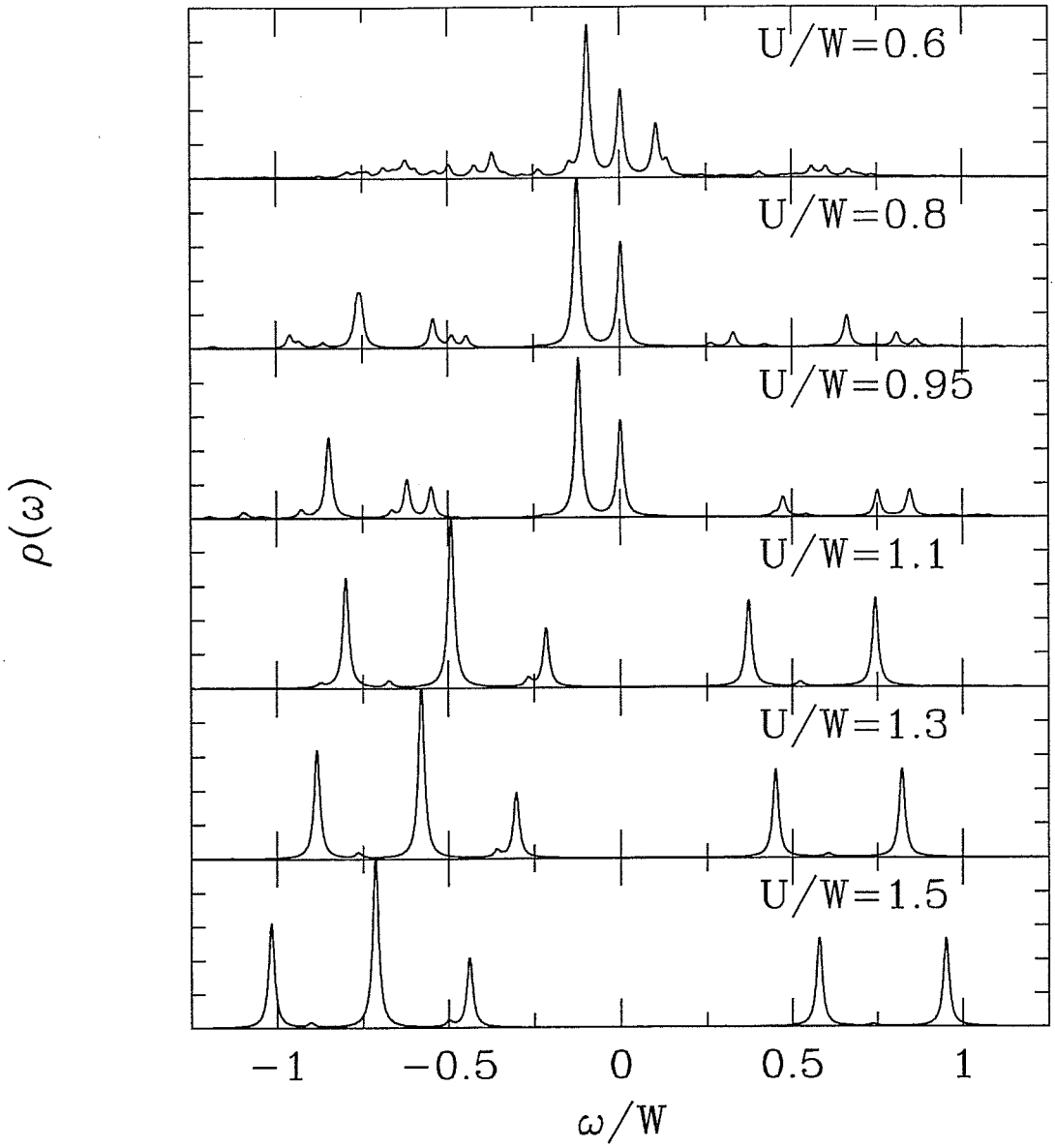

Figure 3.6: The evolution of the spectral density $\rho(\omega) = -1/\pi \mathcal{I}mG(\omega)$ for $n = 4$ and for $J_H/W = -0.01$. Clearly, the three top solutions are metallic and the bottom ones are insulating. $\rho(\omega)$ is expressed in arbitrary units.

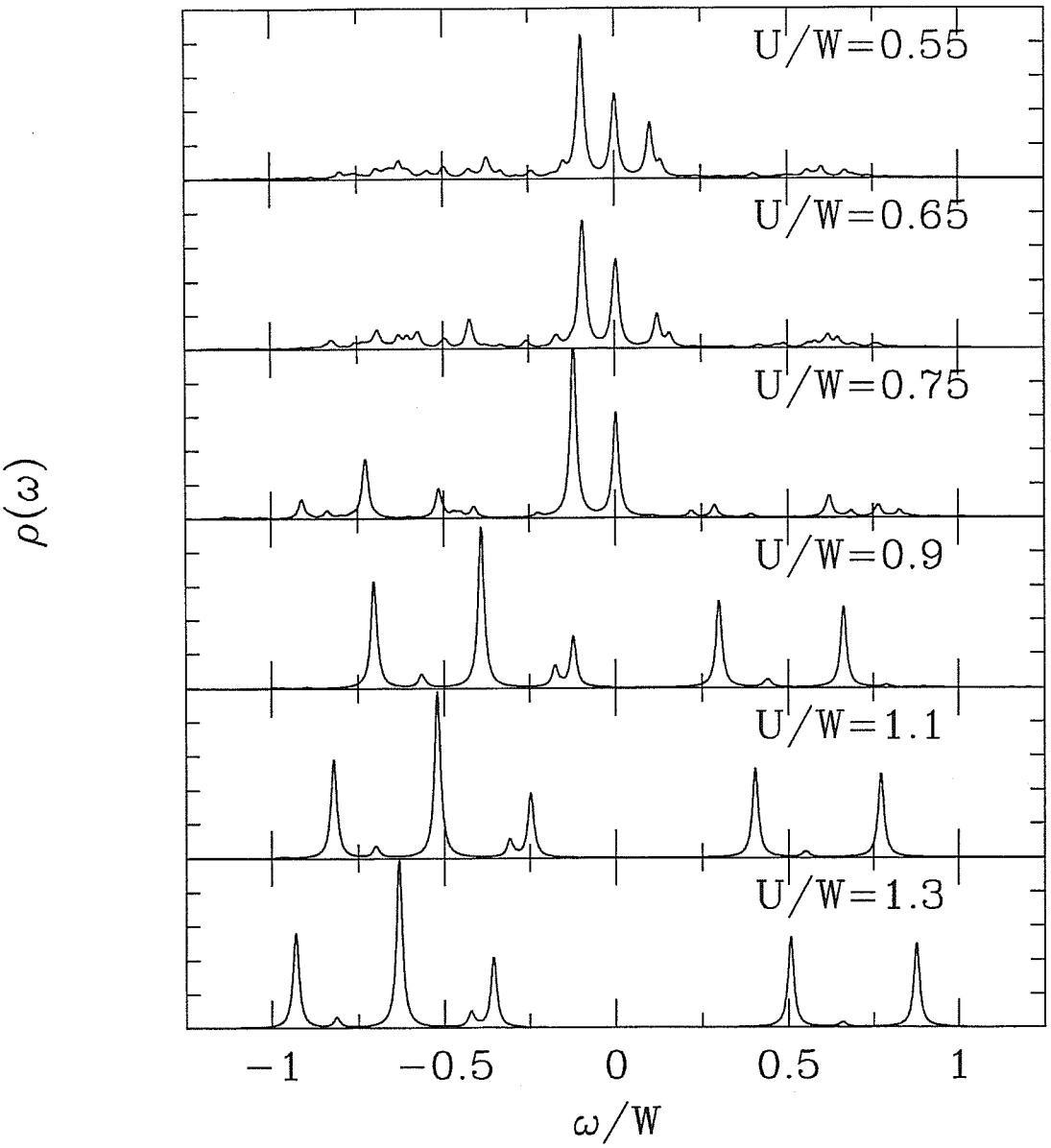

Figure 3.7: The evolution of the spectral density $\rho(\omega) = -1/\pi \mathcal{I}mG(\omega)$ for $n = 4$ and for $J_H/W = -0.02$. Clearly, the three top solutions are metallic and the bottom ones are insulating. $\rho(\omega)$ is expressed in arbitrary units.

The possibility of a band-like transition in which the gap closes due to the multiplet-exchange, leading to a band insulator, is ruled out by the above results. Nevertheless, the argument in the previous section rules out the possibility of a direct second-order transition from a Fermi-liquid and a zero-entropy Mott insulator.

The second possibility is that the transition ceases to be second-order. In fact, if the effective mass was not divergent at the transition, it would be in principle possible to connect the non-critical Fermi-liquid to the insulator. For numerical reasons, it is hard to clearly discriminate between a continuous vanishing of Z, and a small sudden drop. We prefer to use the total energy to prove if the transition is first or second order. Even if the effective mass (or, equivalently, the quasiparticle weight) is not a derivative of the free energy, if this quantity has a jump at the transition (i.e., if it is finite just below U_{c2}, becoming negative for $U > U_{c2}$), the energy is expected to present a discontinuity in its first derivative. The explicit computation of the groundstate energy

$$\frac{E}{N} = t^2 T \sum_n G(i\omega_n)^2 + T \sum_n [(i\omega_n + \mu)G(i\omega_n) - 1]e^{i\omega_n 0^+}$$

rules out also this possibility, since the energy vs U curve is smooth, at least within the numerical accuracy.

A closer look to the numerical results helps us to reconcile the theoretical expectations with the numerical findings. As discussed in Chapter 1, every solution of the DMFT equations involves a recursive procedure. After each step, new parameters are computed according to the self-consistency Eq. (1.10). The quantity

$$\chi = \frac{1}{2(n_s - 1)} \sum_{k=2}^{n_s} (\tilde{\varepsilon}_k - \tilde{\varepsilon}_k^{old})^2 + (V_k - V_k^{old})^2$$

is computed at every iteration to measure the degree of convergence. For $J_H = 0$, or deeply in the metallic and the insulating region, just a few steps (~ 10) are needed to obtain $\chi \sim 10^{-12}$, signaling a good convergence. In the present case, we find that in a small region of U values in the immediate neighbourhood of the transition, convergence is not so easily achieved, and even after more than 20 iterations, the value of χ^2 does not go below 10^{-5}–10^{-6}, and further iterations only lead to fluctuations.

This finding suggest an alternative interpretation of the results obtained for the spectral function. The Fermi-liquid phase that seems to survive up to the critical point may be a metastable state, while another phase, unaccessible to our calculation, may be the groundstate in this region. Remarkably, the interval of couplings in which we are not able to obtain truly converged results scales with the value of the multiplet-exchange coupling, supporting the idea that this numerical problem is the signature of a real physical mechanism taking place.

The analysis of the spectral function and of the total energy across the MIT rule out two of the three options we had for the MIT in the presence of a non-degenerate Mott insulating state. Moreover, even if the paramagnetic solution of the DMFT in absence of broken-symmetries provides a metallic solution up to the MIT, it turns out that in the vicinity of the transition, the Fermi-liquid phase seems to be a metastable phase.

A natural candidate for the groundstate in this region of parameters is a superconducting state, in which the tendency to local pairing given by the multiplet-exchange leads to a coherent superposition of pairs. A possible scenario is the following: for small values of U the system is a regular Fermi-liquid, in which the e-e correlation renormalizes the electronic properties. Once the correlation has strongly renormalized the electronic properties, the multiplet-exchange leads to the formation of pairs, breaking the Fermi-liquid in favour of a superconducting state. A further increase of the coupling finally leads to the Mott-insulating state. In the remainder of this chapter we discuss the possible instability of this system with respect to pairing.

3.4 Superconducting instability of a Fermi liquid

Let us consider how one can detect a pairing instability in a Fermi liquid. The relevant quantity is the particle-particle (Cooper) bubble

$$\chi^{sc}(\tau) = -\langle T_\tau \left(c_{k\uparrow}(\tau) c_{-k\downarrow}(\tau) c^\dagger_{-k\downarrow}(0) c^\dagger_{k\uparrow}(0) \right) \rangle. \tag{3.8}$$

The Matsubara transform of this quantity for free fermions is given by

$$\chi^{sc}(i\omega_n) = \frac{1}{V} \sum_k \frac{1 - 2n_k}{i\omega_n - 2\epsilon_k}, \tag{3.9}$$

where n_k is the occupation number in momentum space. It is also important to stress that the true physical response function is obtained by the analytical continuation $i\omega_n \to \omega + i\eta$ and, for stability reasons, has to be analytic in the upper half-plane [90].

Let us roughly estimate $\chi^{sc}(i\omega_n)$ for complex frequency $i\omega_n \to z$. For energies close to the Fermi energy, and assuming a constant density of states, we get for the free Fermi gas

$$\begin{aligned} \chi_0^{sc}(z) &\simeq \rho_0 \int_0^{\omega_c} dx \left(\frac{1}{z - 2x} - \frac{1}{z + 2x} \right) = \\ &= -\frac{1}{2} \rho_0 \ln \frac{4\omega_c^2 - z^2}{-z^2} \simeq -\frac{1}{2} \rho_0 \ln \frac{4\omega_c^2}{-z^2}, \end{aligned} \tag{3.10}$$

where ω_c is a high energy cut-off. Within the Landau-Fermi liquid theory, we can assume that this function is given by the RPA result

$$\chi^{sc}(z) = \frac{\chi_0^{sc}(z)}{1 - \lambda \chi_0^{sc}(z)}, \tag{3.11}$$

where λ is some coupling in the Cooper channel, and the density of states appearing in χ_0^{sc} contains the effective quasiparticle mass. For positive λ, $\chi^{sc}(z)$ has no poles at low frequency $|z| \ll \omega_c$. On the contrary, for negative λ, it has a pole at

$$z_*^2 = -4\omega_c^2 \mathrm{e}^{-2/(|\lambda|\rho_0)}. \tag{3.12}$$

Upon analytic continuation in the upper half-plane, the pole is for

$$z_* = 2i\omega_c \mathrm{e}^{-1/(|\lambda|\rho_0)} = i\omega_*. \tag{3.13}$$

In other words, the true response function becomes non analytic in the upper half-plane, signaling the Cooper instability. By expanding Eq. (3.11) around the pole, one finds

$$\chi^{sc}(\omega) \simeq -\frac{1}{\lambda^2 \rho_0} \frac{i\omega_*}{\omega - i\omega_*} = \frac{1}{\lambda^2 \rho_0} \frac{1}{\omega^2 + \omega_*^2} \left(\omega_*^2 - i\omega\omega_*\right). \tag{3.14}$$

On the other hand, for positive λ, upon analytic continuation in the upper half-plane,

$$\chi_0^{sc}(\omega) = -\rho_0 \ln \left| \frac{2\omega_c}{\omega} \right| - i\rho_0 \frac{\pi}{2}. \tag{3.15}$$

The imaginary part of $\chi^{sc}(\omega)$ is now

$$\mathcal{I}m\chi^{sc}(\omega) \simeq -\frac{\pi}{2}\rho_0 \frac{1}{\left(1 + \lambda\rho_0 \ln \left|\frac{2\omega_c}{\omega}\right|\right)^2 + \left(\rho_0 \frac{\pi}{2}\right)^2}, \tag{3.16}$$

while the real part reads

$$\begin{aligned} \mathcal{R}e\chi^{sc}(\omega) \simeq & -\left[\rho_0 \ln \left|\frac{2\omega_c}{\omega}\right| + \lambda \left(\rho_0 \ln \left|\frac{2\omega_c}{\omega}\right|\right)^2 + \lambda \left(\rho_0 \frac{\pi}{2}\right)^2\right] \times \\ & \times \frac{1}{\left(1 + \lambda\rho_0 \ln \left|\frac{2\omega_c}{\omega}\right|\right)^2 + \left(\rho_0 \frac{\pi}{2}\right)^2}. \end{aligned} \tag{3.17}$$

We see that the instability manifests itself in the imaginary part only as a different frequency behavior, while the main difference between the two cases is the sign of the real part at small frequency, which is positive for attractive λ and negative otherwise.

Let us better understand this point on the basis of the analytical properties of the response functions. For a given an operator Δ, we define the function

$$\begin{aligned} \frac{1}{\pi}\chi''_{sc}(\omega) = & \sum_n \left|\langle\phi_n|\Delta^\dagger|\phi_0\rangle\right|^2 \delta\left(\omega - E_n + E_0\right) + \\ & - \left|\langle\phi_n|\Delta|\phi_0\rangle\right|^2 \delta\left(\omega + E_n - E_0\right), \end{aligned} \tag{3.18}$$

where $|\phi_0\rangle$ is the ground state at a given chemical potential, $|\phi_n\rangle$ are the states of energy E_n connected to $|\phi_0\rangle$ by Δ.

(3.18) is the dissipative part of the response function

$$\chi^{sc}(\omega) = \sum_n \frac{|\langle\phi_n|\Delta^\dagger|\phi_0\rangle|^2}{\omega - E_n + E_0 + i\eta} - \frac{|\langle\phi_n|\Delta|\phi_0\rangle|^2}{\omega + E_n - E_0 + i\eta}, \tag{3.19}$$

i.e., $\chi''_{sc}(\omega) = -\mathcal{I}m\chi^{sc}(\omega)$. If the system is stable, the response function is analytic in the upper half-plane, and the Kramers-Kronig relations hold. In particular,

$$\mathcal{R}e\chi^{sc}(\omega) = \frac{1}{\pi}\int_{-\infty}^{\infty} d\omega' \chi''_{sc}(\omega') P\left(\frac{1}{\omega - \omega'}\right). \tag{3.20}$$

We notice that, at $\omega = 0$,

$$\mathcal{R}e\chi^{sc}(0) = -\frac{1}{\pi}\int_{-\infty}^{\infty} d\omega' \chi''_{sc}(\omega') P\left(\frac{1}{\omega'}\right). \tag{3.21}$$

Since, by the definition (3.18), $\chi''_{sc} > 0$ for positive frequency and $\chi''_{sc} < 0$ otherwise, then $\mathcal{R}e\chi_{sc}(0) < 0$. Notice that the above property of χ''_{sc} does imply that we are exploring the phase space within a region in which $|\phi_0\rangle$ is a stable lowest energy state. In DMFT this is possible since the states are solution of some self-consistency equation.

In such a case, the instability of the system outside that specified region in the phase space would be signaled for instance by the presence a pole at $i\omega_*$ on the positive imaginary axis, which modifies the Kramers-Kronig relations according to

$$\mathcal{R}e\chi^{sc}(\omega) = -\frac{1}{\pi}\int_{-\infty}^{\infty} d\omega' \mathcal{I}m\chi^{sc}(\omega') P\left(\frac{1}{\omega - \omega'}\right) + 2\mathcal{R}e\frac{Res[\chi^{sc}(i\omega_*)]}{\omega - i\omega_*}, \tag{3.22}$$

$$\mathcal{I}m\chi^{sc}(\omega) = \frac{1}{\pi}\int_{-\infty}^{\infty} d\omega' \mathcal{R}e\chi^{sc}(\omega') P\left(\frac{1}{\omega - \omega'}\right) + 2\mathcal{I}m\frac{Res[\chi^{sc}(i\omega_*)]}{\omega - i\omega_*}. \tag{3.23}$$

Indeed, the presence of the additional pole may change the sign of the real part.

We are therefore in the position to establish a clear-cut criterion for the pairing instability of a Landau Fermi-liquid. The instability occurs when the small-frequency real part of the paring susceptibility Eq. (3.11), or equivalently, of the dissipative part of the response function (3.18) changes sign from positive to negative.

3.4.1 DMFT calculation of the pairing susceptibility

Since the calculations we perform in this thesis do not support superconducting long-range-order, we can only detect the eventual instability of the metal with respect to

pairing, as described in the previous section. We compute the imaginary part of the dynamical susceptibility for pair creation [6]

$$\begin{aligned}\frac{1}{\pi}\chi''_{sc}(\omega) &= \mathcal{I}m\langle\phi_0^N|\Delta^\dagger\frac{1}{\omega-H}\Delta|\phi_0^N\rangle = \\ &= \sum_n |\langle\phi_n^{N+2}|\Delta|\phi_0^N\rangle|^2\delta(\omega-(E_n-E_0)),\end{aligned} \tag{3.24}$$

where $|\phi_0^N\rangle$ is the groundstate for N particles, of energy E_0, and $|\phi_n^{N+2}\rangle$ are the eigenstates with $N+2$ particles, of energies E_n. The pair creation operator $\Delta^\dagger$ is given by

$$\Delta^\dagger = \frac{1}{\sqrt{3}}(c_{1\uparrow}^\dagger c_{1\downarrow}^\dagger + c_{2\uparrow}^\dagger c_{2\downarrow}^\dagger + c_{3\uparrow}^\dagger c_{3\downarrow}^\dagger).$$

A quantity of the form (3.24) is easily obtained with the Lanczos algorithm without the knowledge of the full spectrum, exactly like the spectral quantities we have considered in Sec. 2.6 [36]. We show the evolution of this quantity in Fig. 3.8 for $J_H = -0.02W$ (the same value of Fig. 3.7). Even if the imaginary part is not expected to have a qualitatively strong modification in presence of pairing instability, the qualitative trend leaves little doubt on the Fermi-liquid instability, despite the usual problem of Lanczos susceptibilities, that are made by a collection of δ-functions.

For $U < 0.85W$ (the three low panels on Fig. 3.8) the system is a stable Fermi liquid, and the low-frequency imaginary part of the susceptibility has some small features at low energy that smoothly decrease by increasing U, in agreement with Eq. (3.14). For $U = 0.85W$, i.e. for a coupling really close to $U_{c2} = 0.86W$ (roughly $J_H/2$ before the transition), the low energy features clearly change. The low-energy weight is enhanced and it tends to move to really low frequency. As U is further increased the system enters the Mott phase, and no low-energy feature is present.

The data shown in Fig. 3.8 strongly suggest that in a small slice of width J_H at the boundary of the transition, the Fermi-liquid solution we get in DMFT is unstable towards pairing. Then the numerical instability that limited the convergence of these solutions has a relevant physical counterpart.

If we perform a Kramers-Kronig transform of the imaginary part of $\chi_{sc}(\omega)$, we obtain the real part χ'_{sc}. As expected, this quantity is positive for $U = 0.85W$ (the value for which the imaginary part is enhanced at low frequencies), as opposed to the negative value in the stable Fermi liquid. In Fig. 3.9 we show the Kramers-Kronig transform of

[6] The properties of the response functions imply that we just need to compute the first term in Eq. (3.18), that contributes to the sum only for positive frequencies, since the second term, which contributes only to negative frequencies, is given by the same quantity changed of sign.

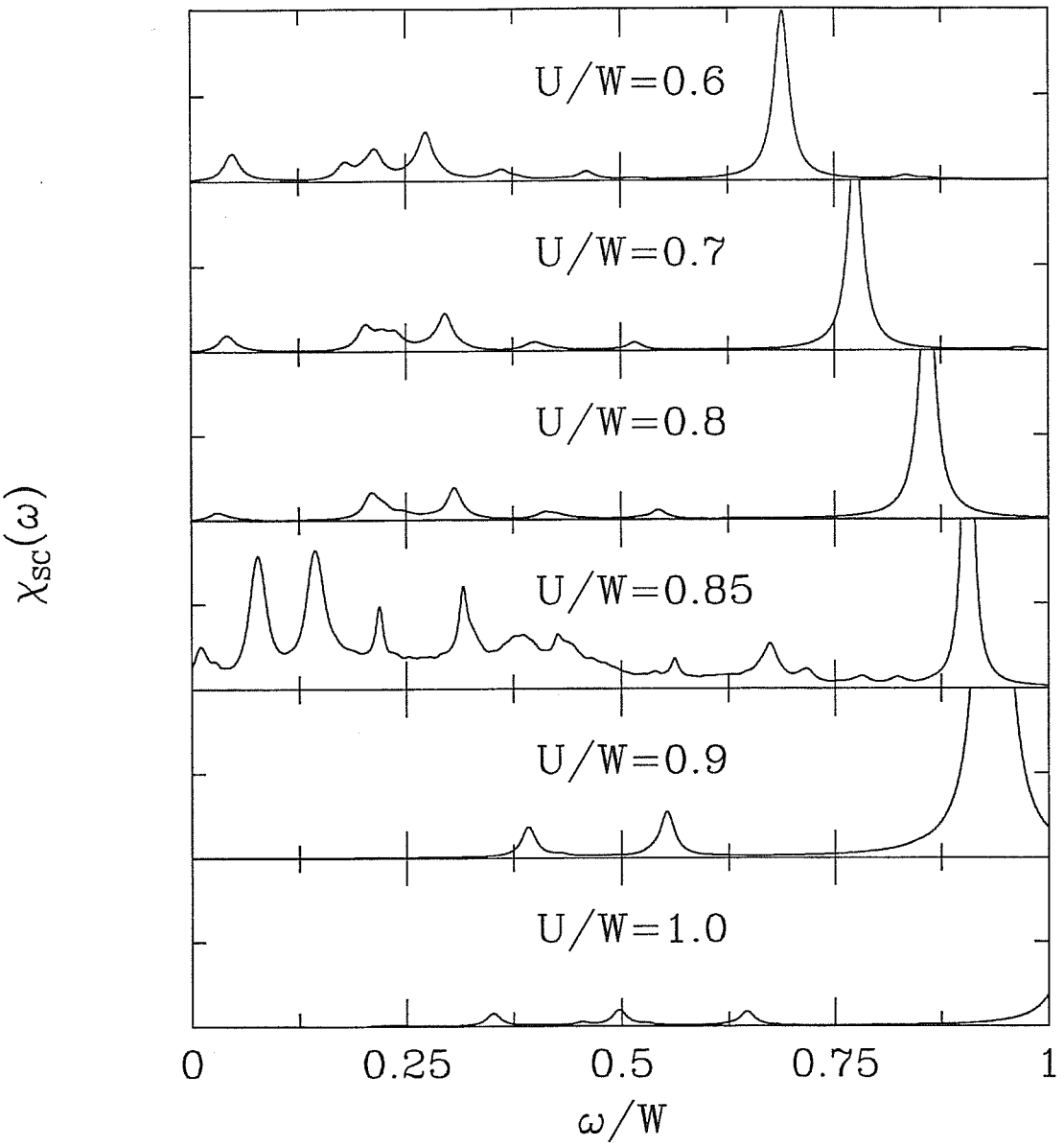

Figure 3.8: The evolution of the imaginary part of the susceptibility for pair creation (3.24) for $n = 4$ and for $J_H/W = -0.02$. U increases from bottom to top. The three low panels are stable Fermi-liquid solutions. For $U = 0.85W$, just $J_H/2$ before the MIT, the low-energy part of this quantity rapidly increases. For $U = 0.9W$ and $U = 1.0$ no low-energy features are present.

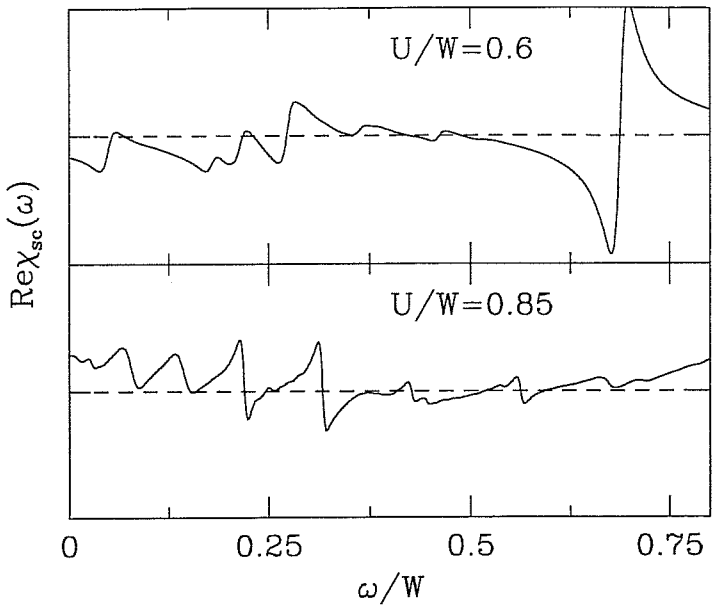

Figure 3.9: The real part of the pair susceptibility for the unstable Fermi-liquid ($U = 0.85W$), and for a stable solution ($U = 0.6W$). The unstable solution is clearly positive for low frequencies , while the stable one is negative.

(3.24) for $U = 0.85W$ and for $U = 0.6W$, a value clearly in the Fermi-liquid regime. The different sign for $\omega \to 0$ for the unstable regime is evident.

3.5 Conclusions

In this chapter we have discussed the role of orbital degeneracy on the Mott transition. First of all, we have considered the pure Hubbard model, in which no interaction between the various orbitals in considered. In this case we have described the successive Mott transitions occurring at integer filling discussing the dependence upon doping of the critical U. The most important issue of this chapter has been the analysis of the effect of a negative multiplet-exchange term. This term, that can be thought as arising from a Jahn-Teller effect, leads, for $n = 4$ electrons per site, to a non-degenerate atomic limit. It is shown that in this case, due to the zero entropy of the atomic limit, it is not possible to characterize the Mott transition within the DMFT as a Kondo effect, and, even more significantly, that it is not possible to have a second-order transition between a Fermi liquid and a zero-entropy insulator. Nevertheless, if the DMFT of this problem is carried out, a Fermi-liquid phase is found up to the transition point in which the system becomes a Mott insulator. We show that this Fermi-liquid is likely to be a metastable solution unstable towards pairing. Therefore, we propose that this model presents a di-

rect superconductor-insulator transition driven by the correlation strength. Starting from a weakly interacting Fermi-liquid, and increasing U, the effective mass of the carriers increases, up to a point in which the effective mass can not increase any more within a Fermi-liquid phase. In this strongly correlates metal, the local correlations that are responsible of the zero-entropy property of the insulator are able to break the Fermi liquid, giving rise to a superconducting state. Increasing the coupling, the system becomes a gapped insulator.

Further investigation is needed to confirm this fascinating scenario. Namely, the DMFT equations must be extended to allow for superconductivity. This work is currently underway.

Chapter 4

The Mott Metal-Insulator transition on the triangular lattice

In this chapter we turn back to the single-band Hubbard model, but we introduce frustration by letting the sites reside on a two-dimensional triangular lattice [91]. This study is relevant both on the theoretical and the experimental side. Recent experimental evidences call for an intensive analysis of strongly correlated electronic models on the triangular lattice. The adlayer structures on semiconductor surfaces, such as SiC(0001) [12] or K/Si(111) : B [13], are Mott insulators, characterized by a $\sqrt{3} \times \sqrt{3}$ arrangement of the dangling-bond surface orbitals, and are likely to be well described by bidimensional strongly correlated Hamiltonians [92] on the triangular lattice. In a completely different context, McKenzie has recently proposed that a similar Hamiltonian in the metallic regime is relevant for organic superconductors like $\kappa - (\mathrm{BEDT} - \mathrm{TTF})_2\mathrm{X}$[14]. From the theoretical point of view, the triangular lattice represents a simple frustrated lattice, in which frustration of the antiferromagnetic (AFM) ordering may lead to remarkable physical properties.

As discussed in Chapter 1, the presence of a MIT at half-filling is a completely general feature of the single-band Hubbard model. In fact the model describes a metal with a half-filled band at least at $U = 0$ and it has to become insulating for $U \to \infty$, due to the localization of the carriers caused by infinite repulsion. The features of the transition may depend on the dimensionality and on the lattice considered. In particular, since at strong-coupling $U \gg t$ the model maps onto an AFM Heisenberg model, the insulator is usually characterized by long-range AFM order.

Some interesting questions naturally arise, even for this simplified model. In this chapter we will try to give an answer to two of the most relevant:

1. Is the system metallic only for $U = 0$ or is there a critical value of U/t separating a (finite) metallic region from an insulating one?

2. Is it possible to describe an insulating state without long-range order within this model?

On the square lattice (and on higher-dimensional cubic lattices) with nearest-neighbours hopping, both questions have a negative answer. As we have discussed in Chapter 1, it turns out that the paramagnetic metal is unstable towards antiferromagnetism for arbitrarily small U. The instability is determined by the divergence of the integral in Eq. (1.3). This is ultimately due to the perfect-nesting property of the non-interacting Fermi surface. In the strong coupling ($U \gg t$) limit the Hubbard model maps onto the AFM Heisenberg model, which is known to present an antiferromagnetically ordered groundstate on the square lattice and on higher dimensionality cubic lattices. There is no reason why intermediate couplings should present metallic behaviour between the limiting AFM insulating solutions found in weak-coupling and strong-coupling.

The MIT then occurs at arbitrarily small U, as a transition between the uncorrelated metal for $U = 0$, and an AFM insulator for every non-zero coupling.

A possible route at least towards a transition taking place at finite U/t, and eventually to a possible insulating state with no broken-symmetry is the introduction of physical effects frustrating the magnetic ordering. The triangular lattice is one of the simplest frustrated lattices. For this model the perfect nesting property is absent for the uncorrelated metal [93]. As consequence, the Stoner criterion does not give a vanishingly small critical coupling for the MIT, and a finite range of couplings presents metallic behaviour.

Nevertheless, there are many evidences for a Néel ordered (insulating) groundstate in the $U/t \to \infty$ (Heisenberg) limit [94, 95]. Notice however that even the classical ordering vector $\mathbf{Q_T} = (4\pi/3, 0)$ (shown in Fig. 4.1) does not give rise to perfect nesting.

Since a metal is expected to be stable at least for small U/t, and an insulator is recovered as $U/t \to \infty$, A MIT is then expected to occur at some finite U. For the same reasons, this transition is not, in principle, necessarily accompanied by antiferromagnetic ordering, as it occurs on the square lattice. This model can be a possible candidate for a "real" Mott transition without magnetic ordering soon after the transition from a metal to an insulator.

Since we are explicitly interested in the peculiar features of the two-dimensional triangular Hubbard model, we will not use the DMFT for this problem, despite the considerable success of this approach in the characterization of the Mott-Hubbard transition. We will rely on the less accurate slave-boson (SB) mean-field theory, which gives any-

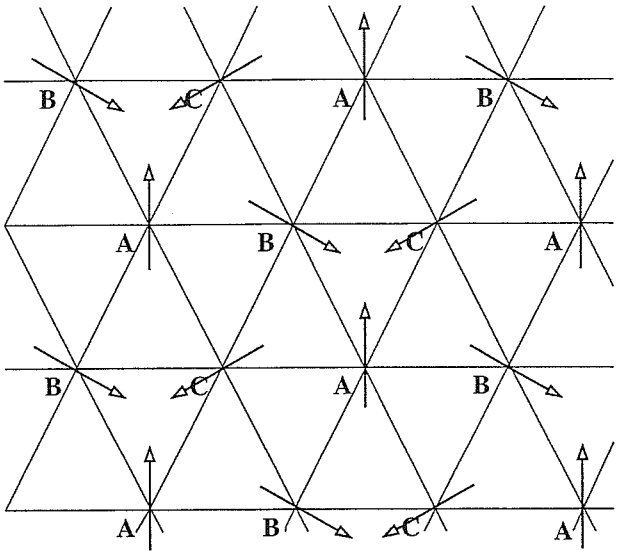

Figure 4.1: The classical Néel state consists of coplanar spins forming $\pm 2\pi/3$ angles between nearest neighbours. This leads to a $\sqrt{3} \times \sqrt{3}$ periodicity with the spins on the three sublattices A,B,C ferromagnetically aligned.

way substantial insight on the transition coming from the metallic side (Brinkman-Rice approach). The comparison with Hartree-Fock (HF) results and with exact diagonalization (ED) of small clusters will help up to correctly interpret the SB results.

4.1 Hartree-Fock calculations

The frustration of the magnetic ordering introduced by the lattice topology reflects itself in a wide variety of competing magnetic phases. Hartree-Fock calculations can help us in understanding which are the most stable magnetic phases and represent a useful starting point for more refined investigations. Note however that the HF scheme is unable to describe an insulating phase without broken symmetry, so that more accurate theories need to be used to answer the questions we asked. The Hartree-Fock phase diagram has been already established by Krishnamurthy and co-workers [96, 97].

Various transitions occur in the intermediate-coupling regime: for small U the system is a paramagnetic metal (PM), which turns to a metal with incommensurate spiral spin-density-wave (Spiral Metal, SM) at $U = U_{c1} = 3.97t$. This phase is characterized by an incommensurate magnetic ordering vector of the form $\mathbf{Q} = (Q_0, 0)$. In other words, as we move along the x-axis, the spin direction rotates of a pitch angle Q_0 every site, as it is shown in Fig. 4.2. The classical Néel phase as shown in Fig. 4.1 can be recovered for $Q_0 = 4\pi/3$. The transition between the PM and the SM is continuous

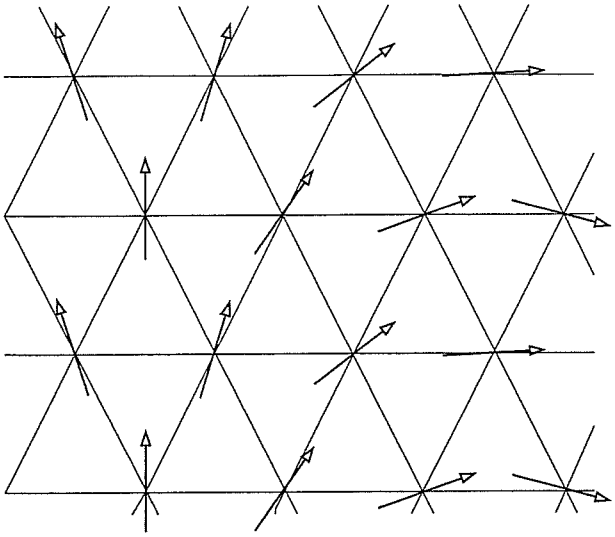

Figure 4.2: A possible spiral phase, with an arbitrary incommensurate ordering vector.

(second order), i.e. the magnetization is $m = 0$ at the transition and then continuously rises. If we follow this solution up to the point in which it crosses the antiferromagnetic insulator, we observe that the magnetization is really close to the saturation value $m = 1$, and the pitch angle to $Q_0 = 4\pi/3$ when the first-order transition occurs.

Indeed, the SM phase is not the most stable up to this crossover: at $U = U_{c2} = 4.45t$ a semi-metallic linear spin-density wave (LSDW) as the one shown if Fig. 4.3 is stabilized. In this phase zig-zag ferromagnetic chains alternate along the x-axis (dashed in Fig. 4.3). The energetic convenience of this phase (at least at the HF level) comes then from its hybrid nature; a significant kinetic energy is still present along the ferromagnetic chains, while the number of broken AFM bonds is not so large.

This latter phase becomes energetically unfavoured at $U = U_{c3} = 5.27t$, where the last first-order transition towards the antiferromagnetic insulator occurs.

In the same work it has also been argued that, at finite temperature, the model should present a Mott transition between a paramagnetic metal and a paramagnetic insulator as that observed, e.g., in V_2O_3.

4.2 The Kotliar-Ruckenstein Slave Boson approach

4.2.1 Formalism

As shown in the previous section, the Hartree-Fock phase diagram presents a rich variety of phases. Four different phases become stable varying the value of U, and three

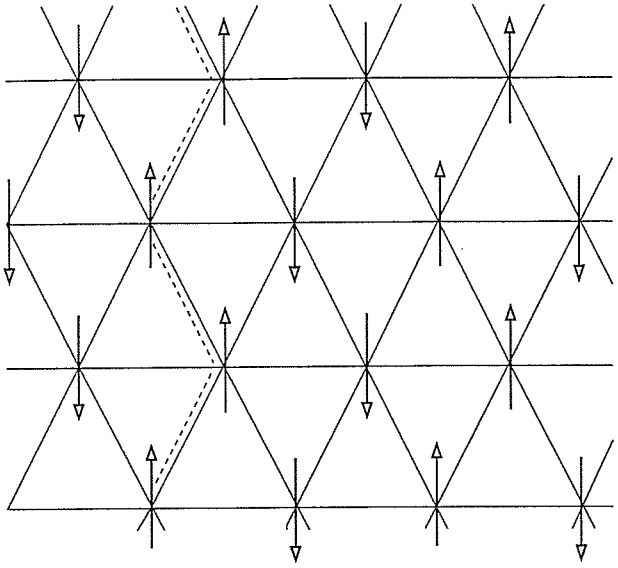

Figure 4.3: The linear spin density wave found in HF. The dashed line denotes the ferromagnetic zig-zag chains

transitions take place, in a relatively small interval of coupling values, namely the continuous transition from the paramagnetic metal to the metal with incommensurate spiral ordering, a first order transition from the spiral phase to the linear spin-density-wave, and finally the first order transition to the antiferromagnetic insulator. However, all the above transitions only occur at relatively large U/t, while the HF approximation is known to be unreliable in the intermediate-coupling regime. Therefore we adopt the more appropriate slave-boson approach [17, 27] which, already at the mean-field level, is exact both in the non-interacting $U = 0$ limit, and in the opposite $U/t \to \infty$ limit, as we shall show in the following. This approximation represents therefore a valuable interpolating scheme between this two limits.

Within the SB approach, we introduce on each site a set of four bosonic operators e_i, $s_{i\uparrow}$, $s_{i\downarrow}$ and d_i to label empty (e), singly (s), and doubly (d) occupied sites, respectively. One, and only one of these bosons is present on each site, besides the fermionic operators. We work therefore in an enlarged Hilbert space, in which auxiliary (slave) bosonic degrees of freedom are introduced. The extended Hilbert space contains unphysical states which can be eliminated by imposing the following constraints:

$$\sum_{\sigma} s_{i\sigma}^{\dagger} s_{i\sigma} + e_i^{\dagger} e_i + d_i^{\dagger} d_i = 1 \tag{4.1}$$

$$c_{i\sigma}^{\dagger} c_{i\sigma} = s_{i\sigma}^{\dagger} s_{i\sigma} + d_i^{\dagger} d_i; \sigma = \pm. \tag{4.2}$$

Eq. (4.1) simply means that no more and no less than one boson must be present on each

site; Eqs.(4.2) state that the fermion number operator $c^\dagger_{i\sigma}c_{i\sigma}$ must be equal to the sum of the proper bosonic number operators (if a down spin is on a given site, than the boson "singly occupied-down" or the boson "doubly occupied" must be present).

Since we are interested in incommensurate magnetic ordering, we use the spin-rotational invariant formulation [98] of the SB approach. The spin projection $\sigma =\uparrow,\downarrow$ is measured with respect to a local quantization axis, which can vary from site to site. To allow for this freedom we introduce the unitary transformation on each site

$$\tilde{c}^\dagger_{i\sigma} = \sum_{\sigma'} = [\mathcal{R}^\dagger(\Omega_i)]_{\sigma\sigma'}c_{i\sigma'}, \tag{4.3}$$

where $\mathcal{R}^\dagger(\Omega_i) = e^{-i(\phi_i/2)\sigma_x}e^{-i(\theta_i/2)\sigma_y} \equiv R^\dagger_i$ is the rotation operator that rotates the z-axis to the direction specified by the spherical angle $\Omega_i = (\theta_i, \phi_i)$, and σ_x and σ_y are the Pauli matrices. The resulting SB Hamiltonian is

$$\begin{aligned}\mathcal{H} = & - t\sum_{\substack{<ij>\\ \sigma\sigma'}}\left[\tilde{c}^\dagger_{i\sigma}z^\dagger_{i\sigma}(\mathcal{R}^\dagger_i\mathcal{R}_j)_{\sigma\sigma'}z_{j\sigma'}\tilde{c}_{j\sigma'} + H.c.\right] \\ & - \mu\sum_{i\sigma}\tilde{c}^\dagger_{i\sigma}\tilde{c}_{i\sigma} + U\sum_i d^\dagger_i d_i \\ & + \sum_i \lambda_i\left(e^\dagger_i e_i + d^\dagger_i d_i + \sum_\sigma s^\dagger_{i\sigma}s_{i\sigma} - 1\right) \\ & + \sum_{i\sigma}\Lambda_{i\sigma}\left(\tilde{c}^\dagger_{i\sigma}\tilde{c}_{i\sigma} - s^\dagger_{i\sigma}s_{i\sigma} - d^\dagger_i d_i\right)\end{aligned} \tag{4.4}$$

where $\tilde{c}_{i\sigma}, \tilde{c}^\dagger_{i\sigma}$ are the pseudo-fermion operators, the Lagrange multipliers λ_i and $\Lambda_{i\sigma}$ enforce on each site the completeness constraint and the correct fermion counting respectively, the operator $\mathcal{R}_i$ rotates the local reference frame back to the laboratory frame.

The operator

$$z_{i\sigma} = \frac{e^\dagger_i s_{i\sigma} + s^\dagger_{i-\sigma}d_i}{\sqrt{1 - d^\dagger_i d_i - s^\dagger_{i\sigma}s_{i\sigma}}\sqrt{1 - e^\dagger_i e_i - s^\dagger_{i-\sigma}s_{i-\sigma}}}$$

is introduced in order to reconstruct the hopping amplitude in the enlarged Fock space, and to yield the correct $U \to 0$ limiting behaviour in the mean-field approximation [27, 98].

We will treat the SB Hamiltonian at a mean-field level, substituting the bosonic operators with average values. In principle, we could let the bosonic fields assume different average values on every site (as in an unrestricted HF calculation). However, the number of self-consistency equations (see below) we can treat is not so large, so we limited

ourselves to fully translationally-invariant solutions, in which the average values of the bosons are site-independent, and to solutions which are still periodic with enlarged unit cells containing three or four sites (see below).

When the angle between two local quantization axes depends only on their relative position, up to a global phase factor one can assume $\mathcal{R}_i^\dagger \mathcal{R}_j = \exp[\mathrm{i}\mathbf{Q}\cdot(\mathbf{R}_i - \mathbf{R}_j)\sigma_y/2]$, where σ_y is the Pauli matrix and $\mathbf{Q}$ is the (incommensurate) modulating wave-vector [98]. In such a case, where the translational invariance is fully preserved, a mean-field description with real site-independent expectation values for the SB operators

$$\langle e_i^{(\dagger)}\rangle = e_0;\ \ \langle s_{i\sigma}^{(\dagger)}\rangle = s_{0\sigma};\ \ \langle d_i^{(\dagger)}\rangle = d_0, \tag{4.5}$$

and for the Lagrange multipliers

$$\langle \lambda_i\rangle = \lambda_0;\ \ \langle \Lambda_{i\sigma}\rangle = \Lambda_{0\sigma}, \tag{4.6}$$

is possible.

In the case of spiral spin ordering, the Hamiltonian (4.4) can be analytically diagonalized by adopting the Bloch representation, and performing a unitary transformation with respect to spin indices, yielding

$$\begin{aligned} E_{\mathbf{k},\pm} &= \frac{1}{2}\left[t(z_{0\uparrow}^2 + z_{0\downarrow}^2)T_e + \Lambda_{0\uparrow} + \Lambda_{0\downarrow}\right] - \mu \\ &\pm \frac{1}{2}\sqrt{\left[t(z_{0\uparrow}^2 - z_{0\downarrow}^2)T_e + \Lambda_{0\uparrow} - \Lambda_{0\downarrow}\right]^2 + 4t^2 z_{0\uparrow}^2 z_{0\downarrow}^2 T_o^2} \end{aligned}$$

where $T_e = -\sum_{\mathbf{l}} \cos(\mathbf{Q}\cdot\mathbf{l}/2)\cos(\mathbf{k}\cdot\mathbf{l})$, $T_o = -\sum_{\mathbf{l}} \sin(\mathbf{Q}\cdot\mathbf{l}/2)\sin(\mathbf{k}\cdot\mathbf{l})$ are the even and odd contribution to the kinetic energy in presence of $\mathbf{Q}$, and $\mathbf{l} = (1,0), (1/2, \pm\sqrt{3}/2)$ are the nearest-neighbour displacements. The saddle-point condition is enforced by minimizing with respect to the mean-field values of the bosons, and to the other parameters (the components of the pitch vectors in our case), the free energy

$$\mathcal{F} = \mathcal{F}_0 - T\sum_{\mathbf{k},\alpha=\pm} \log\left(1 + \mathrm{e}^{-E_{\mathbf{k},\alpha}/T}\right), \tag{4.7}$$

where

$$\mathcal{F}_0 = N[Ud_0^2 + \lambda_0(e_0^2 + d_0^2 + s_{0\uparrow}^2 + s_{0\downarrow}^2 - 1) - \Lambda_{0\uparrow}(d_0^2 + s_{0\uparrow}^2) - \Lambda_{0\downarrow}(d_0^2 + s_{0\downarrow}^2) + \mu n], \tag{4.8}$$

N is the number of sites, and n is the electron density per site. Minimization leads to the set of self-consistency equations

$$\frac{\partial \mathcal{F}_0}{\partial \mathcal{X}} + \sum_{\mathbf{k},\alpha=\pm} \frac{\partial E_{\mathbf{k},\alpha}}{\partial \mathcal{X}} f(E_{\mathbf{k},\alpha}) = 0, \tag{4.9}$$

where $f(E) = [e^{E/T} + 1]^{-1}$ is the Fermi function and $\mathcal{X}$ represents generically one of the parameters (4.5), (4.6) and the two components of the pitch vector $\mathbf{Q}$. The chemical potential μ is fixed by the condition

$$\sum_{\mathbf{k},\alpha=\pm} f(E_{\mathbf{k},\alpha}) = nN.$$

We assume henceforth $n = 1$ (half-filling).

The formalism just outlined allows for a description of the paramagnetic metal, the metallic phase with spiral magnetic ordering, and the antiferromagnetic insulator (which is a special case of spiral ordering).

We have also studied configurations with broken translational symmetry, taking unit-cells containing N_s sites. In these cases, it is not possible to obtain explicit expressions for the eigenvalues of the mean-field SB Hamiltonian, equivalent to Eq. (4.7), and the solution involves a numerical diagonalization of matrices $2N_s \times 2N_s$[1].

In particular we considered solutions in which in the bosons have different values on each of the three sublattices, which amounts to have 21 self-consistency equations for the bosons, plus the ones for the chemical potential and for the pitch vector. This kind of solutions involve diagonalization of a 6×6 matrix.

We have also studied solutions analogous to LSDW found in Hartree-Fock[97]. The latter solutions can be found considering a four-sites unit cell (see Fig. 4.3). In this case, since we were just looking for phases with the same symmetry of the LSDW found in HF, we did not introduce rotations of the local quantization axis to avoid further complications. The Hamiltonian is therefore diagonal in the spin index and numerical diagonalization only involves 4×4 matrices.

The self-consistency equations (4.9) can easily be generalized to the broken-symmetry case, once different bosons are introduced on different sites in the unit-cell.

4.2.2 Phase diagram

A similar SB mean-field theory for this problem has been carried out in Ref. [99]. The result reported was quite similar to the HF phase diagram, but no region of stability was found for the spiral metal. We now describe our results, that present some differences with respect to [99], and later discuss what makes our calculation more careful and complete. The self-consistency equations (4.9) yield the same solutions found in HF, namely a paramagnetic metal, a metal with incommensurate spiral ordering, and an

[1]The factor 2 comes from the spin degree of freedom, since the Hamiltonian is not diagonal in the spin as soon as a pitch vector is considered.

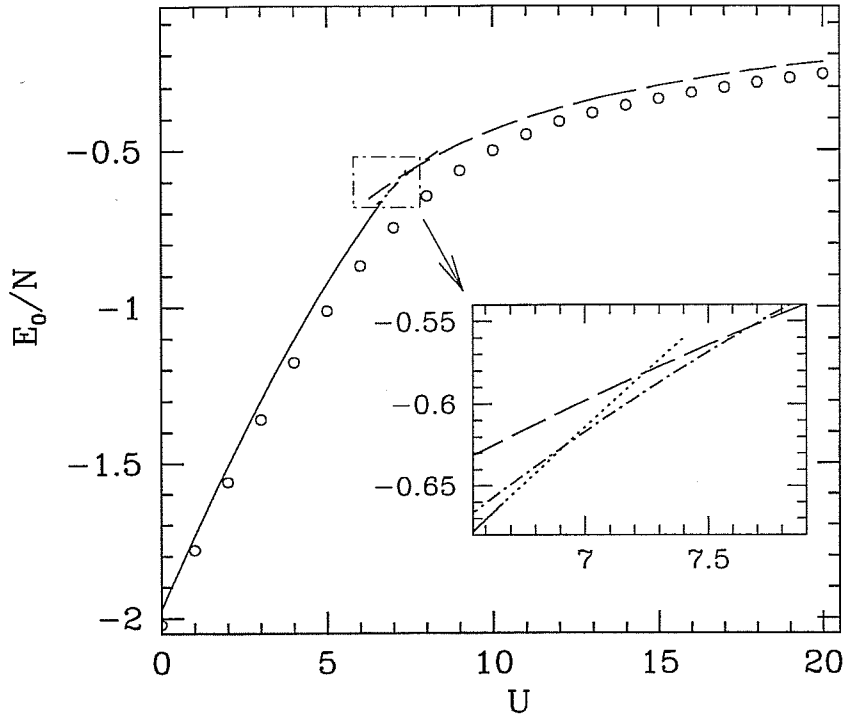

Figure 4.4: U dependence of the groundstate energy per site. SB results: PM (solid line), SM (dotted line), LSDW (dot-dashed line), and AFMI (dashed line). Open dots are the exact diagonalization results for the 12−site cluster.

antiferromagnetic insulator. As in HF, the PM-SM transition is continuous, and the other two transitions are of first order, but all of them occur at larger coupling values, $U_{c1} = 6.68t$, $U_{c2} = 6.84t$, and $U_{c3} = 7.68t$. The energy curves corresponding to the above phases are reported in Fig. 4.4. Our results agree with Ref. [99] as far as the PM, AFMI, and LSDW phases are concerned, but we also find a region of stability for the SM phase, which was not detected in Ref. [99]. These authors were indeed looking for spiral phases starting from the strong-coupling side, and following them to weaker coupling at fixed vector **Q**. On the other hand, our analysis shows that a spiral phase develops continuously from the PM at intermediate coupling and it ends in a critical point soon after the level-crossing with the AFMI (see the inset in Fig. 4.4), and does not exist at strong-coupling. The pitch vector, as well as the magnetization smoothly evolve from the metallic solution, and continuously change increasing the coupling. Therefore, our SM phase is the correct generalization of the corresponding phase found within HF [97], and it is unrelated to the high-energy SM phases of Ref. [99].

However, the region of existence of the SM is narrower within SB as compared to HF, and the magnetization $m = \frac{1}{2}(n_\uparrow - n_\downarrow)$ is always less than 0.1, a really small value with respect to the HF value (≤ 0.4). Therefore the jump of the magnetization at the SM-AFMI transition is substantially larger than in the HF approximation. We point

out that, contrary to nesting models, where the presence of free particles (doping) is a necessary condition for spiral ordering [98, 100, 101], here the spiral phase exists at half-filling, as previously shown in Ref. [96], within the HF approximation. Despite the overall qualitative agreement between the HF and the SB phase diagrams, the main outcome of the comparison between them is that the stability of the SM phase is strongly reduced. Furthermore, the SM is hardly distinguishable from the PM in its whole region of stability. It is reasonable to expect that the inclusion of quantum fluctuations washes out these phases leaving the way open for a transition between a PM and the AFMI.

Despite the strong frustration of the antiferromagnetic (AFM) order on the triangular lattice [94, 95], both the HF and SB approaches indicate no paramagnetic Mott insulating phase in the zero-temperature phase diagram of the half-filled Hubbard model.

4.2.3 The Brinkman-Rice transition

The phase diagram emerging from the mean-field approximation of the Kotliar-Ruckenstein SB Hamiltonian does not present, among the different transitions, a Mott transition from a paramagnetic metal and a paramagnetic insulator (PI), being the insulating phase characterized by magnetic ordering. The second question we asked ourselves at the beginning of this chapter has therefore a negative answer.

Within the SB approach it is possible to restrict to paramagnetic solutions. In a such a restricted space, a MIT occurs between a paramagnetic metal and a paramagnetic insulator. It should be clear from the above discussion that in the case of the triangular lattice, and, even more obviously, for nested lattices, this procedure amounts to follow the paramagnetic solution beyond its region of stability, and that the paramagnetic insulator represents a high-energy excited state. Nevertheless, the investigation of this transition proves useful for at least two reasons: it can be viewed as clue on what it would happen if some other physical effect inhibited magnetism, and it gives an estimate on how far from the Mott transition the system really is. We mean that, if the critical value for the Mott transition is really close to a point in which the metallic solution is still stable, then we expect that the inclusion of small terms which oppose to magnetism can stabilize the paramagnetic insulator.

Since the SB mean-field theory is equivalent to the Gutzwiller variational approach (see Par. 1.1.2,1.1.3), the search of a PM-PI transition is completely equivalent to the Brinkman-Rice [25] approach.

If the possibility for magnetic ordering is neglected, the paramagnetic metallic phase undergoes a transition associated with a vanishing value of the double-occupancy boson

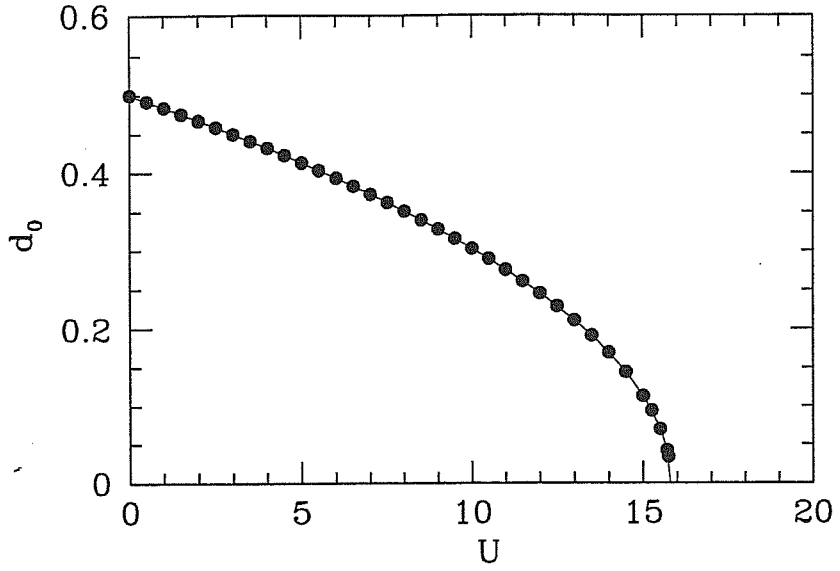

Figure 4.5: Average double occupation as a function of U for the paramagnetic SB solution. The vanishing of d_0 is associated with the paramagnetic insulating solution.

d_0 (reported in Fig. 4.5), and consequently a vanishing $z_{i\sigma}$, which determines in turn a zero effective hopping ($z_{i\sigma}$ is an effective renormalization of the hopping amplitude). As usual the BR transition is associated with the disappearance of the quasiparticles.

The critical value (at $T = 0$) of the Hubbard interaction is given by

$$U_{BR} = \frac{32t}{N} \sum_{\mathbf{k}} \varepsilon_{\mathbf{k}} \theta(2t\varepsilon_{\mathbf{k}} + \mu), \tag{4.10}$$

where $\varepsilon_{\mathbf{k}} = T_e(\mathbf{Q} = 0)$ are the single particle eigenvalues for the paramagnetic solution (i.e. in absence of a pitch vector $\mathbf{Q}$), and μ is the chemical potential chosen to fix the density to $n = 1$ [25, 27]. Using the suitable values for the triangular lattice we obtain $U_{BR}/t \simeq 15.8$ ($\mu = 0.82t$).

As we see this value is much larger than U_{c1}/t, U_{c2}/t and U_{c3}/t found above. The system is therefore not even close to the Brinkman-Rice transition when the MIT occurs.

At least from SB mean-field calculations, the degree of frustration of the triangular lattice is not strong enough to let the system become insulating without taking advantage of the magnetic degrees of freedom. The inclusion of quantum fluctuations beyond the mean-field can in principle wash out the intermediate magnetic phases, but is hard to imagine that the effect would be strong enough to stabilize the paramagnetic insulator.

4.3 Exact Diagonalization

In order to understand to which extent the picture we found within the mean-field SB theory survives in an exact treatment of the model, we performed exact diagonalization of small clusters by means of the standard Lanczos algorithm. The largest lattice compatible with all the symmetries of the model that can be handled with exact diagonalization is a $N = 12$ site cluster [94]. Unfortunately, we can not perform a finite-size scaling analysis of this problem, since the next lattice with the proper symmetries is a $N = 27$ site one, which is far beyond the presently computable sizes. This ED study will anyway help us in further understanding the MIT in the half-filled triangular lattice, providing us with a complementary point of view with respect to the SB mean-field, in which the thermodynamic limit was reached, but the correlation was treated approximately. Especially for really small clusters, attention must be payed to the choice of boundary conditions. In particular, it is crucial to ensure to always work in closed-shell configurations. If a Lanczos calculation is performed with open-shell configurations, the algorithm filters an arbitrary superposition of the degenerate levels, that can break the symmetries of the Hamiltonian, and in a last instance, may not be representative of the actual physics of the system. This may be particularly dangerous when conduction properties of the system are under inspection. 12 electrons in the $12-$site lattice are not in a closed-shell configuration if periodic or anti-periodic boundary conditions are used. It is therefore necessary to resort to twisted boundary conditions, i.e. a phase χ_i ($i = 1, 2$ labels the independent directions on the lattice) must be imposed when hopping around the boundaries. Various values of χ_1 and χ_2 give closed-shell configurations. We always choose (for every value of U) the ones that minimize the energy.

It turns out that the boundary conditions that minimize the energy in a closed-shell configuration for $U = 0$ leave the system in a closed-shell configuration at all U. The energy is shown as a function of U in Fig. 4.4 (open dots). The overall agreement with the mean-field SB results is good, the largest deviations ($\sim 20\%$) being, as expected, at intermediate coupling ($U/t \sim 7$).

The energy curve alone does not allow us to gain enough information on the nature of the MIT in the finite cluster. It is really hard to understand from the energy curve if a single transition occurs, and eventually the order of the transition(s). Fortunately, in ED calculations, we can access almost every groundstate and dynamical property.

To check the occurrence of a discontinuous phase transition we evaluated the overlap between the GS wave function and the two limiting cases of $U = 0$, and for large U (namely, $U = 100t$) representative of the AFM state. As shown in Fig. 4.6 on the large-

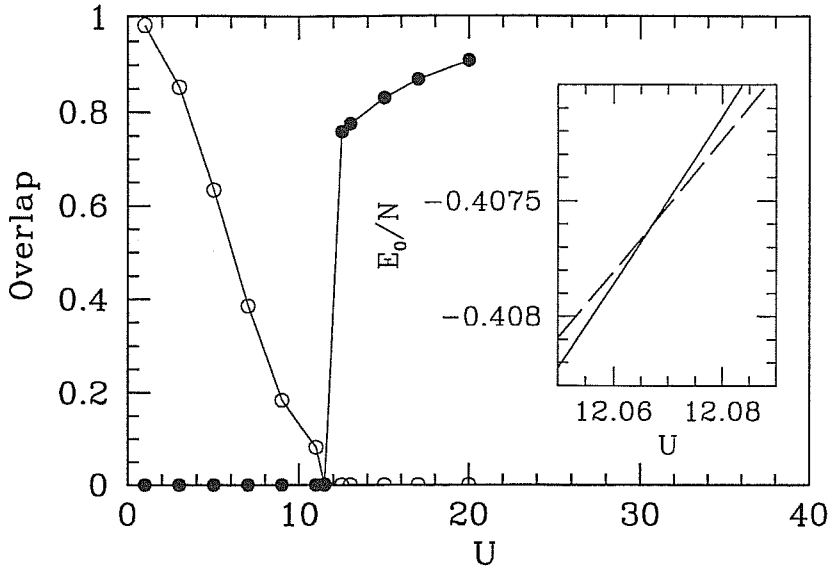

Figure 4.6: Overlap of the finite-U GS with the $U = 0$ (empty dots) and the $U = 100t$ (full dots) GS's, for $N = 12$. In the inset the GS energy per site in the $\mathbf{k} = (0, 0)$ (solid line) and $\mathbf{k} = (2\pi/3, 0)$ (dashed line) subspaces is plotted versus U.

U side of the diagram the GS has a large overlap with the AFM strong-coupling state and a vanishing overlap with the non-interacting metallic one. On the metallic side the overlap with the non-interacting state is always finite, but it is a decreasing function of U; in this regime the GS has anyway a vanishing overlap to the AFM state. We have therefore a clear evidence for a strongly correlated metal with a decreasing coherent part. In particular the sharp change of the GS wave function at $U_{MIT} \simeq 12.07t$ is due to a level-crossing occurring between a metallic and an antiferromagnetic solutions, that correspond to different quantum numbers, as shown in the inset in Fig. (4.6). At least for the $12-$site lattice, the transition is therefore a level-crossing between a solution that maintains a metallic contribution up to the critical coupling and an insulator that soon after the transition strongly resembles the $U/t \to \infty$ limit. These results, however, do not rule out the possibility of a continuous transition within the metallic phase without changing the symmetry of the state, i.e. the PM-SM transition found with SB. The overlap between the GS wavefunction and the $U = 0$ non-interacting metal can be interpreted as a sort of quasiparticle weight renormalizing the non-interacting Green's function. This quantity changes rather abruptly its behaviour at $U \sim 7t$, where the curvature changes sign. This change could be also interpreted as a finite-size counterpart of a second-order transition, but the impossibility of a finite-size scaling does not allow for a reliable confirmation of this hypothesis. In principle this shadow of a second-order

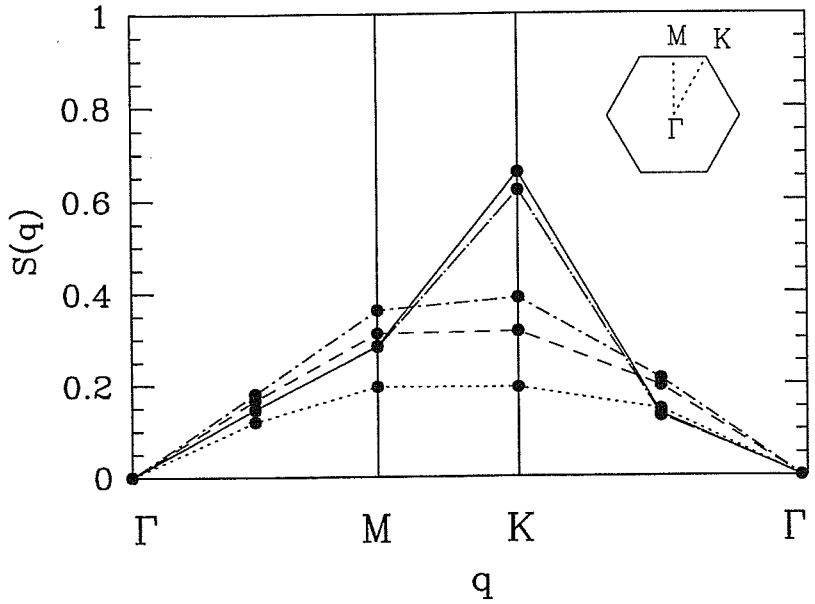

Figure 4.7: Spin structure factor $S(\mathbf{q})$: U=2t (dotted line), U=8t (dashed line), U=11.5t (dot-short-dashed line), U=12.5t (dot-long-dashed), U=40t (solid line).

transition could be considered as the counterpart of the PM-SM transition found in HF and SB. Some magnetic effect would occur if this was the case.

To discuss the possibility of peculiar magnetic phases developing before the transition to an almost perfect AFM at U_{MIT} we have computed the static spin structure factor,

$$S(\mathbf{q}) = \frac{1}{N}\sum_{i,j} S_i^z S_j^z \exp[\mathbf{q}\cdot(\mathbf{r}_i - \mathbf{r}_j)], \tag{4.11}$$

for different values of U. The results, reported in Fig. 4.7, do not suggest any intermediate state between a metallic state without magnetic order and the AFM insulator, as $S(\mathbf{q})$ abruptly changes from a structureless behaviour for metallic couplings to an AFM pattern peaked at the classical ordering wave-vector, i.e. $\mathbf{Q_0} = (4\pi/3, 0)$. The sudden change is coincident with the level crossing shown in Fig.4.6 at U_{MIT}. Although we suspect that the intermediate spiral phases are an artifact of the mean-field approach, the weakness and the strong size-dependence of the spiral phases suggested by the SB results, may make them unaccessible on our 12−site lattice.

As a last quantity, we also computed the finite-frequency optical conductivity $\sigma(\omega)$ and the Drude weight, measuring the electronic mobility. The real part of the xx component of the conductivity tensor for a tight-binding model at zero temperature may be expressed in terms of the Kubo formula [102]

$$\sigma_{xx}(\omega) = D_{xx}\delta(\omega) + \mathcal{I}m\langle 0|J_x^\dagger \frac{1}{\omega - \mathcal{H} + E_0 - i\delta} J_x|0\rangle, \tag{4.12}$$

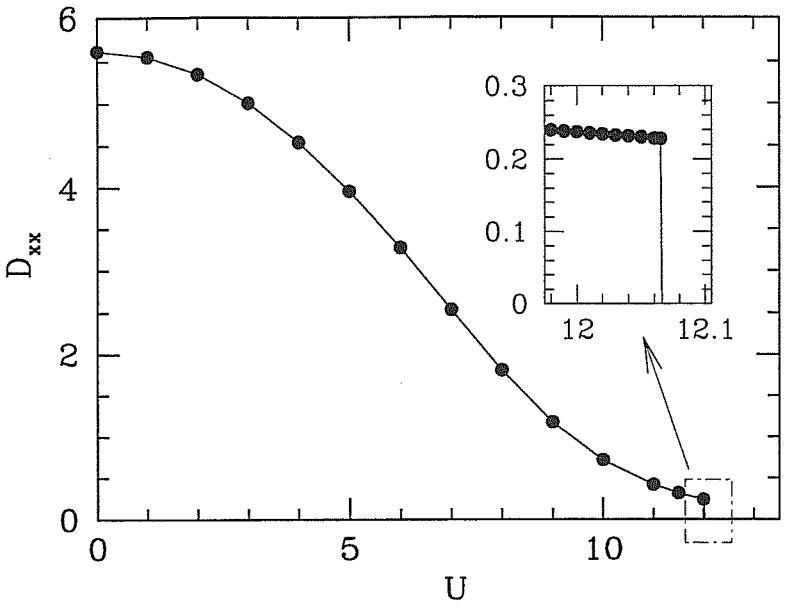

Figure 4.8: Exact calculation of the Drude weight as a function of U for the $N = 12$ cluster.

where $J_x = \sum_{i\sigma,\mathrm{l}} l_x (c^\dagger_{i\sigma} c_{i+\mathrm{l}\sigma} - h.c.)$ is the $x-$component of the current operator (l_x are the $x-$components of the primitive displacements l). vector[36]. The coefficient of the zero-frequency delta function contribution D_{xx}, the Drude weight, is given by the f-sumrule[102]

$$D_{xx} = -\frac{\pi e^2}{2}\langle \mathcal{H}^t_x \rangle - \sum_{n\neq 0} \frac{|\langle \phi_0 | J_x | \phi_n \rangle|^2}{E_n - E_0}, \tag{4.13}$$

where $\mathcal{H}^t_x = \sum_{i\sigma,\mathrm{l}} l_x^2 (c^\dagger_{i\sigma} c_{i+\mathrm{l}\sigma} + h.c.)$, and $|\phi_n\rangle$ is the eigenfunction of $\mathcal{H}$ with eigenvalue E_n. The second term on the right-hand side of Eq. (4.12) can be easily computed with the Lanczos method, without knowing the whole spectrum $|\phi_n\rangle$, E_n, but simply knowing the groundstate $\langle \mathcal{H}^t_x \rangle$ is straightforwardly computed, so D_{xx} is obtained as a difference.

The latter quantity, which is reported in Fig. 4.8 is a direct measure of the metallic character of the state, and the MIT is signaled by the vanishing of D_{xx} [103]. For a finite system, D_{xx} is never vanishing for any value of U, but an abrupt change takes place at the level-crossing point. For $U < U_{MIT}$, D_{xx} is a decreasing function of the interaction, which resembles the overlap in Fig. 4.6. An abrupt change takes place at the level-crossing point and for $U > U_{MIT}$ it becomes negative, a common phenomenon in the insulating phase of a small-size system [36].

All the results of exact diagonalization point towards the same direction: the metal-AFMI level-crossing found within the SB mean-field approach is shifted to sizeably larger values of U. The metallic solution exhibits a continuous loss of metallicity with

increasing U. The Drude weight is finite up to the MIT on the $12-$site lattice although it is quite small (4% of the non-interacting value). We remark that, due to finite-size effects, we cannot exclude the possibility that, for larger systems, the change in slope of D_{xx} (and analogously of the overlap between the groundstate vector and the non-interacting solution) may transform in a real transition in which the quantity vanishes before the transition to the AFMI is reached. In such a case, there would be a region of stability for the paramagnetic insulator, though the SB results point in the opposite direction.

4.4 Conclusions

Using the slave boson technique and the exact diagonalization, we have investigated the zero-temperature phase diagram of the half-filled Hubbard model on a two dimensional triangular lattice. The mean-field SB approach displays a rich phase diagram which qualitatively resembles the one from HF calculations, but, on the other hand, drastically reduces the stability of the spiral metal and of the linear spin-density-wave states. Namely, the weak-coupling paramagnetic metal continuously evolves into a spiral metal at $U = U_{c1} = 6.68t$, which crosses the linearly polarized spin-density-wave groundstate at $U = U_{c2} = 6.84t$. The latter phase undergoes a further first-order transition towards an antiferromagnetic insulator at $U = U_{c3} = 7.68t$. All these transitions occur for coupling constants substantially smaller than the critical value for the Brinkman-Rice transition to a paramagnetic insulator ($U_{BR} = 15.8t$).

The exact-diagonalization results present instead just a first order transition between the paramagnetic metal and the antiferromagnetic insulator at $U_{MIT} = 12.07t$, without intermediate "exotic" phases.

The absence of perfect-nesting is only sufficient to shift the MIT to finite (and quite large) values of U, but the frustration of AFM is unlikely to be strong enough to give rise to a Mott-Hubbard transition within the paramagnetic sector. More frustrated models, like, e.g. the Kagomé lattice, must be invoked to look for a PM-IM transition for the single-band Hubbard model.

Conclusions

In this thesis we have studied some relevant examples of correlation-driven metal-insulator transitions (Mott transitions) with a variety of techniques, ranging from exact diagonalization of small clusters to the slave-boson mean-field theory, from Hartree-Fock to the Dynamical Mean-Field Theory. The latter is the most reliable tool for the study of the Mott transition. The Mott phenomenon is based on the competition between the delocalization effect of the kinetic energy, and the effect of the correlations, that constraint the electronic motion. This basic competition can be studied within the framework of the single-band Hubbard model. The study of this model has enormously contributed to the understanding of the mechanism leading to the Mott transition, but many interesting features of real compounds and many theoretical aspects can only be understood if other physical mechanisms are considered.

One of the most interesting open points regarding the Mott transition is the possibility of a "real" Mott transition, without broken-symmetry in the insulating state. For the single-band Hubbard model, in the absence of frustration , the transition is always accompanied by AFM ordering. We investigated the Mott transition on the most relevant frustrated lattice, the triangular lattice. We have given a substantial contribution to solve this open issue. Our results rule out the possibility of a real Mott transition, since both a slave-boson and an exact diagonalization study find only a transition to an antiferromagnetic insulator. The Brinkman-Rice transition to a paramagnetic insulator occurs for a coupling much larger than the the critical coupling for the transition to the AFM insulator. In the slave-boson approach many exotic magnetic phases are found in the proximity of the MIT. All these findings have an experimental counterpart in Mott insulators on triangular lattices like $SiC(0001)$ or $K/Si(111) : B$, or organic superconductors like $\kappa - (BEDT - TTF)_2X$. a MIT to an AFM state.

An alternative route to a Mott transition without symmetry-breaking is the inclusion of orbital degrees of freedom. This is a point of crucial interest because in most Mott insulators, starting from the prototypical V_2O_3, the orbitals primarily involved in the transition are degenerate.

Among the many experimental realization of Mott insulator, we have concentrated on the alkali-metal doped fullerides A_4C_{60}. These compounds are nonmagnetic insulators, even if they have a partially filled band. Band-structure calculation completely fail in their description, giving a metallic state. Even if the strong correlation is the natural reason for the insulating behaviour, the single-band Hubbard model is definitely not able to account for the properties of these compounds. We have reported strong evidences that the properties of the alkali-metal doped fullerides can only be understood by considering the combined effect of orbital degeneracy, multiplet-exchange, strong electronic correlation and Jahn-Teller effect. The Dynamical Mean Field Theory provides a unique framework in which all these effects can be treated on the same footing.

We have concludes that these compounds can be labeled as Mott-Jahn-Teller insulators. We have shown that the on-site Coulomb repulsion is strong enough to lead to a Mott insulating state, as soon as the multiplet-exchange is considered. The Jahn-Teller coupling further enhances the tendency towards an insulator.

Once the electronic motion is strongly suppressed by the correlation, the solid can be thought as a collection of isolated molecules. Each molecule is free to choose the configuration that minimizes the energy. We have seen that on each molecule, the Jahn-Teller effect is strong enough to overcome Hund's rule, and stabilize a singlet groundstate. As a result, the solid is nonmagnetic. Moreover, we have found that, as soon as the system becomes insulating, the spectral properties become essentially molecular. Our DMFT results are able to completely reproduce all the experimental features of these compounds, ranging from the nonmagnetic properties, to the precise values of the relevant excitations (spin and optical gaps).

The model successfully introduced in the explanation of the fullerides has an important role also from a theoretical point of view. If we consider the antiadiabatic limit for the Jahn-Teller effect on each molecule, then we obtain a purely electronic model with a negative multiplet-exchange coupling J_H. As a result, the atomic limit has an inverted multiplet structure, in which the less degenerate levels are favoured. In particular, for $n = 4$ (or $n = 2$), the molecular groundstate becomes the non-degenerate spin and orbital singlet with $S = 0$ and $L = 0$. The Mott limit is expected to be a zero-entropy insulator. This property has dramatic effects on the Mott transition. First of all, the usual interpretation of the Mott transition in the single band Hubbard model as a Kondo screening of the spin degrees of freedom is not possible for this case, since the insulator has zero entropy.

Moreover, we have shown that a direct second-order transition between a Fermi liquid and a zero-entropy insulator is not possible if the electron effective mass diverges

at the metal-insulator transition. Nevertheless, the DMFT results display a transition between a Fermi-liquid and a Mott insulator. After having ruled out the possibilities that this transition acquires a band-like character, or that it becomes first-order, we have considered a more exciting possibility. A careful analysis of the Fermi liquid solution in the proximity of the Mott transition suggests that this phase is unstable towards pairing in the Cooper channel. We have computed the pairing susceptibility and found that the criteria for the pairing instabilities are satisfied. This finding suggests that, if we allow for superconducting long-range-order, the system would become superconducting before the Mott transition, leading to a direct superconductor-insulator transition. A new fascinating scenario emerges from our results. Upon increasing interaction, the metallic state becomes more and more correlated, and the quasiparticle effective mass strongly increases. When the correlation exceeds a given value ($\sim U_{c2} - J_H$), the local exchange interaction gives rise to a pairing leading to local singlets, that form a superconducting state. At $U = U_{c2}$ the insulator disappears in the Mott insulator. This is the first realization of a direct superconductor-insulator transition to our knowledge. Besides the great theoretical relevance, this result has lots of interesting experimental implications, like the the possible superconducting state in $\mathcal{A}_4C_{60}$ that could be realized by suitably tuning the pressure, putting the system really close to the Mott transition. This finding has to be taken into account also in the description of the superconducting A_3C_{60}.

This scenario still needs a more solid foundation. In particular, the DMFT equations must be extended allowing for pairing. The study of this broken-symmetry case is underway.

Acknowledgments

The first words must be dedicated to my supervisors: first of all Michele Fabrizio, who has continuously stimulated me, sometimes forcing me to follow the right direction. Thank you for the patience and for all the things you teached me. Second, but not least, Erio Tosatti, for his enlightening physical insight, and helpfulness. Many of the good physical ideas in this thesis arise from his intuitions.

I also thank Sandro Sorella, that has guided me in some trips in the land of Green's Function Monte Carlo, that are not presented in this thesis. Alberto Parola and Giuseppe Santoro deserve thanks as well for many interesting discussions on various topics. My office-mates have always been wonderful scientific collaborators, besides good friends, so thanks to Federico Becca, Matteo Calandra and Luca Capriotti. Ilaria Meccoli is definitely a very good friend, but she must also be acknowledged as a great physicist, as everybody who has worked with her knows. A special acknowledgement goes to Sergio Caprara. His enthusiasm and passion are one of the most beautiful things I have ever seen in the world of physics (and of life). I am really endebted with Claudio Castellani for many exciting conversations and for a relevant contribution to some important points of this thesis.

Marco Grilli's office in Rome has been always open to me, whenever I needed, not just as a place to work, or use the PC, but as a nice place to stay. Obviously, I thank Marco for this and for the physics he has teached me in all these years.

I did not have many occasion to talk to Carlo Di Castro, but each of these was really significant. I thank him for this and hope to have more occasions to learn from him.

Sergio Ciuchi, has always believed in me, and he has always fought with my thousands problems, to try to work with me. Meanwhile, he has been a great guide to the Dynamical Mean Field Theory, and that's just one of the reasons to thank him.

I am also endebted with Gaby Kotliar, for having pointed out the problems of the Mott transition to a zero-entropy insulator, and for the interest shown for my work.

Many thanks to Erik Koch for many discussions ranging from various pysical problems to art.

I also thank Denis Feinberg, Giovanni B. Bachelet, and Claudio Grimaldi, for many discussions about physics of subjects related to the work of this thesis, and for the collaborations that I had with them.

I remember many conversations with A. J. Millis, R. Raimondi, W. Stephan, E. Cappellutti, J. Lorenzana, A. Liechtenstein, L. Benfatto and S. Fratini. Thanks to D. Cassi and R. Burioni for the warm hospitality in Parma, to R. De Renzi and M. Acquarone for interesting discussions in that occasion and in other times.

I have just a few minutes to submit my thesis, so I really can not thank everybody as I should. But I would prefer not submitting the thesis than forgetting to thank all of you.

Thanks to you, mamma e papà, who always believed in me (sometimes too much!), have

always been close to me, and have done everything you expect from your parents and sometimes even more. Thanks to Daniele, one of the most surprising persons. I really love the way we are friends besides brothers. Thanks to Alessandro, even if we don't speak so much in these times. You are great, like the time I spent with you in my life.

I am really in trouble to find adequate words for you, Stefania. I can only say that you give significance to my life, and I hope to deserve all that you do to me. Thanks and baciotti.

I can not forget to deeply thank the "amichelli", Alessandro, Marco, Maurizio and Mimmo (rigorously in alphabetical order), for all the time I spent with them, for the patience they have shown to me when I was in bad periods, for being always there.

A kiss to Ilaria, a great friend. Thanks for all the times you listened to my complaints, and stupid speaches. I am running out of time, I hope to thank all of my friends in Trieste, that helped me to live better. Thanks to Luca (my guide and master) Michele (and his experience), and to Giulia and Michela, for a wonderful (though a bit stressing) period. Thanks to Federico, I am sorry I have not been a good coworker, but I hope I have been at least a good guide in NY. Thanks to the prince of non-sense, Mattéo, I have missed you a lot in this year. Thanks to Gabriele and Paul, two wonderful persons. Thanks to Leonardo, who standed me as a bad house-mate. Thanks to Andrea (il Tromba) a guy who knows how to live. I should show you I am not a quaquaraquá. Ciao Mario. (There's no need for more words). Thanks to Andrea (and wife), Gianluca, Antonio, Gianni, Lore, Stefano, Paola, and all the others (I know I am forgetting somebody, I am sorry!!)

This is for you, Giancarlo.

Appendix A

Spectrum of an isolated C_{60}^{n-} ion

The t_{1u} orbitals are the counterparts of the p orbitals within the icosahedral point group, and the multiplet exchange splitting is governed by the Hamiltonian (2.3), that we rewrite here

$$\mathcal{H}_{int} = \frac{2J_H}{3}\sum_{\alpha} n_{\alpha}^2 - \frac{2J_H}{3}\sum_{\alpha<\beta} n_{\alpha}n_{\beta} + \frac{J_H}{2}\sum_{\alpha<\beta}\Delta_{\alpha\beta}^2, \tag{A.1}$$

with $\Delta_{\alpha\beta} = \sum_{\sigma}(c_{\alpha\sigma}^{\dagger}c_{\beta\sigma} + h.c.)$. In this Appendix we show the solutions of this Hamiltonian for different number of particles. Due to symmetry with respect to the $n = 3$ (half-filling) case, the only independent values are $n = 3, 2, 1$.

- For $n = 3$, the possible multiplets, labeled by the total spin S and total angular momentum L, are:

  1. $L = 0$ and $S = 3/2$ with energy $E(n, S, L)$ given by

  $$E\left(3, \frac{3}{2}, 0\right) = 0.$$

  The four eigenstates are

  $$c_{1\uparrow}^{\dagger}c_{2\uparrow}^{\dagger}c_{3\uparrow}^{\dagger}|0\rangle;$$
  $$c_{1\downarrow}^{\dagger}c_{2\downarrow}^{\dagger}c_{3\downarrow}^{\dagger}|0\rangle;$$
  $$\frac{1}{\sqrt{3}}\left(c_{1\downarrow}^{\dagger}c_{2\uparrow}^{\dagger}c_{3\uparrow}^{\dagger} + c_{1\uparrow}^{\dagger}c_{2\downarrow}^{\dagger}c_{3\uparrow}^{\dagger} + c_{1\uparrow}^{\dagger}c_{2\uparrow}^{\dagger}c_{3\downarrow}^{\dagger}\right)|0\rangle;$$
  $$\frac{1}{\sqrt{3}}\left(c_{1\uparrow}^{\dagger}c_{2\downarrow}^{\dagger}c_{3\downarrow}^{\dagger} + c_{1\downarrow}^{\dagger}c_{2\uparrow}^{\dagger}c_{3\downarrow}^{\dagger} + c_{1\downarrow}^{\dagger}c_{2\downarrow}^{\dagger}c_{3\uparrow}^{\dagger}\right)|0\rangle.$$

  2. $L = 2$ and $S = 1/2$ with energy

  $$E\left(3, \frac{1}{2}, 2\right) = 3J_H.$$

The ten eigenstates can be written in the following way: Six are written as

$$\frac{1}{\sqrt{2}}\left(c^\dagger_{\alpha\uparrow}c^\dagger_{\alpha\downarrow}c^\dagger_{\gamma\sigma} - c^\dagger_{\beta\uparrow}c^\dagger_{\beta\downarrow}c^\dagger_{\gamma\sigma}\right)|0\rangle,$$

with $\{\alpha,\beta,\gamma\}$ given by a permutation of $\{1,2,3\}$, and the other four are

$$\frac{1}{\sqrt{2}}\left(c^\dagger_{1\downarrow}c^\dagger_{2\uparrow}c^\dagger_{3\uparrow} - c^\dagger_{1\uparrow}c^\dagger_{2\downarrow}c^\dagger_{3\uparrow}\right)|0\rangle;$$

$$\frac{1}{\sqrt{2}}\left(c^\dagger_{1\uparrow}c^\dagger_{2\downarrow}c^\dagger_{3\downarrow} - c^\dagger_{1\downarrow}c^\dagger_{2\uparrow}c^\dagger_{3\downarrow}\right)|0\rangle;$$

$$\frac{1}{\sqrt{6}}\left(c^\dagger_{1\downarrow}c^\dagger_{2\uparrow}c^\dagger_{3\uparrow} + c^\dagger_{1\uparrow}c^\dagger_{2\downarrow}c^\dagger_{3\uparrow} - 2c^\dagger_{1\uparrow}c^\dagger_{2\uparrow}c^\dagger_{3\downarrow}\right)|0\rangle;$$

$$\frac{1}{\sqrt{6}}\left(c^\dagger_{1\uparrow}c^\dagger_{2\downarrow}c^\dagger_{3\downarrow} + c^\dagger_{1\downarrow}c^\dagger_{2\uparrow}c^\dagger_{3\downarrow} - 2c^\dagger_{1\downarrow}c^\dagger_{2\downarrow}c^\dagger_{3\uparrow}\right)|0\rangle.$$

3. $L = 1$ and $S = 1/2$ with energy

$$E\left(3,\frac{1}{2},1\right) = 5J_H.$$

The six states are given by

$$\frac{1}{\sqrt{2}}\left(c^\dagger_{\alpha\uparrow}c^\dagger_{\alpha\downarrow}c^\dagger_{\gamma\sigma} + c^\dagger_{\beta\uparrow}c^\dagger_{\beta\downarrow}c^\dagger_{\gamma\sigma}\right)|0\rangle,$$

with $\{\alpha,\beta,\gamma\}$ given by a permutation of $\{1,2,3\}$. The overall energy within the $n = 3$ manifold can be written as

$$E(3,S,L) = \frac{15}{2}J_H - J_H\left(2S^2 + \frac{1}{2}L^2\right).$$

- For $n = 2$ (and $n = 4$) we have

1. $S = 1$ and $L = 1$ with energy

$$E(2,1,1) = \frac{5}{3}J_H.$$

The nine eigenstates are obtained applying the spin lowering operator to the state

$$c^\dagger_{\alpha\uparrow}c^\dagger_{\beta\uparrow}|0\rangle,$$

with $\alpha \neq \beta$.

2. $S = 0$ and $L = 2$ with energy

$$E(2,0,2) = \frac{11}{3} J_H.$$

The eigenstates are

$$\frac{1}{\sqrt{2}} \left(c_{1\uparrow}^\dagger c_{1\downarrow}^\dagger - c_{2\uparrow}^\dagger c_{2\downarrow}^\dagger \right) |0\rangle;$$

$$\frac{1}{\sqrt{6}} \left(c_{1\uparrow}^\dagger c_{1\downarrow}^\dagger + c_{2\uparrow}^\dagger c_{2\downarrow}^\dagger - c_{3\uparrow}^\dagger c_{3\downarrow}^\dagger \right) |0\rangle,$$

and, for $\alpha \neq \beta$,

$$\frac{1}{\sqrt{2}} \left(c_{\alpha\uparrow}^\dagger c_{\beta\downarrow}^\dagger + c_{\beta\uparrow}^\dagger c_{\alpha\downarrow}^\dagger \right) |0\rangle.$$

3. $S = 0$ and $L = 0$ with energy

$$E(2,0,0) = \frac{20}{3} J_H,$$

and eigenstate

$$\frac{1}{\sqrt{3}} \left(c_{1\uparrow}^\dagger c_{1\downarrow}^\dagger + c_{2\uparrow}^\dagger c_{2\downarrow}^\dagger + c_{3\uparrow}^\dagger c_{3\downarrow}^\dagger \right) |0\rangle.$$

The energy for two electrons can be written as

$$E(2,S,L) = \frac{20}{3} J_H - J_H \left(2S^2 + \frac{1}{2} L^2 \right).$$

- For $n = 1$ (and $n = 5$) the energy is

$$E\left(1, \frac{1}{2}, 1\right) = \frac{5}{3} J_H.$$

The Hund's rules are satisfied in every manifold. The states are in fact ordered by decreasing spin, and, among the states with the same S, the maximum L has lower energy.

Bibliography

[1] N. F. Mott, *Metal-Insulator Transitions* (Taylor and Francis, London, 1974).

[2] A. Georges, G. Kotliar, W. Krauth, and M. J. Rozenberg, Rev. Mod. Phys. **68**, 13 (1996).

[3] M. Imada, A. Fujimori, and Y. Tokura, Rev. Mod. Phys. **70**, 1039 (1999).

[4] J.H. de Boer, and E.J.W. Verway, Proc. Phys. Soc. London, A **49**, 59 (1937).

[5] R. Peierls, Proc. Phys. Soc. London, A **49**, 72 (1937).

[6] N.F. Mott, Proc. Phys. Soc. London, A **62**, 416 (1949).

[7] J. C. Slater, Phys. Rev. **82**, 538 (1951).

[8] Y. J. Uemura, W. J. Kossler, X. H. Yu, J. R. Kempton, H. E. Schone, D. Opie, C. E. Stronach, D. C. Johnston, M. S. Alvarez, and D. P. Goshorn, Phys. Rev. Lett. **59**, 1045 (1987); J. M. Tranquada D. E. Cox, W. Kunnmann, H. Moudden, G. Shirane, M. Suenaga, P. Zolliker, D. Vaknin, S. K. Sinha, M. S. Alvarez, A. J. Jacobson, and D. C. Johnston, Phys. Rev. Lett. **60**, 156 (1988).

[9] O. Gunnarsson, Rev. Mod. Phys. **69**, 595 (1997).

[10] K. I. Kugel and D. I. Khomskii, Sov. Phys. JETP **37**, 725 (1973); K. I. Kugel and D. I. Khomskii, Sov. Phys. Usp. **25**, 231 (1982).

[11] W. Brückner, H. Oppermann, W. Reichelt, J.I. Terukow, F. A. Tschudnowski, and E. Wolf, *Vanadiumoxide Darstellung, Eigenschaften, Anwendung* (Akademie, Berlin, 1983).

[12] L. I. Johansson, F. Owman, and P. Mårtensjon, Surf. Sci. **360**, L478 (1996); J.-M. Themlin, I. Forbeaux, V. Langlais, H. Belkhir, and J.-M. Debever, Europhys. Lett. **39**, 61 (1997).

[13] H. H. Weitering, X. Shi, P. D. Johnson, J. Chen, N. J. DiNardo, and K. Kempa, Phys. Rev. Lett. **78**, 1331 (1997).

[14] R. H. McKenzie, Comments Cond. Matt. Phys. **18**, 309 (1998); J. Merino and R. H. McKenzie, Phys. Rev. B **61**, 7996 (2000).

[15] M. Fabrizio and E. Tosatti, Phys. Rev. B **55**, 13465 (1997).

[16] M. Capone, M. Fabrizio, P. Giannozzi, and E. Tosatti, Phys. Rev. B **62**, 7619 (2000).

[17] S. E. Barnes, J. Phys. F **6**, 1375 (1976); N. Read and D. Newns, J. Phys. C **16**, 3273 (1983); P. Coleman, Phys. Rev. B **29**, 3035 (1984).

[18] J. Hubbard, Proc. R. Soc. London A **276**, 238 (1963).

[19] M. C. Gutzwiller, Phys. Rev. Lett. **10**, 159 (1963).

[20] J. Kanamori, Prog. Theor. Phys. **30**, 275 (1963).

[21] A. Auerbach, *Interacting electrons and quantum magnetism* (Springer-Verlag, New York, 1994).

[22] H. Eskes, A. M. Olés, M. B. J. Meinders, and W. Stephan, Phys. Rev. B **50**, 17980 (1994).

[23] J.D. Reger and A.P. Young, Phys. Rev. B **37**, 5978 (1998).

[24] E.M. Lieb and F.Y. Wu, Phys. Rev. Lett. **20**, 1455 (1968).

[25] W. F. Brinkman and T. M. Rice, Phys. Rev. B **2**, 4302 (1970).

[26] J. Hubbard, Proc. R. Soc. London A **281**, 401 (1964).

[27] G. Kotliar and A. E. Ruckenstein, Phys. Rev. Lett. **57**, 1362 (1986).

[28] R. Raimondi and C. Castellani, Phys. Rev. B **48**, 11453 (1993).

[29] C. Castellani, G. Kotliar, R. Raimondi, M. Grilli, Z. Wang, and M. Rozenberg, Phys. Rev. Lett. **69**, 2009 (1992).

[30] W. Metzner, and D. Vollhardt, Phys. Rev. Lett. **62**, 324 (1989).

[31] E. N. Economou, *Green's Functions in Quantum Physics* (Springer & Verlag, Berlin, 1983).

[32] X. Y. Zhang, M. J. Rozenberg, and G. Kotliar, Phys. Rev. Lett. **70**, 1666 (1993).

[33] J. E. Hirsch and R.M. Fye, Phys. Rev. Lett. **56**. 2521 (1986).

[34] M. Caffarel and W. Krauth, Phys. Rev. Lett. **72**, 1545 (1994).

[35] W. Krauth, Phys. Rev. B **62**, 6860 (2000).

[36] E. Dagotto, Rev. Mod. Phys. **66**, 763 (1994).

[37] A. Georges and G. Kotliar, Phys. Rev. B **45**, 6497 (1992).

[38] E. Müller-Hartmann, Z. Phys. B **74**, 507 (1989).

[39] M. J. Rozenberg, X. Y. Zhang, and G. Kotliar, Phys. Rev. Lett. **69**, 1236 (1992).

[40] G. Möller, Q. Si, G. Kotliar, M. J. Rozenberg, and D. S. Fisher, Phys. Rev. Lett **74**, 2082 (1995).

[41] H.W. Kroto, J.R. Heath, S.C. O'Brien, R.F. Curl,and R.E. Smalley, Nature **318**,162 (1985).

[42] W. Krätschmer, L.D. Lamb, K. fostiropulos, and D.R. Huffman, Nature **347**, 354 (1990).

[43] S.C. Erwin, in *Buckminsterfullerenes*, ed. by W.E. Billups and M.A. Ciufolini (VCH Publishers, New York, (1992).

[44] R.C. Haddon, A.F. Hebard, M.J. Rosseinsky, D.W. Murphy, S.J. Duclos, K.B. Lyons, B. Miller, J.M. Rosamilia, R.M. Fleming, A.R. Kortan, S.H. Glarum, A.V. Makhija, A.J. Muller, R.H. Eick, S.M. Zahurak, R. Tycko, G. Dabbagh, and F.A. Thiel, Nature **350**, 320 (1991).

[45] T. T. M. Palstra, A .F. Hebard, R. C. Haddon, and P.B. Littlewood, Phys. Rev. B **50**, 3462 (1994).

[46] D. W. Murphy, M. J. Rosseinsky, R. M. Fleming, R. Tycko, A. P. Ramirez, R. C. Haddon, T. Siegrist, G. Dabbagh, J. C. Tully, R. E. Walstedt, J. Phys. Chem. Solids **53**, 1321 (1992).

[47] R.F. Kiefl, T. L. Duty, J. W. Schneider, A. MacFarlane, K. Chow, J. Elzey, P. Mendels, G. D. Morris, J. H. Brewer, E. J. Ansaldo, C. Niedermayer, D. R. Noakes, C. E. Stronach, B. Hitti, and J. E. Fischer, Phys. Rev. Lett. **69**, 2005 (1992).

[48] P. J. Benning, F. Stepniak, D. M. Poirier, J. L. Martins, J. H. Weaver, L. P. F. Chibante and R. E. Smalley, Phys. Rev. B **47**, 13843 (1993).

[49] R. W. Lof, M. A. van Veenendaal, B. Koopmans, H. T. Jonkman, and G. A. Sawatzky, Phys. Rev. Lett. **68**, 3924 (1992).

[50] V. P. Antropov, O. Gunnarsson, and O. Jepsen, Phys. Rev. B **46**, 13647 (1992).

[51] O. Gunnarsson, E. Koch, and R.M. Martin, Phys. Rev. B **54**, R11026 (1996); Phys. Rev. Lett. **83**, 620 (1999).

[52] O. Gunnarsson, E. Koch, and R.M. Martin, Phys. Rev. B **56**, 1146 (1997).

[53] J. E. Han, M. Jarrell, and D. L. Cox, Phys. Rev. B **58**, R4199 (1998).

[54] L. Pietronero, and S. Strässler, Europhys. Lett. **18**, 627 (1992); C. Grimaldi, L. Pietronero, and S. Strässler, Phys. Rev. Lett, **75**, 1158 (1995).

[55] A. J. Millis, P. B. Littlewood, and B. I. Shraiman, Phys. Rev. Lett. **74**, 5144 (1995).

[56] see, *e.g.*, A. P. Ramirez, Superconductivity Review **1**, 1 (1994).

[57] M. Knupfer and J. Fink, Phys. Rev. Lett. **79**, 2714 (1997).

[58] G. Oszlányi, G. Baumgartner, G. Faigel, L. Gránásy, and L. Forró, Phys. Rev. B **58**, 5 (1998).

[59] G. Ruani, P. Guptasarma, C. Taliani, and J. Fisher, Physica C **235-240**, 2477 (1994).

[60] G. Zimmer, M. Helmle, M. Mehring, and F. Rachidi, Europhys. Lett. **27**, 543 (1994); G. Zimmer, M. Mehring, G. Goze, and F. Rachdi, in *Physics and Chemistry of Fullerenes and Derivatives*, ed. by H. Kuzmany, O. Fink, M. Mehring, and S. Roth, World Sci. (1995).

[61] I. Lukyanchuk, N. Kirova, F. Rachidi, C. Goze, P. Molinie, and M. Mehring Phys. Rev. B **51**, 3978 (1995).

[62] R. Kerkoud, P. Auban-Senzier, D. Jérome, S. Brazovkii, I. Luk'yanchuk, N. Kirova, F. Rachdi, and C. Goze, J. Phys. Chem. Solids **57**, 143 (1996)

[63] C.A. Kuntscher, G.M. Bendele, and P.W. Stephens, Phys. Rev. B **55**, R3366 (1997).

[64] O. Gunnarsson, Phys. Rev. B **51**, 3493 (1995); N. Manini and E. Tosatti, in *Recent Advances in the Chemistry and Physics of Fullerenes and Related Materials: Volume 2*, edited by K.M. Kadish and R.S. Ruoff (The Electrochemical Society, Pennington, NJ, 1995), p. 1017.

[65] M. Capone, W. Stephan, and M. Grilli, Phys. Rev. B **56**, 4484 (1997); M. Capone, S. Ciuchi, and C. Grimaldi, Europhys. Lett. **42**, 523 (1998).

[66] N. Manini, E. Tosatti, and A. Auerbach, Phys. Rev. B **49**, 13008 (1994); A. Auerbach, N. Manini, and E. Tosatti, Phys. Rev. B **49**, 12998 (1994).

[67] N. Manini and E. Tosatti, Phys. Rev. B **58**, 782 (1998); M. C. M. O'Brien, J. Phys. C **5**, 2045 (1972).

[68] W. A. Harrison, *Electronic Structure and the Properties of Solids* (Dover, New York, 1989).

[69] S. Satpathy, V. P. Antropov, O. K. Andersen, O. Jepsen, O. Gunnarsson, and A.I. Liechtenstein, Phys. Rev. B **46**, 1773 (1992).

[70] S. Suzuki and K. Nakao, Phys. Rev. B, **52**, 14206 (1995).

[71] L.F. Chibotaru, A. Ceulemans, and S.P. Cojocaru, Phys. Rev. B **59**, R12728 (1999).

[72] W. Andreoni, P. Giannozzi, and M. Parrinello, Phys. Rev. B **51**, 2087 (1995).

[73] P. Paul, Z. Xie, R. Bau, P.D.W. Boyd, and C.A. Reed, J. Am. Chem. Soc. **116**, 4145 (1994).

[74] J. E. Han, E. Koch, O. Gunnarsson, Phys. Rev. Lett. **84**, 1276 (2000).

[75] A.J. Millis, R. Mueller, and B.I. Shraiman, Phys. Rev. B **54**, 5389 (1996), *ibidem* **54**, 5405 (1996).

[76] S. Ciuchi, F. de Pasquale, S. Fratini, and D. Feinberg, Phys. Rev. B **56**, 4494 (1997).

[77] P. W. Anderson, J. Phys. Soc. Japan **9**, 316 (1954); R. Kubo, J. Phys. Soc. Japan **9**, 935 (1954).

[78] Th. Pruschke, D.L. Cox, and M. Jarrell, Phys. Rev. B **47**, 3553 (1993).

[79] A. Khurana, Phys. Rev. Lett. **64**, 1990 (1990).

[80] E.L. Shirley and S.G. Louie, Phys. Rev. B **41**, 133 (1993).

[81] H. Kajueter, G. Kotliar, and G. Möller, Phys. Rev. B **53**, 16214 (1996).

[82] M. J. Rozenberg, G. Kotliar, H. Kajueter, G.A. Thomas, D. H. Rapkine, J.M. Honig, and P. Metcalf, Phys. Rev. Lett. **75**, 105 (1995).

[83] M. J. Rozenberg, I. H. Inoue, H. Makino, F. Iga, and Y. Nishihara, Phys. Rev. Lett. **76**, 4781 (1996).

[84] C. Castellani, C. R. Natoli, and J. Ranninger, Phys. Rev. B **18**, 4945 (1978).

[85] J.P. Lu, Phys. Rev. B **49**, 5687 (1994).

[86] M.J. Rozenberg, Phys. Rev. B **55**, R4855 (1997).

[87] H. Kajueter, and G. Kotliar, Int. J. Mod. Phys. B **11**, 729 (1996); G. Kotliar, and E. Kajueter, Phys. Rev. B **54**, R14221 (1996).

[88] E. Koch, O. Gunnarsson, and R.M. Martin, Phys. Rev. B **60**, 15714 (1999).

[89] P. Mahadevan and D.D. Sarma, Phys. Rev. B **59**, 1739 (1999).

[90] A. A. Abrikosov, L. P. Gor'kov, and I. E. Dyaloshinski, *Methods of Quantum Field Theory in Statistical Physics* (Dover, New York, 1975).

[91] M. Capone, L. Capriotti, F. Becca, and S. Caprara, e.print cond-mat/0006437.

[92] C. S. Hellberg and S. C. Erwin, Phys. Rev. Lett. **83**, 1003 (1999); G. Santoro, S. Sorella, F. Becca, S. Scandolo, and E. Tosatti, Surf. Sci. **402**, 802 (1998).

[93] E. Tosatti and P. W. Anderson, Solid State Comm. **14**, 773 (1974).

[94] B. Bernu, C. Lhuillier, and L. Pierre, Phys. Rev. Lett. **69**, 2590 (1992); B. Bernu, P. Lecheminant, C. Lhuillier, L. Pierre, Phys. Rev. B **50**, 10048 (1994).

[95] L. Capriotti, A. E. Trumper, and S. Sorella, Phys. Rev. Lett. **82**, 3899 (1999); A. E. Trumper, L. Capriotti, and S. Sorella, Phys. Rev. B **61**, 11529 (2000).

[96] H. R. Krishnamurthy, C. Jayaprakash, S. Sarker, and W. Wenzel, Phys. Rev. Lett. **64**, 950 (1990).

[97] C. Jayaprakash, H. R. Krishnamurthy, S. Sarker, and W. Wenzel, Europhys. Lett. **15**, 625 (1991).

[98] E. Arrigoni and G. C. Strinati, Phys. Rev. B **44**, 7455 (1991).

[99] C. J. Gazza, A. E. Trumper, and H. A. Ceccatto, J. Phys.: Condens. Matter **6**, L625 (1994).

[100] V. V. Tugushev, in *Electronic Phase Transitions*, edited by W. Hanke and Yu. Kopaev (Elsevier North-Holland, Amsterdam, 1992), p. 237, and references therein.

[101] S. Caprara, M. Avignon, and V. Tugushev, Phys. Lett. A **255**, 98 (1999).

[102] F. P. Maldague, Phys. Rev. B **16**, 2437 (1977).

[103] W. Kohn, Phys. Rev. **133**, A171 (1964).